

https://dspace.org/

Investigating alternative voltammetric methodologies to study complex formation

Ndlovu, Mapule Prudence

2017

https://hdl.handle.net/10539/24999

Ndlovu, Mapule Prudence (2017) Investigating alternative voltammetric methodologies to study complex formation,University of the Witwatersrand, Johannesburg, <http://hdl.handle.net/10539/24999>

Downloaded from a DSpace repository. https://dspace.org/

Investigating Alternative Voltammetric Methodologies to Study Complex Formation.

by

Mapule Ndlovu

A Dissertation submitted to the Faculty of Science, University of the Witwatersrand, in fulfilment for the requirements for a degree in Masters of Science.

November 2017, Johannesburg

Declaration

I, Mapule Ndlovu, declare that this dissertation is my own, unaided work. It is being submitted for a degree in Master of Science at the University of the Witwatersrand, Johannesburg. It has not been submitted before for any degree or for examination at any other university.



_____

(Mapule Ndlovu)

_____ day of _____ in _____

I dedicate this work to my family. Mama, papa, Vusi, Tshepo and Karabo, thank you for all your support throughout my studies.

Acknowledgements

I would like to acknowledge my supervisor Dr Caren Billing. Thank you for all your support, teaching, kindness and generosity. I have definitely learned so much from you and I enjoyed my research here at Wits because of you. I so blessed to meet you and I wish you all the best for the future.

I would also like to acknowledge the NRF for the funding and the School of Chemistry and Wits University for giving me a platform to do my research.

A huge thank you to Adam and Kgomotso who I have worked with in this research. Family and friends who always support me in my studies and career, I am forever grateful.

Conferences and Seminars

- ✓ The work in this project was presented at an electrochemistry workshop on the 15th of March 2017 at Mintek.

- ✓ A poster was presented on this work at an Inorganic Chemistry Conference and Carman Physical Chemistry symposium of the South African Chemical Institute in Hermanus Western Cape from 25th -29th June 2017.

Table of Contents

Declaration……i

Dedication……ii

Acknowledgement……iii

Conferences and seminars……iv

Abstract……viii

List of Figures……ix

List of Tables……xvi

List of Abbreviations……xix

Chapter 1 -Introduction

1.1) Chemistry of complex formation……1

1.2) Applications of metal complexes……3

1.2.1) Medicinal applications……3

1.2.2) Catalytic applications……5

1.3) Conventional methods used in formation constant determination……7

1.4) The use of DPASV for bismuth complexes……10

1.4.1) Hydrolysis and precipitation of bismuth……10

1.4.2) Differential pulse anodic stripping voltammetry……12

1.5) Determining Formation Constants……15

1.6) The use of film electrodes……16

1.6.1) Mercury film electrodes……17

1.6.2) Bismuth film electrodes……21

1.6.3) Gold film electrodes……24

1.6.4) Summary of Film Electrodes……26

1.7) Aims and objectives……27

1.7) References……28

Chapter 2-Experimental

2.1) General Experimental setup……33

2.2) Experimental Bi^{3+} study……36

2.2.1) The use of Tl^{+} in Voltammetry……36

2.2.2) DPASV reversibility and detection limit study.....38
2.3) Experimental for the use of mercury film electrode.....39
2.4) NOVA software development.....41
2.4.1) Getting started and connecting external devices.....41
2.4.2) Setting new procedures.....45
2.5) NOVA developed procedures.....51
2.5.1) Automated GE calibration procedure.....51
2.5.2) Automated pH titration.....53
2.5.3) NOVA procedure for film formation and analysis.....55
2.6) References.....57
Chapter 3- Results: The Study of Bi^{3+}
3.1) Investigating the Influence of Tl^{+} on the Bi^{3+} Stripping Peak.....58
3.2) Optimisation of E_{dep}.....62
3.3) DPASV Reversibility.....64
3.4) Optimising Parameters to Improve Reversibility.....68
3.4.1) Optimising Parameters to Improve Reversibility of Bi^{3+}.....68
3.4.2) Optimising Parameters to Improve Reversibility for Tl^{+}.....74
3.5) Study of DPASV detection limit.....76
3.6) pH Titration at Low Bi^{3+} Concentration.....79
3.6.1) Glass Electrode Calibration.....79
3.6.2) pH Titration.....80
3.7) Chapter Summary.....85
3.8) References.....86
Chapter 4 – Investigating the Use of MFEs for Determining Formation Constants
4.1) Preparation of the MFE.....87
4.2) Ex Situ Analysis of Cd^{2+}.....91
4.2.1) Reproducibility Study.....91
4.2.2) Thick vs Thin Film.....96
4.2.3) An Attempt to Stabilise the Film.....97
4.2.4) Effect of pH.....97
4.3) In Situ Analysis of Cd^{2+}.....99

4.3.1) Reproducibility study……99

4.3.2) Full pH Study of Free Cd^{2+}……101

4.3.3) Cd^{2+}-PA system……104

4.4) In situ Pb^{2+} Analysis……107

4.4.1) Reproducibility Study……107

4.4.2) In Situ Lead-Glycine (Pb-Gly) Complex Formation Studies……109

4.5) Ex situ Pb^{2+} Analysis……118

4.5.1) Optimisation……118

4.5.2) Reproducibility Study……120

4.5.3) Ex situ Pb-Gly Complex Formation Studies……121

4.6) Chapter Summary……125

4.7) References……126

Chapter 5 – Conclusion……127

Appendix 1……129

Appendix 2……136

Abstract

Metal complexes have a wide range of applications in fields such as medicinal, industrial, environmental and so on. Determining the formations constants for metal complexes is thus essential to gather information on complexes. Conventional methods used to study complexation include spectroscopic methods and the use of voltammetric techniques such as direct current polarography using a mercury drop electrode. In this work alternative voltammetric methods to study complex formation are investigated.

Bismuth complexes have important medicinal applications but not much is known about them because of the difficulties in studying them due to extensive bismuth hydrolysis and precipitation of hydrolysis products from very low pHs. The aim of this work was to investigate whether using low concentrations of bismuth (10^{-6} M) would prevent precipitation in nitrate solutions as predicted in literature. Differential pulse anodic stripping voltammetry (DPASV) was the technique of choice because of its low detection limit, even though it has not been widely used in complex formation studies before. The study revealed that electrochemical response for Bi^{3+} was not fully reversible using this technique. Additionally, even at the low concentration precipitation was observed in the acidic region (investigated via pH titration) and was suspected to be the formation of $BiONO_3$ species.

The second alternative method investigated was the use of mercury film electrodes to replace the use of the toxic mercury drop electrodes which are being phased out worldwide. This work looked at using in situ and ex situ plated films, where the in situ measurements proved more reproducible. A number of challenges were encountered, such as film degradation, peak splitting and ligand adsorption to the film electrode. Nonetheless, formation constants of lead-glycine complexes were determined under different experimental conditions and these were found to be reasonably compared to the literature values.

List of Figures

Chapter 1

Figure 1.1: Schematic diagram of Bi^{3+} complexes showing the solid state forms……..11

Figure 1.2: pBi vs pH diagrams of Bi^{3+} in a) 1 M perchlorate background and b)1 M nitrate background……..12

Figure 1.3: Measurement parameters involved in DPV……..13

Figure 1.4: A typical differential pulse voltammogram measured during the stripping step……..14

Figure 1.5: Micrographs of MFEs plated on GCE in solutions with 30 µM Hg^{2+} using a deposition potential and deposition time of -1.3 V and 60 s, respectively. A) and D) were formed at pH 3.4 without thiocyanate; B) and E) at pH 3.4 and 5 mM thiocyanate; C) and F) at pH 5.7 and 5 mM thiocyanate……..20

Figure 1.6: Diagram of the construction of the two gold working electrodes for double deposition……25

Chapter 2

Figure 2.1: General experimental cell setup for all voltammetric experiments……34

Figure 2.2: Metrohm Autolab Instrumental setup used for all voltammetric measurements. ……..35

Figure 2.3: Positions of Tl^{+} and Bi^{3+} peaks on a DPASV voltammogram……..37

Figure 2.4: Transferring procedures from an old NOVA version to a new version……42

Figure 2.5: Pictures of the Teflon shaft and the RDE which can be used as stirrers……43

Figure 2.6: Inserting serial number of the magnetic stirrer……43

Figure 2.7: Insertion of a serial number and using the Dosino……44

Figure 2.8: Preprogramed electrochemical methods and initial preprogramed commands……46

Figure 2.9: Autolab control command showing the setup for a) PGSTAT302N b) IME663 and c) pX1000 port……48

Figure 2.10: Window showing *Export ASCII data* command for saving data and linking measured data to saved data……49

Figure 2.11: The display of the *analysis view* window and peak analysis……50

Figure 2.12: Automated calibration procedure showing a) Part A of the calibration and b) Part B and C of the calibration……52

Figure 2.13: The pH titration procedure for Bi^{3+} hydrolysis studies made up of a) Part A and b) Part B……54

Figure 2.14: The procedure for preplating Hg at the glassy carbon electrode……56

Figure 2.15. The procedure used in situ analysis and ligand titrations……56

Chapter 3

Figure 3.1: Voltammograms at t_{dep} = 60 s and different E_{dep} values. The orange curve shows the both Bi^{3+} and Tl^{+} were deposited and the blue curve shows only Bi^{3+} was deposited……59

Figure 3.2: Peak potentials at varying t_{dep} for the oxidation peaks of Bi at each E_{dep}. ……60

Figure 3.3: The peak of a voltammogram fitted using the Skew Gaussian model……60

Figure 3.4: Peak currents at varying t_{dep} for the oxidation peaks of Bi at each E_{dep}……61

Figure 3.5: a) E_p vs E_{dep} and b) I_p vs E_{dep} for Bi^{3+} peaks without the reduction of Tl^{+} in solution (t_{dep} = 60 s)……62

Figure 3.6: a) E_p vs E_{dep} and b) I_p vs E_{dep} for Bi^{3+} peaks when reduction of both Bi^{3+} and Tl^{+} occurred (t_{dep} = 30 s)……63

Figure 3.7: Voltammogram of Bi^{3+} data fitted using the Gaussian model……65

Figure 3.8: Voltammogram of Bi^{3+} data fitted using the skewed Gaussian model……66

Figure 3.9: Voltammogram of Tl^{+} data fitted using the Gaussian model……67

Figure 3.10: Voltammogram of Tl^{+} data fitted using the skewed Gaussian model……67

Figure 3.11: E_p (from the skewed Gaussian fit) vs E_{mod} of the Bi peaks at different modulation times using an interval time of 1 s……69

Figure 3.12: I_p (from the skewed Gaussian fit) vs E_{mod} of the Bi peaks at different modulation times using an interval time of 1 s……69

Figure 3.13: Asymmetric factor (α) vs E_{mod} at different t_{mod} using an interval time of 1 s……70

Figure 3.14: W (from the skewed Gaussian fit) vs E_{mod} of the Bi peaks at different modulation times using an interval time of 1 s……71

Figure 3.15: Area vs t_{mod} of the Bi peaks at different modulation amplitudes using an interval time of 1s……71

Figure 3.16: E_p (from the skewed Gaussian fit) vs interval time of the Bi peaks using E_{mod} = 5 mV and t_{mod} = 80 ms……72

Figure 3.17: I_p (from the skewed Gaussian fit) vs interval time of the Bi peaks using E_{mod} = 5 mV and t_{mod} = 80 ms……72

Figure 3.18: Asymmetric factor (α) vs interval time of the Bi peaks using E_{mod} = 5 mV and t_{mod} = 80 ms……73

Figure 3.19: Peak width (from the skewed Gaussian fit) vs interval time of the Bi peaks using E_{mod} = 5 mV and t_{mod} = 80 ms……73

Figure 3.20. I_p (from the skewed Gaussian fit) vs E_{mod} of the Tl peaks at different modulation times….74

Figure 3.21: Peak width (from the skewed Gaussian fit) vs E_{mod} of the Tl peaks at different modulation times……75

Figure 3.22: Asymmetry factor (α) vs E_{mod} of the Tl peaks at different modulation times……75

Figure 3.23: I_p vs t_{dep} for Bi^{3+} at 10^{-6} M, with the initial linear region indicated……77

Figure 3.24: I_p vs t_{dep} for Bi^{3+} at 10^{-7} M, with the initial linear region indicated……77

Figure 3.25: I_p vs t_{dep} for Bi^{3+} at 10^{-8} M, with the initial linear region indicated……78

Figure 3.26: Glass electrode calibration curve obtained for the titration of 0.1 M HNO_3 with 0.1 M KOH at 25°C……80

Figure 3.27: E_p vs pH for Tl^+ data obtained from the titration. The grey line shows the free Tl^+ potential and the deviation due to the diffusion junction potential below about pH 2 is fitted with a polynomial……81

Figure 3.28: I_p vs pH for Tl^+ data obtained from the low concentration titration……82

Figure 3.29: I_p vs pH for Bi^{3+} data obtained from the low concentration titration……82

Figure 3.30: Bi^{3+} peak potentials vs pH and the values corrected for the diffusion junction potential and potential shifts due to the formation of Bi^{3+} nitrate and hydroxide species……84

Figure 3.31: species distribution diagram of 10^{-6} M Bi^{3+}in nitrate background……84

Chapter 4

Figure 4.1: Microscopic image of an unplated glassy carbon electrode……..88

Figure 4.2: Microscopic images of the mercury film formed at rotation speeds a) 500, b) 1000 and c) 1500 rpm. The deposition potential was -900 mV and deposition time was 300 s in 10^{-3} M $Hg(NO_3)_2$….88

Figure 4.3: Microscopic images of the mercury film at deposition times a) 480 s and b) 600 s. The deposition potential was -900 mV and the rotation speed at 1000 rpm in 10^{-3} M $Hg(NO_3)_2$……..89

Figure 4.4: Microscopic images of the mercury film at deposition potentials a) -750 mV b) -800 mV and c) -850 mV. Deposition time was set at 600 s and the rotation speed at 1000 rpm in 10^{-3} M $Hg(NO_3)_2$…….90

Figure 4.5: Microscopic images of the mercury film at deposition times a) 60 s, b) 120 s and c) 180 s The deposition potential was -900 mV and the rotation speed at 1000 rpm in 10^{-2} M $Hg(NO_3)_2$……90

Figure 4.6. Checking reproducibility of DPV measurements for 10^{-4} M Cd^{2+} in 0.1 M HNO_3 on an ex situ plated MFE (plated at -900 mV for 120 s from 10^{-2} M $Hg(NO_3)_2$ solution). The black vertical line indicates the peak position of the first voltammogram to allow for easy comparison……92

Figure 4.7: Testing reproducibility using DPASV for 10^{-4} M Cd^{2+} in 0.1 M HNO_3 on an ex situ plated MFE (plated at -900 mV for 120 s from 10^{-2} M $Hg(NO_3)_2$ solution) with Cd^{2+} deposited at -800 mV for 60 s. To allow for easy comparison the solid vertical line indicates the peak position of the first voltammogram and the dotted vertical line indicates that for the last voltammogram……..93

Figure 4.8: DPASV at MFE for 10^{-4} M Cd^{2+} and 0.015 M PA. The study was done in 0.1 M HNO_3 with Cd^{2+} deposited at -800 mV for 60 s……95

Figure 4.9: Species distribution diagram of 1×10^{-4} M Cd^{2+} and 0.015 M PA……95

Figure 4.10. DPASV at MFE for 10^{-4} M Cd^{2+} and 0.015 M PA. The study was done in 0.1 M HNO_3 with Cd deposited at -800 mV for 60 s and with mercury preplated for a longer time (240 s)……..96

Figure 4.11: DPASV at MFE for 10^{-4} M Cd^{2+} and 0.015 M PA. The study was done in 0.1 M HNO_3 with Cd^{2+} deposited at -800 mV for 60 s and with mercury preplated at 240 s……97

Figure 4.12: DPASV at MFE for 10^{-4} M Cd^{2+} and 0.015 M PA. The study was done at pH 3.8 with Cd^{2+} deposition at -800 mV for 60 s and with mercury preplated for 120 s……98

Figure 4.13: I_p from consecutive DPASV measurements at a MFE for 10^{-4} M Cd^{2+} in 0.1 M HNO_3 with 10^{-3} M $Hg(NO_3)_2$. Measurements were done at E_{dep} = -900 mV with various t_{dep}……..100

Figure 4.14: DPASV peak currents at the MFE for 10^{-4} M Cd^{2+} (with 10^{-3} M Hg^{2+}) and 0.015 M PA. The in situ study with solutions adjusted to pH 3.8 using E_{dep} = -900 mV and t_{dep} = 300 s……..101

Figure 4.15: DPASVs of 10^{-4} M Cd^{2+} at a MFE obtained from solutions at pH 1, 1.5, 2 and 2.5, also containing 10^{-3} M $Hg(NO_3)_2$. The in situ study was done in HNO_3 with E_{dep} = -900 mV and t_{dep} = 300 s. The voltammograms with the highest currents were the first to be measured……..102

Figure 4.16: DPASVs of 10^{-4} M Cd^{2+} at a MFE obtained from solutions at pH 3, 4, 5 and 7, also containing 10^{-3} M $Hg(NO_3)_2$. The in situ study was done in HNO_3 with E_{dep} = -900 mV and t_{dep} = 300 s. The voltammograms with the highest currents were the first to be measured……103

Figure 4.17: DPASVs obtained from the ligand titration at an MFE for 10^{-4} M Cd^{2+} and PA in the range [L]:[Cd] = 100-1500. The in situ study was done in HNO_3 pH 2.5 with E_{dep} = -900 mV and t_{dep} = 300s at 0.1 M ionic strength……..104

Figure 4.18: DPASVs for 10^{-4} M Cd^{2+} at a MFE. The in-situ study was done in HNO_3 at pH 2.5 with E_{dep} = -900 mV and t_{dep} = 300s……106

Figure 4.19: The fifth voltammograms of 10^{-4} M Pb^{2+} (and 10^{-3} M Hg^{2+} in situ plated) at different pHs (E_{dep} and t_{dep} at -900 mV and 300 s, respectively)……..109

Figure 4.20: Example of a derivative plot of change in current vs average potential for a voltammogram obtained from the Pb-Gly titration……..110

Figure 4.21: The straight-line graph fitted through the points close to the x-intercept (from Figure 4.20) to calculate the peak potential……110

Figure 4.22: Experimental complex formation curve for the Pb-Gly ligand titration at pH 4.01 in the range [L]:[Cd] = 47-14 375 on the MFE…… …111

Figure 4.23: Peak current vs log [L] for the Pb-Gly ligand titration at pH 4.01 in the range [L]:[M] = 47-14 375 on the MFE. ……112

Figure 4.24: Slope analysis of the ECFC for the Pb-Gly ligand titration, also showing the deleted points. The CCFC is also shown……..113

Figure 4.25: Slope analysis of the ECFC and the CCFC for the duplicate Pb-Gly ligand titration……116

Figure 4.26: Peak current vs log [L] for the duplicate Pb-Gly ligand titration at pH 4.01……116

Figure 4.27: DPASV recorded with E_{dep} = -0.75 V and t_{dep}= 90 s showing the position of Pb^{2+} on a MFE……119

Figure 4.28: DPASV recorded at E_{dep} = -0.65 V of Pb^{2+} at different t_{dep} values……119

Figure 4.29: Ex situ Pb-Gly titration with 10^{-4} M Pb^{2+} showing peak splitting……121

Figure 4.30: Ex situ Pb-Gly titration at lower concentrations (with 10^{-5} M Pb^{2+}) showing a reduced amount of peak splitting……122

Figure 4.31: The ECFC and CCFC for the Pb-Gly titration at pH 5.12 with 10^{-5} M Pb^{2+}, together with the slope analysis……..

Figure 4.32: Peak current vs log [L] for the Pb-Gly ligand titration at pH 5.12 on the ex situ plated MFE……132

Appendices

Figure A1.1: species distribution diagram for 10^{-4} M Pb^{2+} in water medium. The diagram was plotted using formation constants in Table A1.1……..130

Figure A1.2: Species distribution diagram for aqueous solutions of Hg^{2+} (1×10^{-4} M) plotted using formation constants in Table A1.2 at 25°C and the indicated ionic strength. ……132

Figure A1.3: Species distribution diagram for aqueous solutions of Bi^{3+} (1×10^{-5} M) in acetate medium (0.1 M) plotted using the literature formation constants in Table A1.1 reported at 25 °C and the indicated ionic strength……132

Figure A1.4: Species distribution diagram for aqueous solutions of Hg^{2+} (1×10^{-4} M) in glycine medium (0.1 M) plotted using formation constants in Table A1.2 at 25°C and the indicated ionic strength……..133

Figure A1.5: Species distribution diagram for the 0.1 M glycine in HNO_3. The species distribution diagram was plotted using the protonation constants im Table A1.3 at 25°C and the indicated ionic strengths……134

Figure A1.6: Species distribution diagram for 10^{-5} M Pb^{2+} and 0.12 M glycine in HNO_3 plotted using the formation constants in Table A1.3 at 25°C and the indicated ionic strength……134

Figure A2.1: Voltammograms for the Pb^{2+} measured consecutively at 1×10^{-4} M and 1×10^{-3} M Hg^{2+} at different pH (E_{dep} and t_{dep} at -900 mV and 300 s). The same colour coding was used in all graphs and at pH 1 it can clearly be seen how the peak current decreases as consecutive measurements were made……137

Figure A2.2: Selected Voltammograms from the Pb-Gly titration showing the almost split peaks……..137

Figure A2.3: Voltammograms measured consecutively for 10^{-4} M Pb^{2+} (E_{dep} and t_{dep} at -650 mV and 120 s, respectively) at different pHs. Peak splitting can be seen in some voltammograms……138

List of Tables

Chapter 2

Table 2.1: General experimental conditions and parameters used in the study of Bi^{3+} reversibility and hydrolysis……..38

Table 2.2: General experimental conditions and parameters used in the experiments involving mercury film electrodes……40

Chapter 3

Table 3.1: Comparison of the fitted parameters for the Gaussian and skewed Gaussian models…….66

Table 3.2: Final optimised DPASV parameters for Bi^{3+}……74

Table 3.3: Log β values for bismuth nitrate species at 25°C……83

Chapter 4

Table 4.1: Peaks currents and % current decrease for consecutive DPASV measurements of Cd^{2+} solutions (deposited at -800 mV for 60 s in 0.1 M HNO_3) on an ex situ plated MFE. The experiment was repeated four times……94

Table 4.2: The average and corresponding standard deviation for the peak potentials, peak currents and peak widths of 7 voltammograms measured consecutively at various pHs. The solution contained 10^{-4} M Pb^{2+} and 10^{-3} M Hg^{2+} and E_{dep} = -900 mV and t_{dep} = 300 s……108

Table 4.3: Experimentally determined formation constants for the Pb-Gly system at pH 4.01 and 25 °C (0.011 M – 0.58 M ionic strength) together with the literature formation constants[9] at the ionic strength stated in brackets……114

Table 4.4: Pb-Gly experimentally determined formation constants at pH 4.01 and 25 °C (0.011 M – 0.578 M ionic strength) and literature formation constants at ionic strengths indicated in brackets……117

Table 4.5: The average and corresponding standard deviation for peak potentials and peak currents of consecutively measured voltammograms at various pHs. The solution contained 10^{-4} M Pb^{2+} and E_{dep} = -0.65 V and t_{dep} = 120 s……120

Table 4.6: Pb-Gly ex situ experimentally determined formation constants at pH 5.12 and 25 °C (0.001 M – 0.061 M ionic strength) and literature formation constants[9] at ionic strengths indicated in brackets……124

Appendices

Table A1.1: Formation constants for the Bi^{3+} hydroxide and Bi^{3+} acetate (Ac) systems as well as the protonation constants for acetate at 25 °C and the given ionic strengths……..129

Table A1.2: Formation constants[1] for the Hg^{2+} hydroxide and Hg^{2+} glycine (Gly) systems as well as the protonation constants for glycine at 25 °C and the given ionic strengths……..131

Table A1.3: Formation constants[1] for lead hydroxide, lead glycine systems and protonation constants for glycine at 25°C and the given ionic strengths……133

List of Abbreviations

AdSV- Adsorptive Stripping Voltammetry

ASV- Anodic Stripping Voltammetry

BFE-Bismuth Film Electrode

BSS -Bismuth Subsalicylate

CBS- Colloidal Bismuth Nitrate

CCFC- Calculated Complex Formation Curve

Cd-PA- Cadmium- Picolinic Acid

CE- Counter Electrode

DADS- Diallyl Disulfide

DAS- Diallyl Sulfide

DCP- Direct Current Polarography

DMDS- Dimethyl Disulfide

DME- Dropping Mercury Electrode

DNA- deoxyribose Nucleic Acid

DPASV -Differential Pulse Anodic Stripping Voltammetry

DPP -Differential Pulse Polarography

DPV- Differential Pulse Voltammetry

ECFC- Experimental Complex Formation Curve

EDTA- Ethylenediaminetetraacetic acid

GCE- Glassy Carbon Electrode

GE- Glass Electrode

H. .*pylori*- Helicobacter Pyroli

HMDE- Hanging mercury Drop Electrode

HSAB - Hard Soft Acid Base

MDE-Mercury Drop Electrode

MFE-Mercury Film Electrode

ML- Metal-Ligand

NMR- Nuclear Magnetic Resonance

Pb-Gly- Lead- Glycine

PCA- Pyrazine Carboxylic Acid

RDE- Rotating Disk Electrode

RE- Reference electrode

RPM- Revolutions per Minute

SSE- Sum of Squares of Errors

UV-Vis – Ultraviolet Visible Spectroscopy

WE- Working Electrode

Nomenclature

I_p – Peak Current

E_p – Peak Potential

E_j – Junction Potential

E_{dep} – Deposition Potential

t_{dep} – Deposition Time

E_{mod} – Modulation Potential

t_{mod} – Modulation Time

Chapter 1 – Introduction

1.1 Chemistry of Complex Formation

Complexes are compounds or ionic compounds in which a central atom or ion is surrounded by negatively charged or neutral molecules possessing a lone pair of electrons. The term is almost exclusively taken to mean an ion of a transition metal which is surrounded by other molecules or ions.[1] These surrounding molecules or ions that are attached to the central metal ion are called ligands. Complexation occurs when the ligands donate lone pairs of electrons making a covalent bond to the central metal ion. In the periodic table the first row transition metals have partially filled 3d orbitals and empty 4d and 4p orbitals which work to accept these lone electron pairs. This enables transition metals to form complexes with multiple ligands on one central metal ion.[1]

The most common ligands include H_2O, OH^-, NH_3 and CN^-. The type of ligands that coordinate to the central atom depend on the local environment of the metal ion. In an aqueous environment, the most common ligands are H_2O molecules with the common complex being a central metal ion surrounded by six H_2O molecules. The formula for this complex would be written as $[M(H_2O)_6]^{2+}$ and named the hexa aqua complex ion. The 2+ ionic charge is due to the oxidation state of the central metal ion. The complex remains ionic because the H_2O ligands are neutral ligands. Ligands are not permanently attached to the metal – if the environment changes, ligand exchange will take place and the metal ion will be surrounded by the most favoured ligand. An example would be addition of chloride to the hexa aqua complex, where the H_2O molecules will be displaced by the chloride ligands.[1]

The mechanism of complex formation occurs through both the inner sphere and the outer sphere. For an aqua complex, the inner sphere is H_2O molecules which are bound directly to the metal ion.[2] The outer sphere is usually H_2O molecules which surround the complex by hydrogen bonding. The initial step in complex formation with another ligand is that the first ligand forms an outer sphere around the complex. These ligands will then start replacing the H_2O molecules that are bound directly to the metal ion. The ligands will then become the inner sphere and thereby complex directly to the metal ion.[2,3,4] Initial formation of the outer sphere is very important for the kinetics of complex formation. When the ligands are in the outer sphere, they can move faster to the inner sphere for complexation to occur.

There are various factors that affect complex formation, these include the affinity of the metal ion for the ligand due to the size, composition, chemistry and the concentration of the metal or ligand.[5] Pearson proposed the idea of hard and soft acids and bases (HSAB) in 1963.[6] Hard metal ions have a

high affinity for ligands with hard donor atoms and soft metal ions prefer ligands with soft donor atoms.[6] Hard metal ions are those with small ionic radii, high positive charge and empty orbitals in the valence shell, with examples being Na^{+}, $Ca^{2+}$and Al^{3+}, and soft metal ions have large radii, lower charge and filled orbitals, such as Ag^{+}, Hg^{2+} and Cd^{2+}. Soft ligands have a large radii with an intermediate electronegativity such as I^{-}, CN, RS^{-} and SCN^{-} to name a few. Some metal ions and donor atoms of ligands are borderline and these include Bi^{3+}, Cu^{2+} and Pb^{2+} metal ions and Br^{-} and N_3^{-} donor ligands.

Steric and electronic factors are other important aspects that affect complex formation. If there is a bulky molecule attached to the metal ion or near the complex, this will cause repulsion of the donor atom on the ligand with the metal ion.[7] Complex formation will be compromised due to this and the complex formed will be weakly stable. The basicity of the ligand and the pH of the solvent also affects the extent to which complexation will occur. The more basic the donor atom of the ligand, the more easily electrons can be transferred from the donor atom to the empty orbital of the metal ion and the greater the chance of complex formation. Protonated ligands would need to be deprotonated in order to be basic and participate in complex formation.[5,7]

Complexes are named using the name of the ligand, the name of the metal ion, its oxidation state and the overall charge of the ion. Complexes come in different shapes and sizes. This is often dependant on the coordination number of the metal ion. Coordination number is essentially the number of pairs of the electrons that can attach to the central metal ion. Some ligands can act as chelators; these are polydentate ligands which can form more than one bond with the metal ion. These kinds of ligands are usually more effective and form stable complexes.[5]

1.2 Applications of Metal Complexes

1.2.1 Medicinal Applications

Medicinal inorganic chemistry is an emerging research area in drug design which uses metal ions as pharmacophores (in other words, they are part of a molecule that is responsible for biological interaction) since they produce structures that cannot be achieved with organic chemistry alone. Currently, metallodrugs are used to treat many diseases.

For more than 200 years, bismuth has been used in preparing medicinal drugs and today new drugs are being developed. Bismuth was first used as an additive in paints and skin products in the seventeenth century. In 1786 for the first time ever Louis Odier used Bi^{3+} to treat dyspepsia.[8,9] In Britain, the use of Bi^{3+} in medicine only started in the nineteenth century.[9] Bismuth subnitrate was the first bismuth compound to be used. It was later used to treat gastric and intestinal disorders. In 1887 Felix Blazer[10] first reported that bismuth may be useful to treat syphilis. Bismuth was still regarded as an important antisyphillic agent even after penicillin was discovered to be the safe and quick treatment for treponemal infections. Bismuth's action was seen to be very valuable in tertiary and quarterly stages of syphilis.[9,10]

Different Bi^{3+} compounds such as subcitrates, subgallates, subsalicylates and subnitrates, have been useful in treating different conditions like hypertension, skin conditions and other infections. BSS (bismuth subsalicylate) and CBS (colloidal bismuth subnitrate) have been used throughout the world since the 1970's for treatment of diahorrea and peptic ulcers respectively.[9,11]

Using bismuth compounds on its own or in conjunction with other compounds has been found to be very effective in the antibacterial action against bacteria such as *Helicobacter Pylori* (*H. pylori)* which causes peptic ulcers. Combining bismuth with some liphophilic thiol compounds enhances bismuth's antibacterial action. Several thiols such as monothioglycerols and dimercecarprol have been combined with $Bi(NO_3)_3$ to enhance the antibacterial action by 25-400 fold. The latter thiol is also very effective against *staphylococcusaureus*.[12]

H. pylori is a gram negative spiral shaped bacterium that causes severe gastric mucosal conditions such as gastric cancer. It has a flagella which enables it to enter the mucosa through the mucus layer. This bacterium produces the enzyme urease which catalyses the hydrolysis of urea according to the reaction:

$$H_2NCONH_2 + H_2O \rightarrow [H_2NCOO^- + NH_4^+] \rightarrow 2NH_3 + CO_2$$

The ammonia produced is toxic to human cells. Bismuth hinders the reproduction and growth of this bacterium although the mechanisms by which it does so are not yet clear.[9]

The radioisotopes isotopes ^{212}Bi and ^{213}Bi have the potential to be anticancer agents. They have short half-lives which are 61 and 46 minutes, respectively.[13] They undergo alpha decay and in so doing they emit radionuclides that transfer energy. In cancer treatment, when they decay they release alpha particles that do not go deep into the tissue of the cancer patients. Penetration is only about 50-80 μm deep. This will minimise the physical harm of healthy tissue in the process of aiming for cancerous tissue. Their very short half-lives require that transport molecules deliver them directly to cancerous cells. Chelating ligands such as polyaminopolycarboxylates and aminocarboxylates are useful for carrying bismuth radionuclides to the cancerous tissue where the release of alpha particles will occur at the cancerous cells and therefore the nearby non-cancerous tissue remains largely unharmed.

Although bismuth has been used in medicine, there is not enough information about bismuth complexes to fully understand their mechanisms of action. Information such as thermodynamic stability and kinetics of Bi^{3+} complexes is insufficient.

Other common metallodrugs include gadolinium compounds which are used to enhance MRI contrast agents and platinum which is used as an anticancer agent.[14] The anticancer activity of the platinum-based complex, cisplatin, was first discovered by Rosenberg in the 1960s.[15,16] It became clinically accepted in 1978 and today it is one of the best and most widely sold metallodrug. The discovery of cisplatin resulted in the use of metal complexes for chemotherapy to block the replication of DNA cells in the nuclear DNA. Cisplatin does this by forming linkages inside the DNA that changes the DNA. This then hinders transcription and replication and subsequently kills the cell.[17,18] However, cisplatin comes with a number of disadvantages and these include toxic side effects, poor stability and resistance of many tumours. These led to its limited use in medicinal applications. Side effects of cisplatin include vomiting, nausea and bone marrow suppression.

The success of platinum-based drugs encouraged research into other metal-based drugs such as ruthenium, bismuth and barium. Ferrocene was first synthesised accidentally in 1951. Decades later, numerous ferrocene complexes were isolated and its application was discovered by the Jaouen group when they attached ferrocene to tamoxinfen which is a drug used in the treatment of breast cancer. This finding led to the discovery of other modified ferrocene drugs such as ferrocifen which is also a cytotoxin.[19]

Current research is mainly focusing on protein-targeting complexes, not DNA-targeting. There is an increase in the development of metal complexes as enzyme inhibitors.[20] The introduction of metal

complexes has also increased the selectivity and activity of free ligands. The metal ion can act to hold the kinetically inert complex together and the ligands will be used in the overall structure of the inhibitor.[21]

1.2.2 Applications in Catalysis

Catalysis is also an essential application of metal complexes. Knowles, Noyoni and Sharpless were awarded a Nobel Prize for a catalytic process involving metal complexes in 2001, and more recently in 2010 Heck, Suzuki and Negishi received a Nobel Prize for palladium based coupling.[16]

Several transition metal sulphides display catalytic activity, such as acting as surfaces for molecular hydrogen and facilitating the reductive transformation of organic molecules.[22] Metal sulphides have catalysed the hydrogenation of unsaturated compounds and aromatic compounds. These metal sulphide catalysts are very useful in fuel processing and during the hydrorefining processes to catalyse isomerisation, dehydration and hydrocracking processes.[22,23] Metal sulphides that have characteristics of a semi-conductor have been used in the making of photo- and electrocatalytic systems, such as tungsten sulphide (WS_2), which has been used as a photocathode and photoanode. Iron sulphide complexes serve as catalysts for the reduction of many substrates using electron donors or hydrides.

Metal complex-based catalysts with pyridine as a ligand are becoming ground breaking because they are able to form complexes with different metal ions that are at different oxidation states, therefore give higher catalytic performances. Metal complexes have also been used in catalysis involving photoexcitation with visible light. Ruthenium and iridium complexes with polypyridine as ligands have the ability to absorb light in the visible region; this absorbed light gives stable and longer photoexcited states.[24,25] These metal complexes have been used as a photoredox catalyst to decompose water into oxygen and hydrogen and reduce carbon dioxide to methane gas.

Light can be converted into electricity by using ruthenium-based metal complexes as light collectors. The ruthenium tris-bipyridine complex not only absorbs light but gives off intense emissions. However, nowadays ruthenium complexes are being replaced because of their scarcity, cost and toxicity. The bis-diamine copper complex is gaining much attention because of its light absorption properties, high abundance, lower toxicity and affordability. This has made these complexes valuable for solar energy conversion and, because of the abundance of copper, solar energy can be converted to electricity and fuels in large quantities.[25]

Vanadium complexes are utilised as catalysts to modify alkanes. They have been used to catalyse organic processes such as oxidation and carboxylation of alkanes.[26] The catalytic activity of these

processes can be enhanced by adding acid, such as nitric acid, sulphuric acid, oxalic acid and pyrazine carboxyl acid (PCA) which are promoters. In 1993 Shul'pin and Kozlov[27] discovered that the vanadate salt (n-Bu_4N)(VO_3) had efficient catalytic activity towards oxidation of the organic compounds when used in combination with PCA and hydrogen peroxide. Following this, Sutradhar *et al*.[28] also reported the importance of PCA in catalytic activity of vanadium complexes for oxidation of alkenes in either liquid or gas form.

1.3 Conventional Methods Used to Determine Formation Constants

To determine the formation constants, any method can be used if it is able to determine the concentration of at least one species involved in complex formation in solution. That concentration will be used together with the stoichiometry of the reaction to determine the concentration of all other species present in solution. Several other equilibrium measurements would have to be done under different conditions (for example different concentrations) to be able to determine the formation constants accurately.[5]

Spectroscopic methods have been used to study complexes and determine their formation constants. UV-vis spectroscopy involves the absorbance of electromagnetic radiation in the UV-vis region of the electromagnetic spectrum. It can give an indication of how much each absorbing species has been absorbed and since absorbance is directly proportional to concentration, it can be used to determine the equilibrium concentrations of each of the species and can be used to calculate formation constants by a series of mass balance equations. More than one species can absorb light at a given wavelength, where the extent of absorption depends on the relative concentrations and the spectral properties of the species.[29] The ligand titration experiment using UV-vis are thus usually repeated at different wavelengths and the formation constants are averaged.

In 1971 Shlayapnikov and Shtern[30] observed that the absorbance increased at 280 nm upon addition of bicarbonate to a copper solution, in other words as copper bicarbonate complexes were formed. In 1977 Jones and Manahan[31] conducted a complexation study where they observed the spectral peaks of $K_2Cu(CO_3)_2$ when copper was added to a potassium carbonate solution. However, neither Shlayapnikov and Shtern[30] nor Jones and Manahan[31] could determine the formation constants of the complex formed or the absorbing species in solution.[29]

By 1996 eighty percent of the formation constants that had been reported in literature were determined by glass electrode (GE) potentiometry.[5] This technique was the preferred method because common ligands are weak acid or bases and are largely responsible for changes in the H^+ concentration of the solution as complexation take place. Determining the H^+ concentration would give direct information about the concentration of uncomplexed ligand that is present at equilibrium and therefore give insight into the affinity of the ligand for the metal ion. Glass electrodes are used for these measurements because the electrode is selective and sensitive to essentially only the free H^+ concentration. For measurements done in the pH range 2-12, the H^+ concentration measured will be accurate enough to use in the determination of formation constants. Some metal ions form stable complexes below pH 2; but potentiometry cannot be used to determine formation constants for such systems.

Potentiometry is often chosen over polarography because the experiment is straight-forward and interpretation of results with GE potentiometry is simple since readily accessible computer programs can be used to analyse data. However, polarography can give information that cannot be obtained by other techniques. It has greater sensitivity and lower detection limits and could be used to study complexation below pH 2 including the cases for metal ions that easily hydrolyse and precipitate. The low detection limit means that metal complexation can be studied at very low concentrations, and precipitation would be delayed and only occur at a higher pH.

Polarography is a unique electrochemical technique that can be used for qualitative and quantitative simultaneous determinations in the study of formation constants and it uses small amounts of sample.[32] In this case both the pH is measured to gain information about the H^+ concentration and the metal-ligand species are looked at through the reduction process. The technique allows determination of the composition and the distribution of different complexes that are formed. Numerous mathematical methods have now been developed to determine stability constants.[33–35] Basic methodology to study complex formation became available before the 1900.[36] In 1901 Bondlander[37] developed a method to determine dominant species in solution using electromotive force measurements in their study of silver and copper complexes. In the 1902 for the first time, Morse[38] and Sherrill[39] studied the stepwise formation of mercury chloride complexes. A few other developments in formation constant determination were made in the early 1900 but sadly progress slowed down significantly after 1920. The Debye -Hückel concept was then introduced which successfully explained the behaviour of dilute solutions and this led to all electrolytes being believed to be dissociated species under very dilute conditions.[36]

The method used in equilibrium studies should ideally not disturb the system that is under study. In polarography, the concentrations of the species at the surface of the electrode are slightly changed during the measurement because the metal ion from the complex is reduced and forms an amalgam with the mercury drop, and any ligand that was bound to the metal ion then moves into solution. Deford and Hume[40,41] used conditions that ensured the disturbance was minimal and did not impact on the results. Their method has been proven to be trustworthy by comparing their results to those found using other methods and techniques. Therefore, equations used in polarography to determine formation constants must use assumption that are applicable in most methods.[41] The two important conditions that are required to determine formation constants using polarography. This first is that the reaction occurring at the electrode should be reversible, whether the metal ion is complexed or not. Reversibility of the electron transfer reaction can be evaluated by studying the polarograms. The second is that the concentration of the ligand at the surface of the electrode be the same in the bulk solution. Since this cannot be strictly the case, a large excess of ligand is often added so that when the

metal ion is reduced at the electrode surface and the ligand moves into solution, the change in concentration is negligible since an extremely small amount of the metal ion is reduced at each step.

Direct current polarography (DCP) is a common type of polarographic method where a dropping mercury electrode (DME) is used. With newer DMEs, the drops are generated by a pressurised inert gas that forces mercury to flow through a narrow capillary and hang on the tip until it is knocked off and a new drop is formed. The timing can be far more readily controlled than when using a mercury drop electrode based on gravitational flow. DCP, differential pulse polarography (DPP) and other voltammetric methods are now being used widely for formation constants determination.[42–47]

Other methods for studying formation complexes include nuclear magnetic resonance (NMR), ion exchange, ion conductivity and many more. These techniques are often used in special circumstances when spectrophotometry, polarography or potentiometry cannot be used. An example would be the use of NMR in a case where formation constants need to be determined for radioactive metal ions at low concentrations.

Up until this point, we have looked at the chemistry of complex formation and highlighted some of the important applications of metal complexes. Various techniques used to study formation constants have been also been discussed. We will now shift our focus to two methodologies that will be used to study complex formation in this work. Firstly the use of differential pulse anodic stripping voltammetry (DPASV) will be considered which is a sensitive method that will be used to study bismuth complexes at low concentrations to postpone bismuth precipitation to higher pHs. Secondly, the use of film electrodes to replace the toxic mercury drop electrode in complex formation will be looked at. These will be discussed in detail in sections 1.4 and 1.5, respectively.

1.4 The Use of Differential Pulse Anodic Stripping Voltammetry for Studying Bismuth Complexes

1.4.1 Hydrolysis and Precipitation of Bismuth

The significant medicinal applications of bismuth complexes have been extensively covered in section 1.2.1. As mentioned, the mechanisms of action of bismuth drugs are still not fully understood because not enough kinetic or thermodynamic information is known about Bi^{3+} complexes. This is because of the difficulties experienced when studying Bi^{3+} such as hydrolysis and precipitation occurring at low pH even at fairly low concentrations.

The hydrolysis of Bi^{3+} has been studied by many authors and has been useful in coming up with techniques that help study hydrolysis reactions.[48] The species $Bi(OH)^{2+}$, $Bi(OH)_3$ and $Bi(OH)_4^-$ were readily found. In 1947 authors Graner and Sillën[49] reported that hydrolysis products that formed by a process of polymerisation and they reported the detection of species Bi_2O^{4+} and $Bi_3O_2^{5+}$. They later found this work to be incorrect due to the erroneous use of quinhydrone electrode.[50] Olin[51] reported a study using bismuth amalgam and glass electrodes over a wide range of Bi^{3+} concentrations. In his study, it was concluded that the polynuclear $Bi_6(OH)_{12}^{6+}$ is more stable than the $Bi(OH)_2^+$ complex since $Bi(OH)_2^+$ could not be detected. However, in another study done by Suganuma *et al.*[52], $Bi(OH)_2^+$ was detected in a solution of pH 0.5 and 7 at Bi^{3+} concentrations as low as 10^{-7} M. It was then concluded that at higher Bi^{3+} concentrations $Bi_6(OH)_{12}^{6+}$ is the dominant species and $Bi(OH)_2^+$ forms at low concentrations. Other polynuclear species also found at higher Bi concentrations were $Bi_9(OH)_{20}^{7+}$, $Bi_9(OH)_{21}^{6+}$ and $Bi_9(OH)_{22}^{5+}$. The Bi^{3+} species distribution in Figure A1.1 in Appendix 1 was drawn for 1×10^{-5} M Bi^{3+} in an aqueous medium using formation constants given in Table A1.1, also in the Appendix. This diagram clearly shows that Bi^{3+} hydrolyses already from pH 0 and experiments have indicated that precipitation also occurs from about pH 2.

The precipitation of hydroxides or oxides limits the pH range where studies of soluble hydrolysis products can be done. Swinehart and Garret[53] reported the solubility product of $BiONO_3$ but this was found to be incorrect. This is due to the fact that they did not take into consideration the possibility that the $BiNO_3^{2+}$ species could have also formed, as well as the fact that they did not do experiments at a constant ionic strength, i.e. maintain the same concentration of nitrate.

Kragten *et al.*[48] determined the complexes of bismuth-oxy complexes in different matrices (chloride, perchlorate and nitrate). The formation constants of bismuth hydroxy species $Bi(OH)_3$ and $Bi(OH)_4^-$ were also determined. The scheme in Figure 1.1 illustrates the reaction of Bi^{3+} in aqueous solutions containing background electrolytes of nitrate, perchlorate and chloride (shown as symbol A) and it clearly shows the species that are in the solid form.

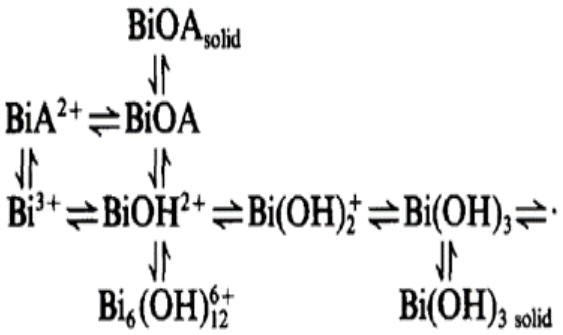


Figure 1.1: Schematic diagram of Bi^{3+} complexes showing the solid state forms.[48]

Figures 1.2a) and b) show pBi-pH plots in 1 M perchlorate and 1 M nitrate, respectively. The dots plotted show the experimental results. The region within the borderlines shows the species that is dominant under those conditions. The precipitation regions of $Bi(OH)_3$ and $BiOClO_4$ for a perchlorate background or $BiONO_3$ for a nitrate background were found by adapting the curves to the experimental data. Kragten *et al*.[48] could not draw the pBi-pH diagram for chloride because BiOCl has a very limited solubility and Bi^{3+} was found to form strong complexes with chloride in solution.

It is a challenge to tell whether O_2^{2-} or OH^- is bound to a metal ion using most experimental techniques, thus it is difficult to say whether the species BiOA or $Bi(OH)_2A$ has formed. Hence when calculating the boundary lines for pBi-pH the solubility products used for BiOA were considered as $Bi(OH)_2A$. In the systems illustrated, both the pH and the bismuth concentration determine the type and concentration of the various species. From these plots it can be observed that the solubility of $Bi(OH)_3$ is low and thus precipitates from concentrations of about 2×10^{-5} M Bi^{3+}. BiOA precipitates in the lower pH range and when placed in alkaline conditions it recrystallizes to $Bi(OH)_3$ in the solid form.

It is thus clear that Bi^{3+} precipitates at a low pH at fairly low Bi^{3+} concentrations. This is problematic because we are forced to start complex formation studies below pH 2 where Bi^{3+} is still soluble. When using DCP the lowest Bi^{3+} concentration that can be reliably studied is 10^{-5} M. The aim of this study was to use a more sensitive voltammetric technique to study Bi^{3+} at lower concentrations to prevent precipitation as far as possible. The technique used was DPASV.

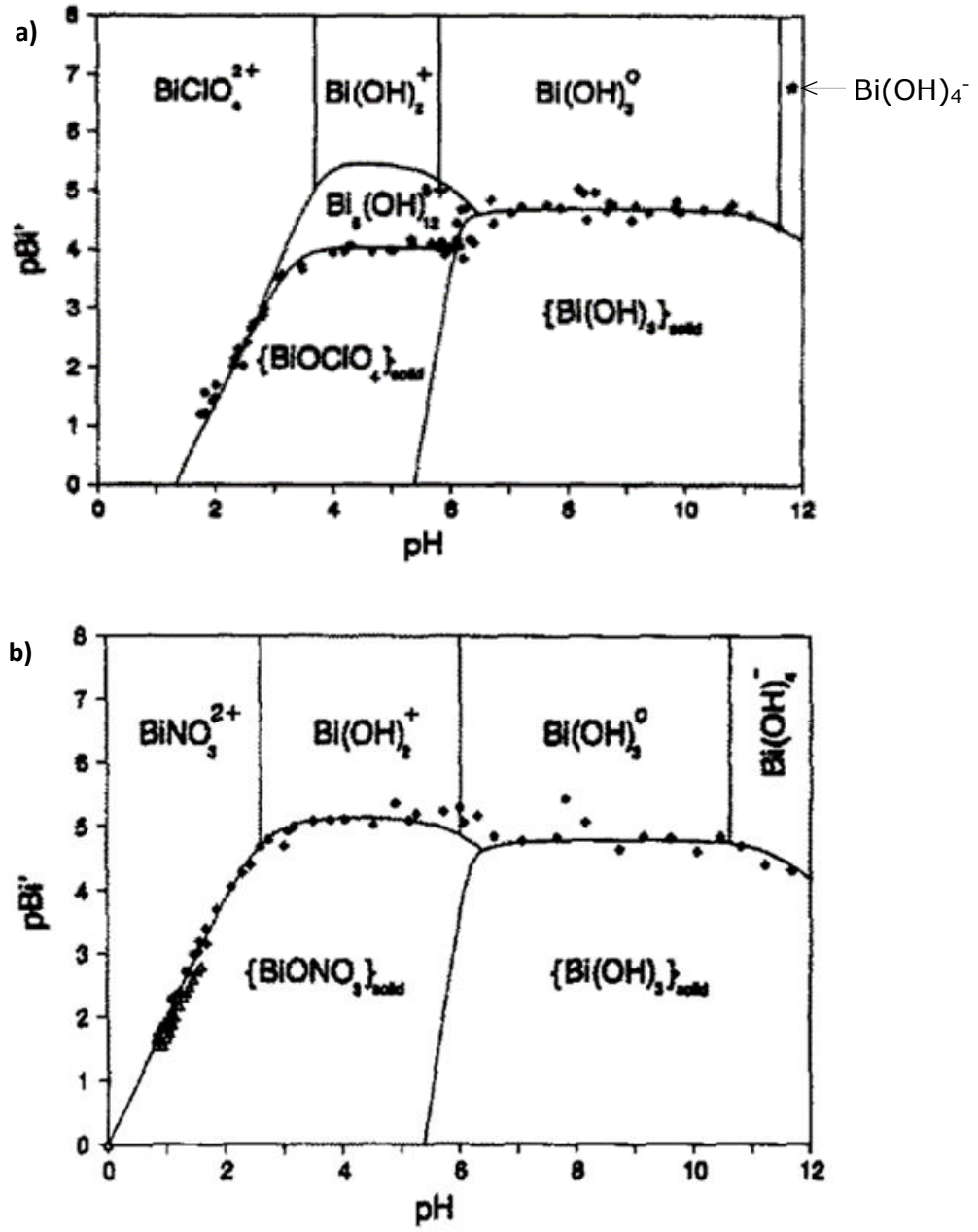


Figure 1.2: pBi vs pH diagrams of Bi^{3+} in a) 1 M perchlorate background and b)1 M nitrate background.[48]

1.4.2 Differential Pulse Anodic Stripping Voltammetry (DPASV)

DPASV is a combination of two techniques, differential pulse voltammetry (DPV) and anodic stripping voltammetry (ASV). In DPV, the potential is increased in a stepwise fashion and a potential pulse is superimposed on this at the end of each step. Figure 1.3 below illustrates the DPV technique and the parameters involved. A start potential is applied and just before the pulse is applied, the current is measured. A pulse is then applied for a certain amount of time. Just before the end of the pulse duration, the current is sampled again. The interval time is the duration of the applied base potential

and the modulation potential together. The pulse height and the duration of the pulse are known as the modulation amplitude and modulation time, respectively. The step potential is the potential increment that is added from one base potential to the next and the cycle repeats. The difference between the current at the pulse and at the base is called the differential current and this is plotted against the base potential in the voltammogram. The current is sampled twice to eliminate non-faradaic currents as far as possible. The start and the end potential refer to the potential range in which the voltammogram is measured.[54,55]

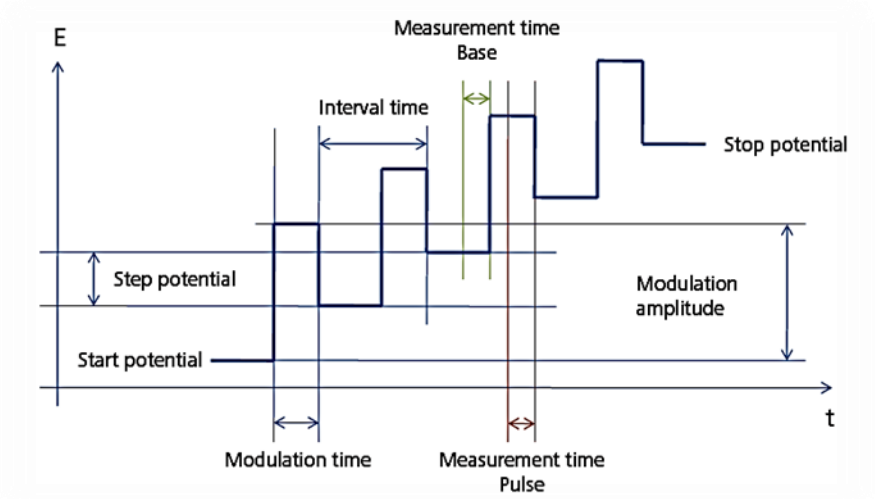


Figure 1.3: Measurement parameters involved in DPV.[56]

ASV works by applying a negative potential to reduce the metal ion. This preconcentrates the metal ion at the electrode surface or forms an amalgam if a mercury electrode is used. This is then followed by applying a potential scan in a positive direction to re-oxidise the metal thereby stripping it from the electrode. The sensitivity of ASV results from the reduction step where the metal gets preconcentrated at the electrode surface. The process below illustrates the reduction of the metal ion at a mercury drop in a ligand free environment:

$$M^{n+} + ne^- \rightarrow M_{Hg}$$

This is then followed by oxidation of the metal as:

$$M_{Hg} \rightarrow M^{n+} + ne^-$$

In complex formation studies, the aim is to measure the resultant peak current and peak potentials that are due to the oxidation together with complex formation. The reduction process when the ligand

is also present in solution would be for example as follows (assuming the charge on the ligand is -1 and the dominant form of the ligand in solution is HL):

$$ML^{(n-1)+} + H^+ + ne^- \rightarrow M_{Hg} + HL$$

In the next step the metal is oxidised followed immediately by complex formation by the ligand at the surface of the electrode as illustrated in the process below.

$$M_{Hg} + HL \rightarrow ML^{(n-1)+} + H^+ + ne^-$$

It is critical that complex formation must be rapid (within the measurement time) or else it will not be detected. A typical voltammogram is given in Figure 1.4 which shows the peak potential (E_p) and peak current (I_p) that are measured. These parameters are used in the calculation of formation constants.

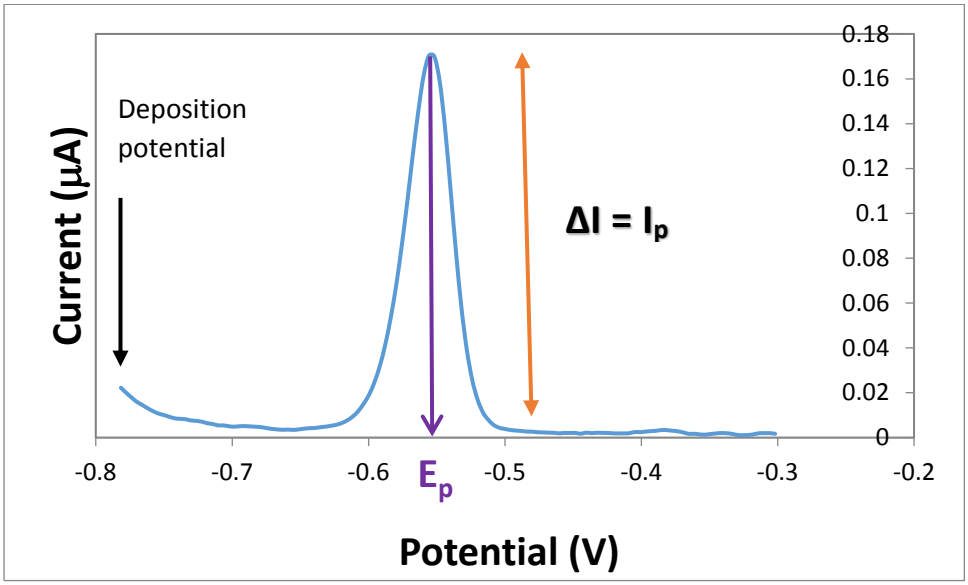


Figure 1.4: A typical differential pulse voltammogram measured during the stripping step.

In this study, the technique DPASV has been chosen for its low detection limit where concentrations as low as 10^{-10} M can be determined in theory.[57] The need for a sensitive technique can be seen from Figure 1.2 where, to avoid precipitation of Bi^{3+} at low pH, the concentration of Bi^{3+} has to be very low (closer to 10^{-6} M). Added benefits of using this technique are that the instrument is inexpensive and multiple electroactive species can be measured simultaneously.

1.5 Determining Formation Constants

Formation constants determined by voltammetry are evaluated by monitoring the change in the peak current and the shift in peak potential as determined for the free metal ion and for the metal-ligand complexes as the pH of the solution is increased or the ligand concentration is increased.[58] Formation constants can be determined via a ligand titration or a pH titration. In ligand titrations, the pH is kept constant and the ligand-to-metal concentration ratio ([L]:[M]) is increased. In pH titrations, the ligand-to-metal concentration ratio is kept constant and the pH is increased. Cukrowski's[58] equation below is used to calculate the formation constants:

$$\{\mathrm{E}(\mathrm{M_{free}}) - \mathrm{E}(\mathrm{M_{comp}})_\mathrm{i}\} - \frac{\mathrm{RT}}{\mathrm{nF}} \ln \frac{\mathrm{I}(\mathrm{M_{comp}})_\mathrm{i}}{\mathrm{I}(\mathrm{M_{free}})_\mathrm{i}} = \frac{\mathrm{RT}}{\mathrm{nF}} \ln \frac{[\mathrm{M_T}]_\mathrm{i}}{[\mathrm{M_{free}}]_\mathrm{i}} \quad (1)$$

where $\mathrm{E}(\mathrm{M_{free}})$ is the peak potential of the free metal ion, $E(\mathrm{M_{comp}})$ is the peak potential of the metal-ligand complex, $I(\mathrm{M_{free}})$ is the peak current of the free metal ion and $I(\mathrm{M_{comp}})$ is the peak current of the metal-ligand complex. $[\mathrm{M_T}]$ and $[\mathrm{M_{free}}]$ are the total concentrations of the metal ion and the concentration of the free metal ion, respectively. The symbol *i* represents either the pH or the ligand concentration at which the measurements are done at every step in the titration.

The left side of the equation is calculated by using experimental data. The most critical term in the calculation is $\{\mathrm{E}(\mathrm{M_{free}}) - \mathrm{E}(\mathrm{M_{comp}})_\mathrm{i}\}$ which is the change in the peak potential (ΔE_p) and the term $\frac{\mathrm{RT}}{\mathrm{nF}} \ln \frac{\mathrm{I}(\mathrm{M_{comp}})_\mathrm{i}}{\mathrm{I}(\mathrm{M_{free}})_\mathrm{i}}$ is the correction term. The left side of the equation is hence named the corrected ΔE_p. To get the most accurate and reliable formation constants, the corrected ΔE_p must only be influenced by changes that are due to complex formation. If there are any other factors that influence the corrected ΔE_p, then the calculated formation constants will not be accurate.

On the right side of the equation [M] is known and $[\mathrm{M_{free}}]$ is found by calculations involving mass balance equations, which contain the formation constants of all the suspected solution species. The formation constants for the metal-ligand species being investigated are refined such that the calculated part represents the experimental data as closely as possible.[58] All known stability constants, such as the protonation constants of the ligand and hydrolysis constants of the metal ion, are kept fixed in this process.

1.6 The Use of Film Electrodes for Formation Constant Determination

Formation constants in electrochemistry have largely been determined with the use of a dropping mercury electrode (DME). The drop is elemental mercury which is very toxic and has become difficult to source due to the efforts of phasing it out. Alternatives to using the DME were thus investigated and in this work the use of film electrodes was considered for formation constant determination. In electrochemical studies of complex formation, an ideal electrode should give reproducible data (both peak potentials and peak currents) that is not influenced by anything other than the metal-ligand complexation.

The success of electrochemical processes depends on the type of working electrode used. An ideal electrode is one that can be used over a considerable range of potentials, has a reproducible surface and displays chemical inertness and mechanical stability. The two general types of electrodes used are the solid and liquid electrodes. Film electrodes can be classified as either of the two types depending on the metal plated on the substrate. There are numerous electrode substrates that can be used for film formation (e.g. carbon, platinum and gold) but there is a limited number of metals that can be plated onto these substrates to form a film.[59] The most common liquid film electrode is mercury. Solid film electrodes include gold, platinum and the more recently bismuth.[60]

The development of polarography by Herovsky in 1922,[61] led to mercury being used as the electrode of choice for analytical studies in the negative potential region. The two common types of mercury drop electrodes are the hanging mercury drop electrode (HMDE) and the dropping mercury electrode (DME). These have been used in numerous applications for determining inorganic and organic compounds, with HMDEs being used to a larger extent than the DMEs. Even though its applications are widely successful, its usage comes with disadvantages.

The biggest disadvantage of HMDEs and especially DMEs is the use of metallic mercury which is very toxic and hence environmentally unfriendly. There is a very high risk of contamination, exposure and poisoning. Many countries have even completely discontinued using metallic mercury and it has become very difficult to source in some countries.[61,62] The electrode consists of a capillary tube through which the mercury flows and then hangs on the tip. This capillary requires regular maintenance to generate a reproducible mercury drop. Also, the mechanical stability of the mercury drop is very limited. The drop can be easily lost during vibrations or when used in flow cells with very high flow rates. This means that the HMDE is not an appropriate electrode for usage in on-site applications where generally the conditions are not very stable. Also, HMDEs cannot be modified and used to enhance detection limits or selectivity.

Current research worldwide aims at developing, studying and understanding alternative electrodes for voltammetric studies. This section discusses recent developments and properties of film electrodes, including mercury film electrodes (MFEs), bismuth film electrodes (BFEs), gold film electrodes and combination electrodes where two or more metals are used in conjunction, such as bismuth-antimony or bismuth-mercury electrodes. In particular the aim is to look at using film electrodes for techniques such as ASV. For the past 20 years MFEs, made by coating an appropriate substrate with a film of mercury, have shown to be effective for electrochemical analysis using ASV and adsorptive stripping voltammetry (AdSV).[63]

1.6.1 Mercury Film Electrodes

Mercury film electrodes have been developed to overcome the mentioned disadvantages that come with mercury drop electrodes. These are simply made by plating mercury on a substrate. Some of the advantages of MFEs are that the surfaces have a greater mechanical stability (unlike the drops) and also the surface areas are generally larger. Flow cell experiments and on-site analysis can be performed with these electrodes. The quantity of mercury used for MFEs is significantly smaller (almost negligible) compared to the DMEs therefore less toxicity and exposure. However, MFEs have a smaller potential range of study and some drawbacks occur in the preparation, regeneration and activation of the film electrode and its substrate.

The most widely used substrates for MFEs are carbon substrates because they are unreactive and have a wide potential region of study. This is important for determining multiple metals that are reduced and oxidized at a different potentials. The carbon substrates have a low background current, are inexpensive and readily available. Additionally, they are easily cleaned by polishing. Glassy carbon (GC) is the most widely used substrate but impregnated graphite and carbon paste (made by combining carbon powder with paraffin which is an inert hydrophobic binder[64]) are more easily constructed and their surfaces can also be easily regenerated. Graphite pencil electrodes on the other hand are readily disposable. Reticulated vitreous carbon (microporous GC) has a huge surface area and when plated with mercury, it functions effectively in coulometry. A more scarce carbon substrate is pyrolytic graphite. New developments have been reported that carbon nanotubes can be coated with mercury and used as substrates.[65] Attempts have also been made to use metals as substrates for coating mercury. Metals such as platinum and gold were largely unsuccessful because they dissolve in mercury and form an amalgam. Additionally, the coated film is uneven and the electroactive species react with the metal surface. Some metal substrates that have been reported for coating mercury are nickel, copper and aluminium to name a few.[61]

Prior to plating the mercury, the substrate has to be properly polished to ensure a smooth surface. For a glassy carbon substrate, aluminium oxide paste is usually used to polish the surface. Metallic mercury is coated onto the substrate by reducing mercury ions from solution. There are three ways of coating the substrate. The ex situ method entails preplating metallic mercury (from an Hg^{2+} containing solution) onto the glassy carbon electrode, followed by transferring the plated electrode to the sample solution where analysis is to take place. Forced convection through stirring the solution with a magnetic stirrer or using a rotating disk electrode usually speeds up the preplating step. Different plating conditions can be used but it is generally recommended that plating solutions be at low pH to prevent mercury hydrolysis which starts to a small extent around pH 2 (as shown in Figure A1.2 in Appendix 1) if there is no other ligand present.

For the in situ analysis, Hg^{2+} ions are added to the sample solution and plated together with the analyte during analysis; this method is less time consuming than the ex situ method. The choice of the type of plating is dependent on the type of analysis that would be carried out. Sometimes a combination of coating methods is used to minimize the loss in the mercury film. The third but more rare method of plating is to use a mercury precursor, such as $HgCl_2$ or HgO (encapsulated on Nafion)[66], whereby the mercury from these compounds will be released and reduced during the analysis reaction. This method is almost similar to in situ plating. Substrates like silver, platinum and gold can be plated by just dipping them in liquid mercury,[67] but as discussed these metals slowly dissolve due to amalgam formation.

The rate at which mercury is deposited can be enhanced by adding a metal such as thallium. This metal enhances nucleation sites and hence increases the rate of film formation. In analyses where plating is done in situ, target metal ions that are plated with mercury do play an important role in enhancing nucleation.[61,68]

After use in cases where a film had been plated, the film would have to be removed. This can be done mechanically by gently wiping the surface of the electrode with a smooth piece of tissue. The electrode substrates are usually very delicate so scratching of the surface should be avoided. It is important that the electrode gets thoroughly cleaned at the end of the analysis to avoid any permanent damage to the electrode and interferences from the residue on the electrode. An unclean electrode substrate could prevent a uniform film from being plated or carry-over effects in the next analysis. Carry-over effects are even more evident in the analysis involving longer preconcentration times. Electrochemical cleaning of substrates is done by applying a positive potential (such as 0.6 V for 60 s) to oxidise species on the surface of the electrode. The electrochemical cleaning process is significantly facilitated in an

acidic solution such as 0.1 M HNO_3.[69] Other chemical methods of removing the film include treatment with iodine or a tetraethylene.

In situ plated MFEs are advantageous because the surface is regenerated with each analysis. Wu[70] conducted a study where in situ plating was done when studying Cd and Pb using ASV. The in situ plated mercury gave reproducible background currents because the film was re-plated at each measurement therefore a fresh surface was made. However, in the same study, the MFE was found to be unstable during measurements as spiking currents were observed. Gollas *et al*.[71] also reported a similar behaviour of spiking currents observed in their work. They rationalized that the spikes were due to mixing of the mercury droplets when mercury was plated hence the spiking currents were caused by the small changes in the structure of the film.

Ex situ MFE studies were also conducted and it was observed that the MFE surface is subject to change. Micrographs were taken after plating before analysis and then again after ten cycles of voltammograms were measured and it was observed that the morphology of the film had changed. Taking the film for imaging also has an effect on the morphology because on drying, the film cracks. Leaving a layer of water on the surface mostly preserves the film. Therefore, in situ formed MFEs are far better than ex situ formed MFEs because the former regenerate the films, gives a more reproducible background, are much more sensitive and the peaks are less broad.[70]

Surface morphology studies reported largely that the MFE is basically small droplets dispersed on the substrate. At a more negative deposition potential, the droplets are smaller and more evenly dispersed.[72] A less negative deposition potential causes deposition of mercury on defect sites. A high negative deposition potential makes a homogeneous film with droplets of mercury packed together. But, a very negative deposition potential might also result in damage to the film caused by H_2 evolution occurring. This was proven when the MFE was deposited at -1.1 V whereby the background currents for the measurements were changing indicating changes in surface morphology of the films due to H_2 evolution.[73]

In situ plating might be the most recommended method, but there are some reports that suggest that it forms the most irreproducible films that are often difficult to remove at the end of the analysis and could also form solid mercuric compounds on the electrode substrate.[72] If solid compounds form, it would compromise the performance and a huge amount of time would be required for polishing and cleaning it. Diederich *et al.*[74] reported a method of coating mercury on a glassy carbon substrate whereby in situ plating was done in the presence of thiocyanate which enhanced the performance of the MFE. Monterroso *et al.*[72] went on to look at the overall effect on the performance of a MFE (on a glassy carbon substrate) also plated in the presence of thiocyanate. They showed how the pH and

deposition potential for plating, affects the morphology of the MFE, its reproducibility, mechanical stability, selectivity and sensitivity. The study (done with both in situ and ex situ plating) found that homogenous films were produced when the plating solutions contained thiocyanates. Films formed in solutions without thiocyanate (see Figure 1.5 A and D) gave surfaces with regions that were uncoated with mercury and the colour of the film was uneven throughout the surface. Figure 1.5 B,E,C and F show films plated in the presence of thiocyanate, where full surface coverage can be seen. These results were obtained at two different pH conditions (3.4 and 5.7). It was therefore concluded that thiocyanates facilitate the nucleation of mercury to produce the uniform MFE. The authors' rationale was that thiocyanates control the kinetics of deposition of mercury by complexing to the mercury ions. However, at low pH (<2.5), thiocyanate is not needed, the presence of protons was more effective in facilitating nucleation. The protons reduce the C-O functionality on the glassy carbon and this unblocks active sites and facilitates nucleation. Additional advantages of using MFEs formed in the presence of thiocyanate (above pH 2.5) is that the reproducibility increased significantly from an RSD of 7-9% to 0.8-0.9% and the MFEs did not show signs of degradation and no changes in the background current were observed as in other cases.[75]

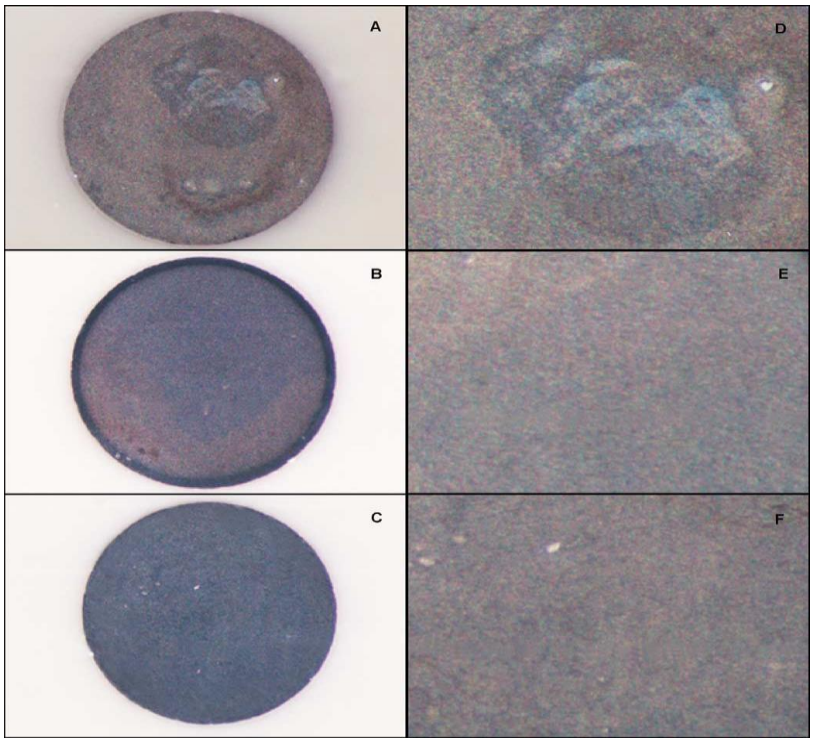


Figure 1.5: Micrographs of MFEs plated on GCE in solutions with 30 µM Hg^{2+} using a deposition potential and deposition time of -1.3 V and 60 s, respectively. A) and D) were formed at pH 3.4 without thiocyanate; B) and E) at pH 3.4 and 5 mM thiocyanate; C) and F) at pH 5.7 and 5 mM thiocyanate.[72]

Brainina and Neyman[76] also demonstrated a method of making a more uniform film on a graphite pencil substrate. Mercury was plated in a solution containing sulphate ions. In the presence of sulphate, the mercury–sulphate interactions are favourable (in terms of hard and soft interactions) therefore this controls the amount of mercury that gets deposited. This results in a film of smaller droplets that covers the substrate uniformly.

Nahar[77] determined the formation constants of zinc with ethylenediamine by the use of DPASV and a mercury film plated on glassy carbon. The MFE was prepared ex situ from a solution of HCl. The zinc-ethylenediamine complexation studies were done by running DPASV in an acetate buffer solution at pH 9 and a ligand titration was performed. The author was able to detect the formation of ML, ML_2, ML_3 and metal hydroxide species. The log β values determined were comparable to the literature values. The high magnitude of the stability constants obtained (6.03, 10.16 and 13.98 for ML, ML_2 and ML_3, respectively) indicated the zinc-ethylenediamine system is very stable under very basic condition. However, the mercury film used was plated ex situ and the stability of the film was not clearly discussed in their paper.

1.6.2 Bismuth Film Electrodes

Bismuth film electrodes (BFEs) are among the various electrodes that are being developed to replace MFEs. Unlike traditional MFEs, BFEs and bismuth salts are less harmful to the environment and non-bioaccumulative.[45] BFEs are made by plating bismuth on an appropriate substrate. They are able to form multicomponent fused alloys with other metals such as cadmium and lead.[78] This property is an advantage since it is very similar to the formation of amalgam by mercury electrodes. The formation of the alloys speeds up the nucleation of bismuth during the deposition of metals to be analysed. In voltammetry, the metal being studied needs to be able to adhere, adsorb, dissolve in or be electrochemically attached to the electrode surface used.

Bismuth is able to plate on common substrates that have been used for MFEs. Substrates made of carbon such as carbon paste, glassy carbon, wax-impregnated graphite and pencil lead have been reported.[60,63] Carbon substrates are inexpensive and simple to prepare and can be modified easily just like in when used in MFEs.[79]

Bismuth films can also be coated in three ways as already described when discussing with MFEs. The plating solution most commonly used for the formation of bismuth films is an acetate buffer solution at pH 4.5 (with a Bi^{3+} concentration 10^{-5} M).[78,80] It is important to note that according to the bismuth species distribution diagram (see Figure A1.3 in Appendix 1), at pH 4.5 in an acetate medium the

dominant species in solution is $Bi(OH)_2^+$. The acetate buffer is added to complex Bi^{3+} to prevent hydrolysis and therefore precipitation. However, comparison between Figures A1.3 and A1.1 shows that there is no difference indicating that complexation with acetate does not take place significantly, not surprising due to the small formation constants shown in Table A1.1. In some work done in our lab, we found that it was still necessary for Bi^{3+} to be added to the acetate buffer after purging the solution and just before plating was initiated to prevent precipitation. In section 1.4.1 we saw that the BiOA (where A= $NO_3^-/ClO_4^-/Cl^-$) precipitated at low pH, where BiOA could also mean $Bi(OH)_2A$. This could indicate that at pH 4.5 the $Bi(OH)_2Ac$ (where Ac = Acetate) species is formed which is more soluble than the other BiOA species studied and that precipitation is very slow.

Krolica and Bobrowski[59] developed a quick and easy method of coating bismuth. Their procedure used a media which had 0.2 M of $Bi(NO_3)_3$ in 0.5 M LiBr and 1 M HCl with deposition done at -0.28 V. Microscopic analysis showed that the experimental conditions and the condition of the electrode substrate greatly influenced the nucleation, growth and overall surface coverage of the bismuth film.[59,78]

In in situ analysis, with most films (including MFEs and BFEs), the metal ion for film formation is added directly to the sample solution and it is important that the concentration of this metal ion be much higher than the target compound (at least 10 fold higher) to prevent any saturation effects.[80] This plating procedure is limited to ASV because a negative potential is applied for preconcentration of the sample metal ions and this negative potential is also used for film plating. With bismuth films, the drawback of in situ coating is that the pH range of the sample solution in which analysis can be done is limited because hydrolysis of Bi^{3+} occurs easily in neutral and basic media. According to Figure 1.2 the insoluble hydrolysis product, $Bi(OH)_3$ is formed from around pH 6. Hence in situ coating is appropriate only for low pH sample solutions.

However, it has been postulated[63] that the coating of BFEs under very basic conditions can be possible due to the formation of the $Bi(OH)^{2+}$ species which is soluble in aqueous media and can be reduced on electrode surfaces. We disagree with this statement because according to the species distribution diagram in Figure A1.3 in Appendix 1, the $Bi(OH)^{2+}$ species is only present up to about pH 5; at very basic pHs (above pH 12) the dominant species is $Bi(OH)_4^-$ which would be soluble. In forming MFEs, mercury hydrolysis also occurs soon after pH 3 (see Figure A1.2 Appendix 1) when there is no ligand present. But with MFEs, and most other metals, if there is ligand present which complexes the mercury, hydrolysis happens at higher pHs depending on the actual and relative concentrations of the ligand and metal ion as well as the formation constants (for example, see Figure A1.4 in Appendix 1).

Ex situ plating is more complicated and time consuming than in situ because an additional preplating step is required and the preplated electrode has to subsequently be transferred to the sample solution. Bismuth coatings can also be formed by using bismuth precursors such as Bi_2O_3 where the precursor is incorporated into a carbon paste and bismuth will get reduced to the metal via the reaction:

$$Bi_2O_{3(S)} + 3H_2O + 6e^- \rightarrow 2Bi_{(S)} + 6OH^-$$

This method is limited to carbon paste electrodes because the bismuth precursor has to be incorporated into it; no bismuth salts are needed in solution.

The potential scanning window of BFEs is from -1.25 V (at pH 4.5) so therefore it can be used to detect metals that appear in the negative potential region such as cadmium, lead and zinc. Bismuth gets oxidized at about 0.05 V so metals that appear at a positive potential cannot be studied using bismuth films electrodes. However, copper is one of the few metals that could be studied using bismuth films in the positive region.[81]

A more recent study done by Yi *et al.*[62] looked at the use of Bi-Sb film electrodes for trace determination of Cd^{2+} in tap waters. Bi-Sb electrodes were first used in the year 2000 to replace the mercury electrodes since the properties of the two electrodes are very similar. These similarities include the fact that the electrode is not highly sensitive to dissolved oxygen, the electrodes can be used for studies at a wide range of potentials and also they have the ability to study organic compounds.[82] This electrode has also been reported to perform satisfactorily for electrochemical studies at low pH (pH < 2).[62] The authors[62] initially studied bismuth and antimony electrodes separately by plating them on a glassy carbon electrode. The performance of the individually plated metals was compared to the electrode with both metals plated (Bi-Sb).There was a higher response to Cd^{2+} when Bi-Sb film electrode was used as compared to when either the bismuth film or antimony film electrodes were used separately. It also appeared that the response of Cd^{2+} on the Sb film electrode was higher than on the Bi film electrode. Overall, the Bi-Sb film electrode produced well-defined Cd^{2+} peaks with no interferences from oxygen. Experimental conditions and parameters were optimised. These included the pH of the background solution, the concentration ratio of bismuth and antimony, the deposition potential and deposition time. At a high negative potential, hydrogen evolution started to be observed. This had to be avoided because the H_2 bubbles accumulate on the film and this results in current decrease because of decrease in electrode surface area. The study found that pH 2 is the optimum pH and beyond this pH the Cd^{2+} response drops which was thought to be due to the hydrolysis of the antimony and possibly bismuth as well.[80]

1.6.3 Gold Film Electrodes

Gold films have attracted much attention due to their mechanical and chemical stability, specific surface area and the electrode surface that can be easily modified. Porous gold films have interested numerous researchers, with publications involving these films increasing significantly over the last decade. These films are used largely in electrical conductivity and catalytic activity of solar cells and electrochemical sensors, amongst others.[83] Other common gold electrodes are the non-porous gold film electrode and the solid gold electrode. Ali *et al.*[44] looked at stability constant determination of lead complexes with different organic compounds: diallyl disulfide (DADS), dimethyl disulfide (DMDS) and diallyl sulfide (DAS) on a solid gold electrode. The gold working electrode was initially prepared by scraping with a fine grade of furriery paper and polished with Al_2O_3 powder. It was then rinsed in 0.2 M NaOH and also rinsed ultrasonically with a mixture of ethanol and water for 180 s.

A ligand titration was done where the background solution (in this case an acetate buffer) was kept at a constant pH of 5.5. Various other electrodes such as the glassy carbon, platinum, mercury film and carbon paste electrodes were also tested against the gold electrode and it was decided that the gold electrode produced the best results because the changes in the voltammograms during titration were adequate for formation constants studies, i.e. the response was much better when the gold electrode was used.[44] Since this was a ligand titration at a specific pH, other pH conditions (in the pH range 3-7) were also studied. It was observed that the current increased as the pH was increased from 3 to 5.5. Above pH 5.5 the current decreased due to the formation of lead hydroxide species. The peak potential of Pb^{2+} in the absence of ligand was constant with an increase in pH up to 5.5 and thereafter it shifted more negative. A pH of 5.5 was chosen as the optimum pH since it gave the maximum current and the peak potential at this pH was very similar to the other values below 5.5. Different background electrolytes, namely acetate, citrate and Britton-Robinson buffer, were tested and the acetate proved to be the best background where reduction of lead was effective.

Korolczuk and co-workers[84] studied trace As^{3+} determination using ASV and two gold working electrodes simultaneously. One of the disadvantages of using ASV is that other metal ions like Cu^{2+} can interfere with the analysis of the target metal. The use of gold nanoparticles, the addition of EDTA and concealing the electrode with a Nafion film[85] are some of the ways to reduce interference of ions. Korolczuk looked at minimizing interference from other metals and lowering the detection limit using ASV. This was achieved by using two gold working electrodes for double deposition.

The study was carried by placing the two working electrodes opposite each other. The first electrode was a gold film plated on a glassy carbon electrode. This gold film electrode was made by electrochemical deposition from a solution containing gold and urea. Then after 15 s the plated gold

was polarized at 0.2 V to remove impurities. The second electrode consisted of an ensemble of four gold microelectrodes made from gold wires sealed with epoxy resin. The deposition potential and time for analysis at the two electrodes were optimised individually and both electrodes (gold film and gold ensemble) produced comparable parameters for deposition potential and deposition time. It was then decided that the same parameters will be used for both electrodes. Figure 1.6 shows the construction of the two working electrodes and the electrochemical reactions that take place at each step in the analysis of the target ion (As^{3+}). Firstly arsenic was deposited at the gold film electrode (Figure 1.6A). The electrode was then disconnected and placed near the second electrode (Figure 1.6B). The arsenic was allowed to be oxidized by dissolved oxygen and then a second deposition was then carried at the gold ensemble electrode. Voltammetric measurements (ASV) were then done at the second electrode.

The main point of the double deposition was to enhance the detection limit. This happened when the two electrodes were brought close together. The electroactive species that were deposited and stripped from the gold film electrode were at close proximity to the gold ensemble electrode where the second deposition took place. This means that mass transport of the electroactive species was enhanced. After the first deposition, the second deposition was carried out from an unstirred solution so that the electroactive species did not diffuse back into the bulk solution. A significantly higher response was achieved with currents more than 10 times greater than when only one working electrode was used. The study used acetate buffer (pH 4.6) as the supporting electrolyte to reduce the occurrence of H_2 evolution as these bubbles could potentially accumulate on the second electrode since no stirring was done. EDTA was added to minimise interferences by other metal ions, but proved to be effective only in masking Pb^{2+} and very little minimisation of Cu^{2+} interference.

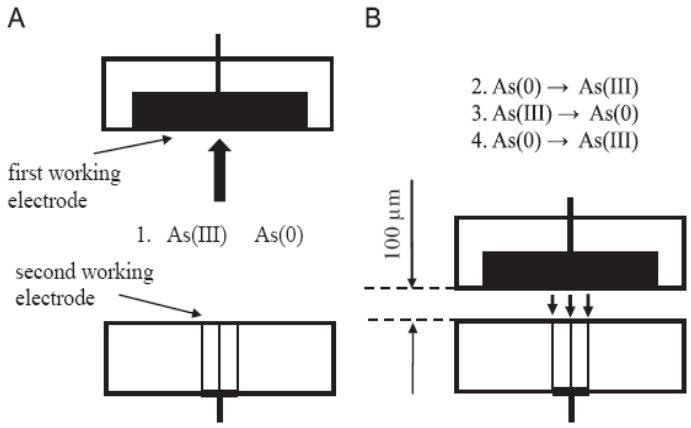


Figure 1.6. Diagram of the construction of the two gold working electrodes for double deposition.[84]

1.6.4 Summary of Film Electrodes

Various film electrodes have been discussed and it seems that these electrodes and hence the measured responses are all largely influenced by pH. This means that if they are used as an alternative to the mercury drop electrode, all experiments for complex formation would have to be ligand titrations and not pH titrations. As it was highlighted at the beginning of the section, in complex formation studies, changes in the peak currents and peak potentials should not be influenced by anything other than complexation. Particularly with bismuth film electrodes we are restricted to acidic pHs because of bismuth hydrolysis. Even Bi-Sb film electrodes only work optimally at pH 2. In that case, current is not only dependent on the concentration, diffusion rate and formation of inert, non-labile or insoluble species, but also on the pH at which the measurement is made. Mercury films have issues of toxicity and film degradation which have to be taken into consideration when doing measurements. However, in this work MFEs were chosen because unlike bismuth they are not as susceptible to hydrolysis.

1.7 Aims and Objectives

The hypothesis is that the use DPASV and film electrodes can replace conventional methods used in studying complex formation. These alternative methods will be investigated in this work. Complex formation studies for bismuth were considered where difficulties arise due to the hydrolysis and precipitation of bismuth at low pH and concentration. It will be investigated whether DPASV can be used as an alternative technique (rather than the usual polarographic techniques). The main reason for this is because DPASV has very low detection limits and would therefore allow bismuth to be studied at low concentrations where precipitation can hopefully be prevented as shown in Figure 1.2.

The second alternative methodology that will be investigated is the use of film electrodes to study complex formation. Formation constants have largely been determined using a mercury drop electrode and very few studies have been reported where film electrodes have been utilised. The main drive for this is to eliminate the use of toxic mercury. Even though mercury film electrodes were employed in this work, the quantity of mercury in the films (obtained by reducing mercury salts) is very low. The film will be tested on studying complexes of Cd^{2+} and Pb^{2+} which are metals that have been extensively studied. The aim is to reproduce the formation constants that are already presented in literature with the use of mercury films.

In both cases, automated procedures will be developed using the NOVA software (which controls the Metrohm potentiostat and other external devices) where possible. Experimental conditions and parameters will be optimised and all reported formation constants will be compared to the literature values. The research outline carried is as follows:

- Software development and programming of automated and non-automated procedures.
- Investigation of the use of Tl^{+} to determine the use of diffusion junction potential for use in Bi^{3+} study.
- Optimisation of voltammetric measurement parameters and investigation of reversibility Bi^{3+} and Ti^{+} on DPASV.
- The study of the detection limit of DPASV.
- Calibration of the glass electrode and pH titration of Bi at low concentration.
- Preparation of MFE and microscopic analysis of the film.
- Ex situ and in situ analysis of Cd^{2+} on MFE.

Ex situ and in situ analysis of Pb^{2+} including complex formation studies with glycine as ligand.

1.8 References

1. Atkins, P. W., Overton, T. L., Rourke, J. P. and Weller, M. T. *Shriver and Atkins' Inorganic Chemistry*, (Oxford University Press, 2010).

2. Warren, J. J., Lancaster, K. M., Richards, J. H. and Gray, H. B. *J. Inorg. Biochem.* **115,** 119–126 (2012).

3. Choppin, G. R. *J. Alloys Compd* **249,** 9–13 (1997).

4. Kravtsov, V. I. *J. Electroanal. Chem.* **69,** 125–131 (1976).

5. Martell, A. E. and Hancock, R. D. *Metal Complexes in Aqueous Solutions*, (Plenum Press, 1996).

6. Pearson, R. G. *Coord. Chem. Rev.* **100,** 403–425 (1990).

7. Irving, B. H. and Williams, R. J. P. *J. Chem. Soc.* 3192-3210 (1949).

8. Yang, Y., Ruizhuo, O., Lina,X., Ning, G., Weiweli, L., Kai, F., Lei., O., Zhuoyuan, Y., Shuang., Z. and Yuqing, M. Y. *J.Coord.Chem.* **8972,** (2015).

9. Sadler, P. J., Li, H. and Sun, H. *Coord. Chem. Rev.* **185-186,** 689–709 (1999).

10. Balzer, F. C. R. *Soc. Biol.* **41,** 537-544 (1889).

11. Briand, G. G. and Burford, N. *Chem. Rev.* **99,** 2601–58 (1999).

12. Yang, N. and Sun, H. *Coord. Chem. Rev* .**251,** 2354–2366 (2007).

13. Keogan, D. M. and Griffith, D. M. *Molecules* **19,** 15258–15297 (2014).

14. Hanif, M., Nawaz, M. A. H., Babak, M. V., Iqbal, J., Roller, A., Keppler, B. K. and Hartinger, C. G. *Molecules* **19,** 8080–8092 (2014).

15. Rosenberg, B., Vancamp, L., Trosko, J. and Mansour, V.H. *Nature* **222,** 385–386 (1969).

16. Turel, I. *Molecules* **20,** 7951–7956 (2015).

17. D'Errico, S., Oliviero, G., Borbone, N., Piccialli, V., Pinto, B., De Falco, F., Carnuccio, R., Costantino, V., Nici, F. and Picallii , G. *Molecules* **19,** 9339–9353 (2014).

18. Wexselblatt, E., Yavin, E. and Gibson, D. *Inorg. Chim. Acta* **393,** 75–83 (2012).

19. Vessières, A., Top, S., Pigeon, P., Hillard, E., Bouberk, L., Spera, D. and Jaouen, G. *J. Med. Chem.* **48,** 3937–3940 (2005).

20. Gasser, G. and Metzler-Nolte, N. *Bioinorganic Medicinal Chemistry*. (Wiley-VCH, 2011).

21. Meggers, E. *Chem. Commun.* 1001–1010 (2009).

22. DuBois, M. R.*Chem. Rev.* **89,** 1–9 (1989).

23. Weisser, 0 and Landa, S. *Sulphide Catalysts, Their Properties and Applications*. (Pergamon Press, 1973).

24. Prier, C. K., Rankic, D. A. and MacMillan, D. W. C. *Chem. Rev.* **113,** 5322–5363 (2013).

25. Sandroni, M., Pellegrin, Y. and Odobel, F. *Comptes Rendus Chim.* **19,** 79–93 (2016).

26. Sutradhar, M., Martins, L. M. D. R. S., Guedes da Silva, M. F. C. and Pombeiro, A. J. L. *Coord. Chem. Rev.* **301-302,** 200–239 (2015).

27. Shul'pin, G. B. and Kozlov, Y. N. *Org. Biomol. Chem.* **1,** 2303–6 (2003).

28. Sutradhar, M., Alegria, E. C. B. A., Mahmudov, K. T., da Silva, M. F. C. & Pombeiro, A. J. L. *RSC Adv.* **6,** 8079–8088 (2016).

29. Zuehlke, R. W. and Kester, D. R. *Mar. Chem.* **13,** 203–226 (1983).

30. Shlayapnikov, D. S. and Shtern, E. K. *Chem. Abs.* **77,** (1972).

31. Jones, D. R. Manahan, S. E. *Anal. Chem.* **39,** 10–12 (1977).

32. Eva, J. *J. Electroanal. Chem.* **196,** 43–51 (1985).

33. Rossottt, F. *The Determination of Stability Constants and Other Equilibrium Constants in Solution*, (McGraw-Hill, 1961).

34. Crow, D. R. *Polarography of Metal Complexes*, (Academic Press, 1969).

35. Gupta, P. N. and Bhat, S. A. *J. Electrochem. Soc.* **31,** 171 (1982).

36. Stuart, R. *J. Chem. Educ.* **35,** 592–599 (1958).

37. Bondlander, G. and Fittig, R. *J. Phys. Chem.* **39,** (1902).

38. Morse, H. *J. Phys. Chem.* **41,** (1902).

39. Sherill, M. S. *J. Phys. Chem.* **43,** (1903).

40. Deford, D. D. and Hume, D. N. *J. Amer. Chem. Soc.* **73,** 5321 (1951).

41. Bond, A. M. and Hefter, G. *J. Electroanal. Chem.* **31,** 477–485 (1971).

42. Billing, C., Cukrowski, I. and Jordan, B. *Electroanalysis* **25,** (2013).

43. Cukrowski, I. and Luckay, R. C. *Anal. Chim. Acta* **372,** 323–331 (1998).

44. Ali, M., Soleymani-bonoti, F. and Zakavi, S. *Chinese Chem. Lett.* **1–6** (2015).

45. Wu, S., Huang, X., Wu, Y., Jin, Y. and Li, G. *Int. J. Electrochem. Sci.* **10,** 8255–8262 (2015).

46. Casassas, E., Quimica, F. De. and Barcelona, D. *J. Electroanal. Chem.* **213,** 235–244 (1986).

47. Foti, C., Lando, G. and Millero, F, J. *Environ. Chem.* **8,** 320–331 (2011).

48. Kragten, J., Decnop-Weever, L. G. and Gründler, P. *Talanta* **40,** 485–490 (1993).

49. Graner, F. and Sillén, L. G. *Acta Chem. Scand.* **1,** (1947).

50. Graner, F., Olin, A. and Sillén, L. *Acta Chem. Scand.* **10,** (1956).

51. Olin, Å. *Acta Chem. Scand.* **11,** 1445–1456 (1957).

52. Sugunama, H., Shimizu, I. and Hataye, I. H. *Chem. Soc.* **60,** 877–883 (1987).

53. Swinehart, D. F. and Garret, A. B. *J. Amer. Chem. Soc.* **73,** (1961).

54. Banks, G. E. and Compton, R. G. *Understanding Voltammetry*, (World Scientific Publishing Co, 2007).

55. Kissinger, P. T. and Heineman, W. R. *Laboratory Techniques in Analytical Chemistry*, (Marcel Dekker, 1984).

56. Metrohm. NOVA Autolab Tutorial. Version 1.10, 20–28 (2013).

57. Barek, J., Fogg, A. G., Muck, A. and Zima, *J. Crit. Rev. Anal. Chem.* **8347,** (2016).

58. Cukrowski, I. and Loader, S. A. *Electroanalysis* **10,** 877–85 (1998).

59. Królicka, A. and Bobrowski, A. *Electrochem. Commun.* **6,** 99–104 (2004).

60. Wang, J., Lu, J., Hocevar, S. B., Farias, P. A. M. and Ogorevc, B. *Anal. Chem.* **72,** 3218–3222

(2000).

61. Economou, A and Fielden, P. R. *Analyst* **128,** 205–212 (2003).

62. Yi, W. J., Li, Y., Ran, G., Luo, H. Q. and Li, N. *Sens. Actuators B Chem.* **166-167,** 544–548 (2012).

63. Economou, A. *Electroanalysis* **24,** 334–340 (2005).

64. Lin, G. G. and Scott, J. G. *Pestic Biochem. Physiol.* **100,** 130–134 (2012).

65. Pan, H., Liu, L., Guo, Z., Dai, L., Zhang, F., Zhu, D., Czerw, R. and Caroll, D.L. *Nano Lett.* **3,** 29–32 (2003).

66. Merkoci, A., Vasjari, M., Fabregas, E. and Alegret, S. *Mikrochim. Acta* **135,** 29–33 (2000).

67. Mo, S., Na, J., Mo, H. and Chen, L. *Anal. Lett.* **25,** 899–909 (1992).

68. Brainina, K. *Anal. Chim. Acta* **305,** 146–153 (1995).

69. Maleki, N., Absalan, G., Safavi, A. and Farjami, E. *Anal. Chim. Acta* **581,** 37–41 (2007).

70. Wu, H. P. *Anal. Chem.* **6,** 3151–3157 (1994).

71. Gollas, J., Galus, Z. and Osteryoung, *J. Anal. Chem.* **59,** (1987).

72. Monterroso, S. C. C., Carapuça, H. M., Simão, J. E. J. and Duarte, A. C. *Anal. Chim. Acta* **503,** 203–212 (2004).

73. Wang, J. and Greene, B. *Anal. Chim. Acta* **144,** (1982).

74. Diederich, H.J., Meyer, S. and Scholz, F. *J. Anal. Chem.* **349,** 670–675 (1994).

75. Wang, J. and Freiha, B.A. *Anal. Chim. Acta* **148,** 79–85 (1983).

76. Brainina, K. and Neyman, E. *Electroanalytical Stripping Methods*. (John Wiley, 1993).

77. Nahar, N. *J. Chem. Sci.* **3,** 5–9 (2013).

78. Wang, J. *Electroanalysis* **17,** 1341–1346 (2005).

79. Guzsvány, V., Papp, Z., Zbiljic, J., Vajdle, O. and Rodic, M. *Molecules* **16,** 4451–4466 (2011).

80. Rehacek, V., Hotovy, I., Vojs, M. and Mika, *Microsyst. Technol.* **14,** 491–498 (2008).

81. Yang, D., Wang, L., Chen, Z., Megharaj, M. and Naidu, R. *Electroanalysis* **25,** 2637–2644

(2013).

82. Hutton, E. A., Ogovevc, B., Hočevar, S.B., Weldon, F., Smyth, M.R. and Wang, *J. Electrochem. Commun.* **3,** 707–711 (2001).

83. Zhang, R. and Olin, H. *Materials* **7,** 3834–3854 (2014).

84. Korolczuk, M., Ochab, M. and Rutyna, I. *Talanta* **144,** 517–521 (2015).

85. Antonova, S. and Zakharova, E. *Electrochem. Commun.* **70,** 33–38 (2016).

Chapter 2 – Experimental

2.1 General Experimental Setup

Figure 2.1 shows the typical voltammetric cell that was used for all voltammetric measurements. The VA stand (Metrohm 663) houses the electrochemical jacketed glass cell which was connected to a circulatory water bath (PolyScience) to maintain a constant temperature of 25.0 °C ± 0.1 °C. It also housed the three electrode system consisting of the working electrode (WE), the reference electrode (RE) and the counter electrode (CE). Two types of WEs were used, namely the mercury drop electrode (MDE) (Metrohm, 6.1246.020) and the mercury film on a 6 mm diameter glassy carbon electrode (GCE) (Metrohm, 6.1204.800). The glassy carbon electrode is connected to a rotator (Metrohm, 6.1204.220) which is rotated using a motor on the VA stand. The RE (Metrohm, 6.0728.010) used was the Ag/AgCl (3 M KCl) that was inserted in a 0.5 M or 0.1 M KNO_3 salt bridge solution housed in an electrolyte vessel with a porous ceramic frit (Metrohm, 6.1245.020). Note that all potentials are quoted in this work is with respect to the 3 M KCl Ag/AgCl reference electrode. A platinum electrode (Metrohm, 6.0343.000) was used as the counter electrode.

A thermocouple (Metrohm 6.1110.100) was used to monitor the temperature in the cell and a glass electrode (6.0234.100 combined with Ag/AgCl (3 M KCl) RE)) was also used to monitor the pH of the cell solution. A 20 mL Dosino unit (Metrohm, 800) with titrant outlet was used in automated titration experiments. All purging was done using 99.999 % nitrogen to eliminate oxygen contamination. This was done at varying duration times but generally a 25 mL solution was purged for 30 minutes and 10 mL solution for 15 minutes. The background was stirred during purging and deposition with either the rotating disk electrode or the magnetic stirrer. The general background solution used was HNO_3 at different pHs depending on the experiment. Millipak Ultrapure water (18.2 MΩ.cm) was used to make up all solutions.

Figure 2.2 below displays the instrumental setup which was used for all voltammetric measurements conducted in this study. The Metrohm instrument consisted of a 663 VA stand connected to the cell and a PGSTAT 302N Autolab potentiostat which is the central component to which all other components were connected. For automated experiments, the components used were the 801 magnetic stirrer, the 800 Dosino (both the stirrer and Dosino were connected via the IME663 interface) and the pH meter (module

pX1000) which is built into the potentiostat. The 20 ml Dosimat and 780 pH meter were used for manual experiments. The computer controlled all components (except those controlled manually) through NOVA (version 1.10) installed on the desktop PC and all experiments, measurements, data capturing and some analysis was done using it. The development of the software procedures will be discussed later in this chapter.

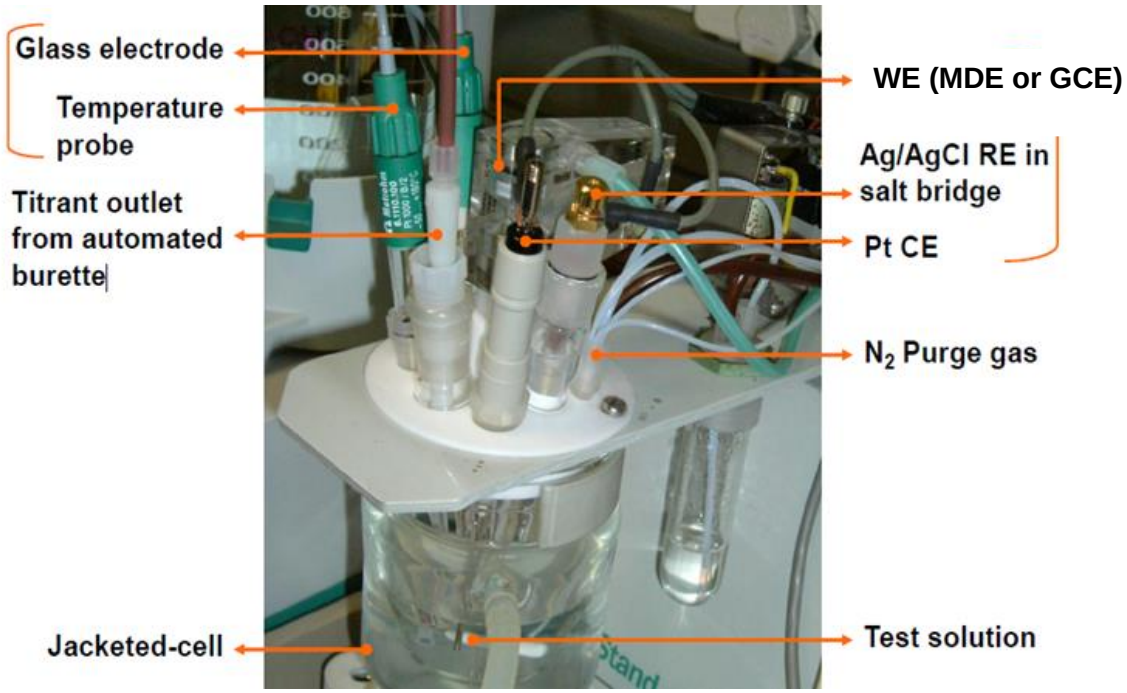


Figure 2.1: General experimental cell setup for all voltammetric experiments.



Figure 2.2: Metrohm Autolab Instrumental setup used for all voltammetric measurements.

Due to nature of mercury being toxic, safety precautions were taken when handling the mercury salts. The correct personal protective equipment (gloves, labcoats and safety glasses) were worn at all times for all experiments involving mercury salts. In the study of bismuth, the electrode used was a mercury drop which is even more toxic. During use we ensured that the drop is always submerged under water to avoid exposure into the atmosphere. Maintenance and filling of the electrode with liquid mercury was always done in the fume hood. Safety precautions were also taken when working with other toxic heavy metal salts such as Tl^{+}, Cd^{2+} and Pb^{2+}.All the heavy metal waste was discarded in a designated waste bottles.

2.2 Experimental for Bi^{3+} Study

2.2.1 The Use of Tl^{+} in Voltammetry

A diffusion junction potential forms at the junction of the sample solution and the salt bridge, i.e. where two different solutions are in contact, and this is due to the unequal mobility of the ions across the ceramic frit.[1] Consider our experiment where the background solution contained 0.5 M HNO_3 and the salt bridge solution contained 0.5 M KNO_3, the diffusion rate of NO_3^- on both sides can be regarded as equal, but H^+ has a higher mobility than K^+ and therefore moves faster across the junction. At the ceramic frit, the side with the salt bridge solution will be more positive than that with background solution and therefore a potential difference is established. The diffusion junction potential is significant when the sample solution is below pH 2, where the hydrogen ions are in high concentration since the mobility of the H^+ is higher than any other cation (such as K^+ in the salt bridge). This potential difference is incorporated in the overall potential difference between the WE and the RE. Therefore the potential measured is $E_{meas} = E(M) + E_j$, where E(M) and E_j are the potentials due to the reduction or oxidation of the metal ion species and the junction potential, respectively. In complex formation studies, a change in the pH of the sample solution could the result in a change E(M) and E_j. It is therefore imperative to accurately determine the magnitude of E_j to be able to correct for it and determine E(M) accurately.

The Henderson equation can be used to theoretically determine the diffusion junction potential, but it has limitations because the assumptions that were made in deriving the equation do not always apply in some experiments. In all our Bi^{3+} studies we experimentally determined the junction potential by using a "witness" ion. This is a method developed by Billing *et al.*[2] where they used Tl^+ to monitor the diffusion junction potential. Changes in the reduction potential of Tl^+ were ascribed to be due to the diffusion junction because Tl^+ does not readily form complexes, especially at low pH.

In previous work, complex formation has been studied via differential pulse polarography or direct current polarography. No sign of interference or interactions between Bi^{3+} and Tl^+ were observed when using polarography. In this study, DPASV which is a newer approach to study complex formation was used. This technique is different from the previously used technique because preconcentration of the metal is done. Preconcentration of the two metals (Bi and Tl) in the mercury drop electrode may form an alloy that could result in interferences in the stripping step. An example of these type of interferences have been reported in the use of films electrodes when lead was studied on a bismuth film and interactions where observed that resulted in distorted peaks for lead stripping.[3] So, the first experiment that we conducted was to determine whether the preconcentration of Tl^+ (which is used a "witness" ion to determine the diffusion

junction potential) had any effect on the electrochemistry of Bi^{3+}. The experiment was conducted in two forms and then compared. In the one experiment, Bi was preconcentrated alone and in another experiment both Bi^{3+} and Tl^{+} where preconcentrated simultaneously. The experiments were conducted in a 25.00 mL of 0.5 M HNO_3 solution with Tl^{+} and Bi^{3+} at 1×10^{-5} M and 4×10^{-5} M respectively and the solution was purged for 1800 s. DPASV was run at deposition potential (E_{dep}) -0.2 V or -0.75 V (vs. Ag/AgCl) and deposition time (t_{dep}) ranging from 5 -120 s. The two E_{dep}'s were chosen because of the positions of the Bi^{3+} and Tl^{+} peaks on the voltammogram (see Figure 2.3). Thus E_{dep} = -0.2 V deposits Bi^{3+} only and E_{dep} = -0.75 V deposits both Bi^{3+} and Tl^{+}. Other measurement parameters were: initial potential = -0.2 or -0.75 V, end potential = 0.15 V, step potential =0.005 V, modulation amplitude (E_{mod}) = 0.025 V, modulation time (t_{mod}) = 50 ms and interval time = 1.0 s. The parameters E_{dep} and t_{dep} were optimised in this experiment and the detailed results will be discussed in Chapter 3, section 3.1.

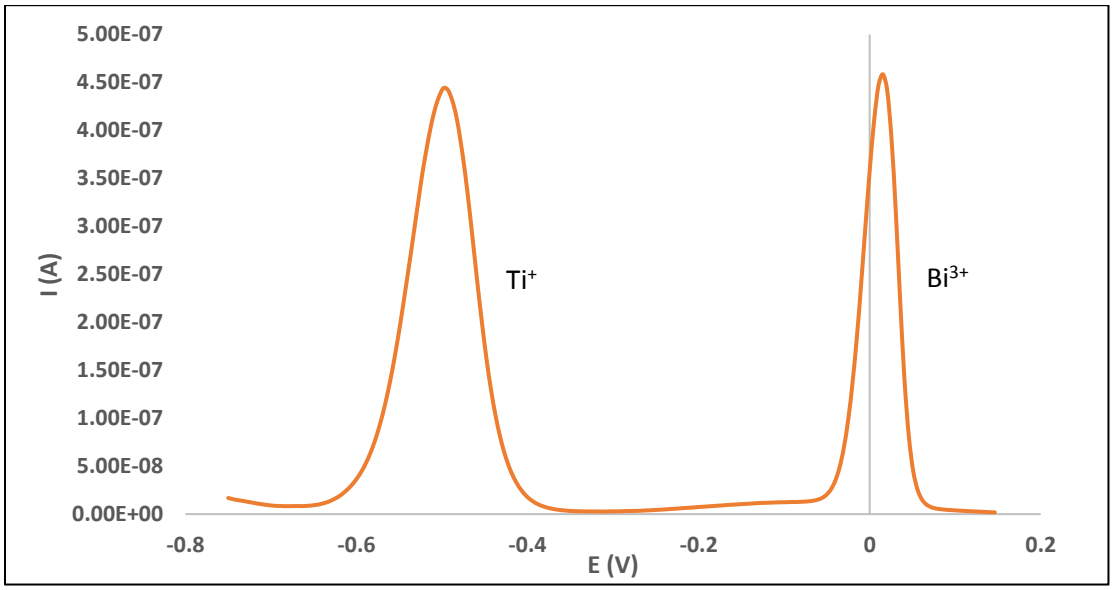


Figure 2.3: Positions of Tl^{+} and Bi^{3+} peaks on a DPASV voltammogram.

2.2.2 DPASV Reversibility and Detection Limit Studies

Before the Bi^{3+} hydrolysis study could be done, we did a detailed study on the reversibility of Bi^{3+} and Tl^{+} using DPASV. This was critical because the model that is used to calculate the formation constants is based on the assumption that the potential measured is reversible. The reversibility study entailed optimising all the parameters such as modulation amplitude, modulation time and interval time. The NOVA software manual[4] indicated that these parameters could affect the shape of the voltammetric peaks and therefore the reversibility. The default parameters (mentioned in the section 2.2.1) were used initially but peaks were found to give fairly broad and asymmetric after significant amount of analysis. Table 2.1 gives the general experimental parameters and conditions that were used for optimisation and reversibility studied. We used the already optimised E_{dep} and t_{dep} to optimise modulation time, modulation amplitude and interval time. Only one parameter was changed at a time. The Bi^{3+} and Tl^{+} results were analysed individually and compared. Following this, the study of the detection limit was done by simply studying Bi^{3+} at 1×10^{-6} M, 1×10^{-7} M an d 1×10^{-8} M (with the Tl^{+} concentration four times more that of Bi^{3+} in all three experiments and different deposition times were used). A pH titration of free Bi^{3+} was also performed where Bi^{3+} was studied at 1×10^{-6} M (and Tl^{+} at 4×10^{-6} M) to see if precipitation was prevented or to what extent it was postponed. The software procedure used for this titration will be explained section 2.4.3.1.

Table 2.1: General experimental conditions and parameters used in the study of Bi^{3+} reversibility and hydrolysis.

	Bi^{3+}	**Bi^{3+} + Tl^{+}**
Concentration	10^{-8} M – 10^{-5} M	10^{-5} M Bi^{3+} 4×10^{-5} M Tl^{+}
E_{dep} (vs. Ag/AgCl)	-0.15 – -0.3 V	-0.7 – -0.8 V
pH	1 – 7	
t_{dep}	5 – 120 s	
E_{mod}	0.025 – 0.05 V	
t_{mod}	40 – 100 ms	
Interval time	1 – 2 s	

2.3 Experimental for the use of Mercury Film Electrodes

Before the MFEs were plated, it was important to ensure that the GC substrate was clean and even. The GCE was polished thoroughly with 0.1 µm aluminium oxide using deionised water as lubricant on a smooth polishing cloth. It was then rinsed with deionised water, sonicated for 2 minutes, rinsed again with water and ethanol and then air dried.

The ex situ plating solution used consisted of 1×10^{-3} M $Hg(NO_3)_2$ and 0.01 M KNO_3 as used by Castro *et al*.[5] A 10 mL aliquot of plating solution was purged for 15 minutes while rotating the disk electrode to stir the solution. Rotating was also done during the deposition of the film on to the electrode. The film plated electrode was then transferred to the analysis solution. The speed of the rotating disk electrode was the first parameter to be optimised, followed by the deposition potential and the deposition time for film formation.

For in situ analysis, no preplating was done, mercury was added directly in the analysis solution. An extensive reproducibility study of the film (at different pH) was done for both in situ and ex situ analysis followed by ligand titration using the experimental parameters and conditions in the Table 2.2. This table illustrates the general conditions and range of parameters that were used in different experiments. The specific conditions are discussed for each experiment in the results and discussions in Chapter 4.

Ligand titrations were used to study the complex formation of Cd^{2+} or Pb^{2+} with ligands, such as picolinic acid and glycine, both in situ and ex situ titrations were done. The ligand titration was done by keeping the pH of the solution constant while changing the ligand-to-metal concentration ratio and this was repeated at different pH values. The ligand solutions were prepared at a high concentration (about 1 M) and adjusted to the pH value that was to be used for the titration (using a KOH solution). The 780 pH meter was used to measure the pH. The glass electrode was first calibrated with buffer solutions at pH 4, 7 and 9 which were kept in a 25 °C water bath. The general parameters, pH values, Hg^{2+} concentration and ligand-to-metal concentration ratios used are in Table 2.2. A procedure for ligand titration was then set up on NOVA (to be discussed later). The titration was carried out by first plating a mercury film (in ex situ the film is preplated in a separate plating solution) and then measuring the background (HNO_3) current. The metal ion was then added to the background solution and pH adjusted to the desired pH that would be used for the titration. A free metal ion DPASV was then measured so that the peak potential and peak current could be established before complex formation takes place. The prepared ligand solution was then added in small volumes to achieve an increasing ligand-to-metal concentration ratio. After each

addition of the ligand, the solution was purged and stirred and at each step of the titration, a DPASV was measured. The titration went on until the last and highest concentration ratio.

Table 2.2: General experimental conditions and parameters used in the experiments involving mercury film electrodes.

	10^{-4} M Cd^{2+}	**10^{-4} M Pb^{2+}**
Picolinic acid	[L]:[M] = 100 -1500	
Glycine		[L]:[M] = 47 - 14375
pH	1-7	1-9
Hg^{2+}	10^{-3} – 10^{-2} M	10^{-3} M
E_{dep} (vs. Ag/AgCl)	-0.75 – -1 V	-0.65 – -1 V
t_{dep}	60 – 600 s	30 – 300 s
E_{mod}	0.025 V	
t_{mod}	0.05 s	
E_{con}	0.6 V	
t_{con}	60 s	
Interval time	1 s	

2.4 NOVA Software Development

NOVA is the latest software designed for Metrohm Autolab electrochemistry instruments. This software gives the user full control of procedures and data analysis. Unlike the previously used GPES software which was useful for once-off measurements only, NOVA has a list of commands that can be used to design and fully automate the experiment according to the user's needs. Added advantages is that it has a faster USB data transfer and can connect to about 16 Autolab instruments unlike GPES which can connect to only 8 instruments. This section will discuss how procedures were designed and automated using this software.

2.4.1 Getting started and connecting external devices

To get started on NOVA first switch on the potentiostat and the IME663 interface, then switch on the computer and open NOVA to ensure the software connects to the hardware. If a newer version of NOVA has just been installed, the procedures saved on the older version would have to be transferred to the newer version. This can be done by opening the new version, clicking *tools*, select *database manager*, then click on *my procedures* and select the version whose procedure you want, as shown in Figure 2.4. All the procedures that were in the old version will be available in the new version.

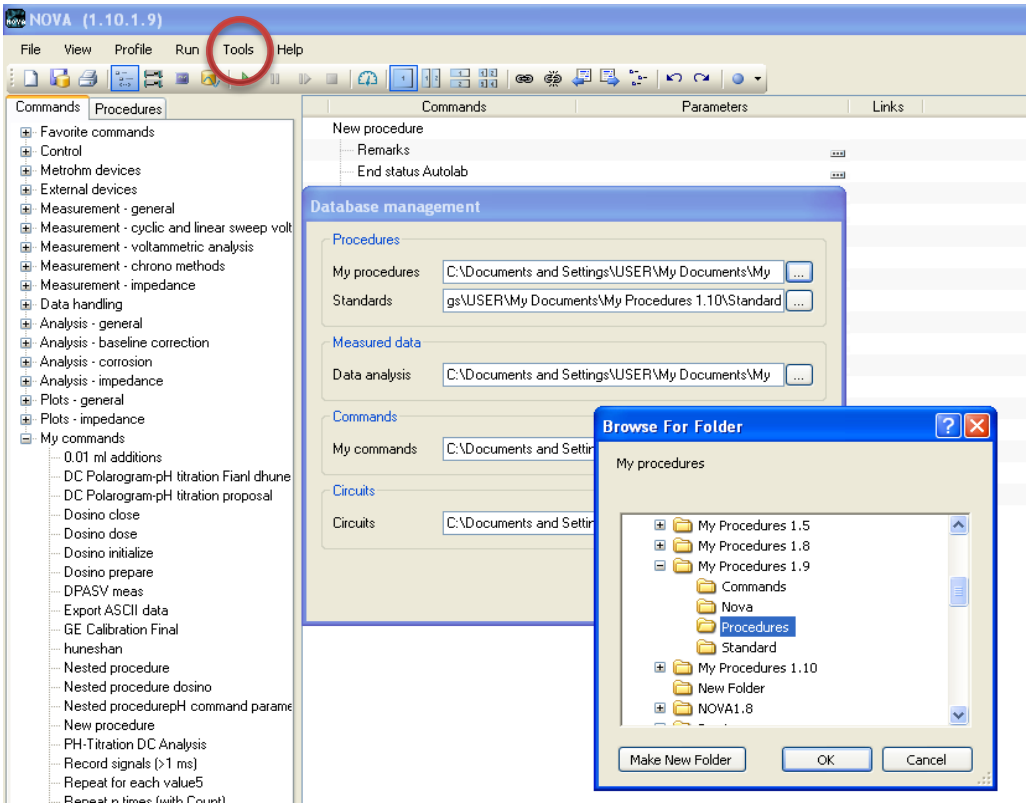


Figure 2.4: Transferring procedures from an old NOVA version to a new version.

Before programming new procedures, one has to ensure that all the hardware is connected and visible on the software. For example the magnetic stirrer and the Dosino have to be recognised by the software. There are two types of stirrers, the magnetic stirrer and the rotating disk electrode (RDE). The RDE can be replaced by Teflon shaft which acts as a stirrer (shown in Figure 2.5). To set the magnetic stirrer on, the correct serial number of the magnetic stirrer has to be inserted for the software to recognise the stirrer. Under *commands*, *stirrer initialize* can be selected by dragging it to the procedure window (all other commands are also activated this way), then click on *settings*. The window in Figure 2.6 shows where the serial number should be written. To set the stirrer on we used these three commands (*stirrer initialize*, *stirrer speed* and *close*) with stirrer speed ≠ 0 if stirring. To stop stirring, set speed = 0. Once an external device is initialised, it must be closed at the end of the procedure or else the procedure would not run. The RDE can be controlled manually or remotely via the IME663 interface stirrer button which can be set on remote or not. The speed can only be set on the VA 663 stand.



Figure 2.5: Pictures of the Teflon shaft and the RDE which can be used as stirrers.

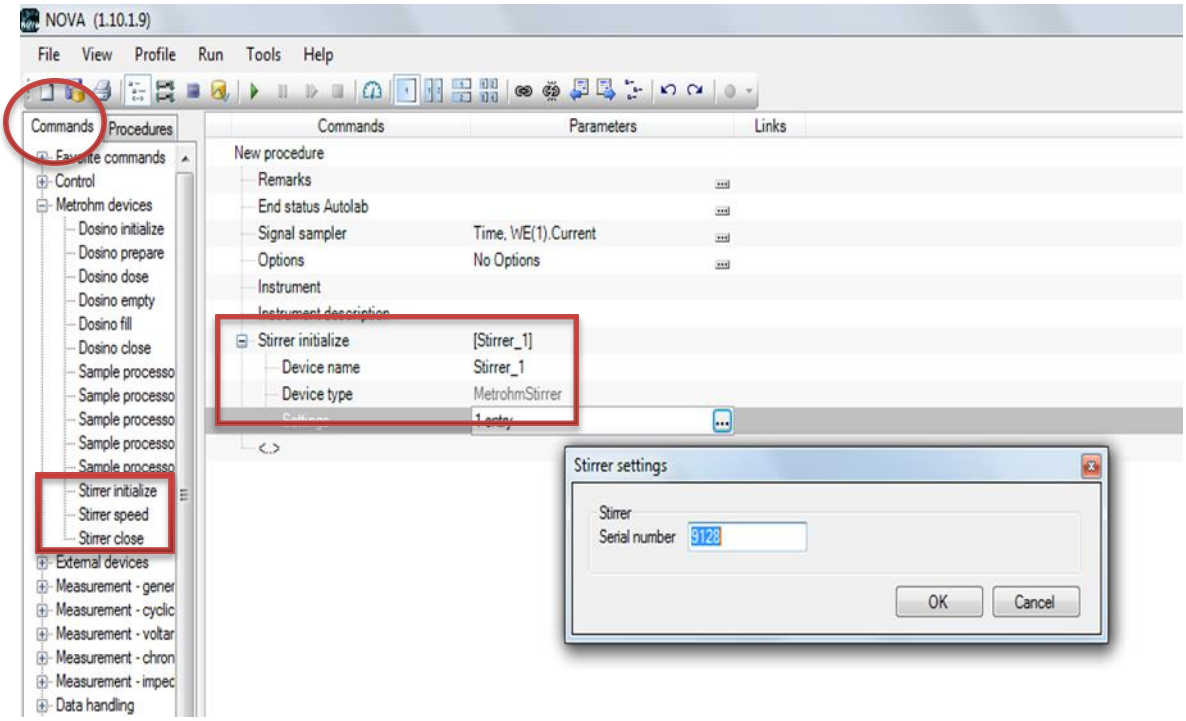


Figure 2.6: Inserting serial number of the magnetic stirrer.

The Dosino can be controlled in a similar manner by using the commands *Dosino initialize*, *Dosino dose* and *Dosino close*. The commands *Dosino prepare*, *Dosino fill* and *Dosino empty* are used for getting the Dosino ready for use, filling it up and emptying it, respectively. The volume to be dosed can be specified on the *Dosino dose* command and the serial number of the Dosino has to again be changed (under the *Dosino initialize* command) to match the one in use as shown in Figure 2.7. The filling rate can be specified

in the same window. Only the built in pX1000 pH meter can be controlled by the software, the 780 pH meter was used manually. The electrodes in the cell are directly connected to the potentiostat.

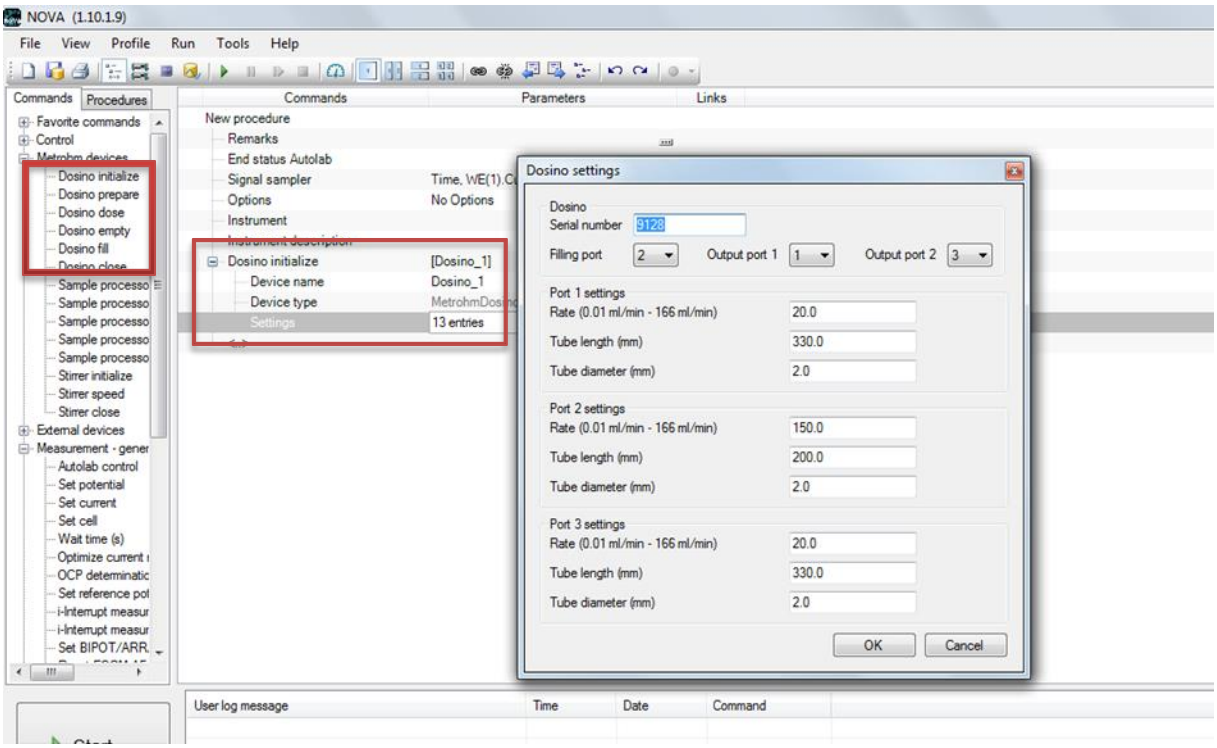


Figure 2.7: Insertion of a serial number and using the Dosino.

For most electrochemical techniques it is important to purge the solutions with N_2. It displaces the air that contains oxygen which dissolves in the solution. N_2 pressure is also used to form the mercury drop by controlling the valves on the VA stand. With DC polarography, a new drop is used for every point on the voltammogram that is recorded. It is therefore imperative that the pressure of N_2 released be high enough to be able to knock off the mercury when needed. The pressure required for the proper functioning of the mercury multimode electrode is about 100 kPa. If the pressure is less than this then the mercury drop will not form properly but, if the pressure is too high, it will damage the membrane in this electrode.

2.4.2 Setting New Procedures

NOVA has a list of preprogramed electrochemical techniques that are commonly used. Users can use these as the starting point and modify the procedure to suit their experimental requirements. By clicking on the *procedure* tab one can view the list of these (left side of Figure 2.8) and open any one by dragging to the right. When setting up a new procedure, the following will appear on the screen: *Remarks*, *End status Autolab*, *signal sampler* and *options* as shown on the right side of Figure 2.8. Under *remarks* you can add information that you would want to remember about the procedure. *End status Autolab* is where you set the state that the instrument must be left in at the very end of the procedure. For example, you can set it to switch the cell off (highly recommended) and switch the purge and stirrer on or off. You can also set the number of drops you want created at the end if using a mercury drop electrode. It is important to leave a drop hanging at the end of the capillary to prevent oxidation of mercury from blocking the capillary (this must be submerged in water for storage such that the mercury does not volatilise). The *signal sampler* is for choosing the type of measurement that is to be done such as current, voltage, pH etc. *Options* is used to set the maximum and minimum current range and integration of signals. There are default settings for each of these that the user can use, but more specific requirements are often needed.

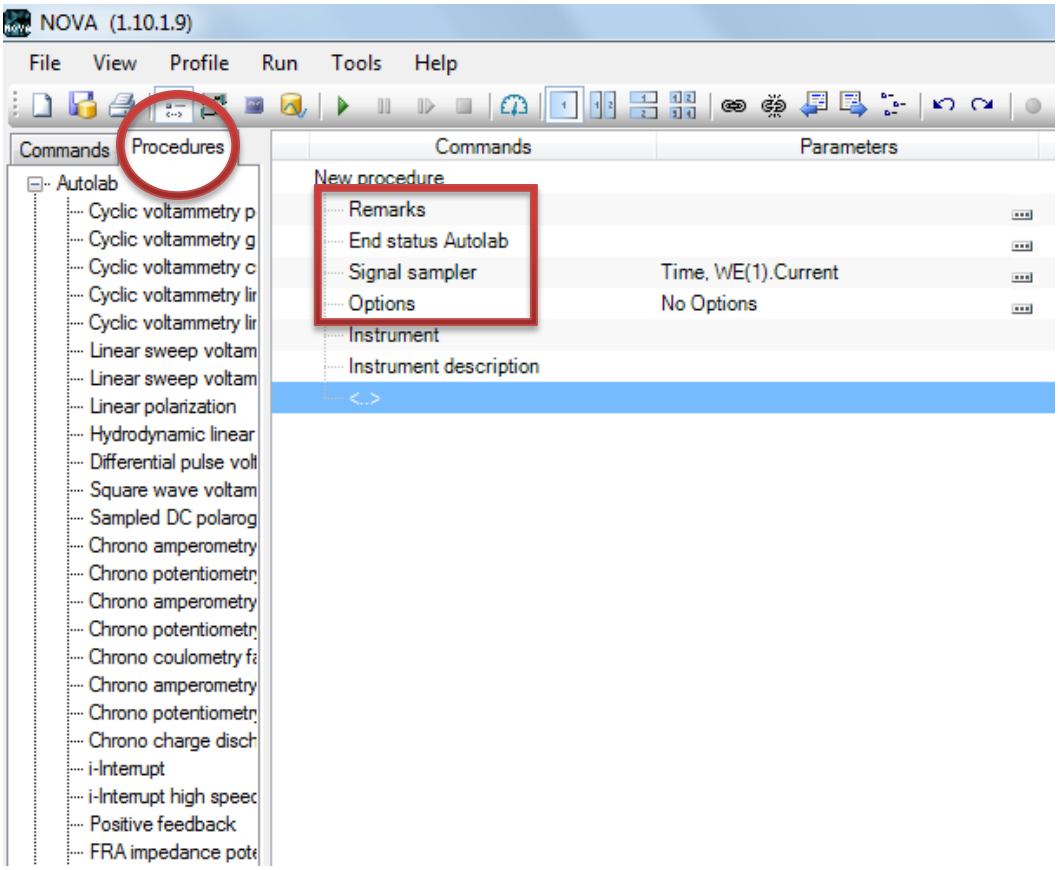
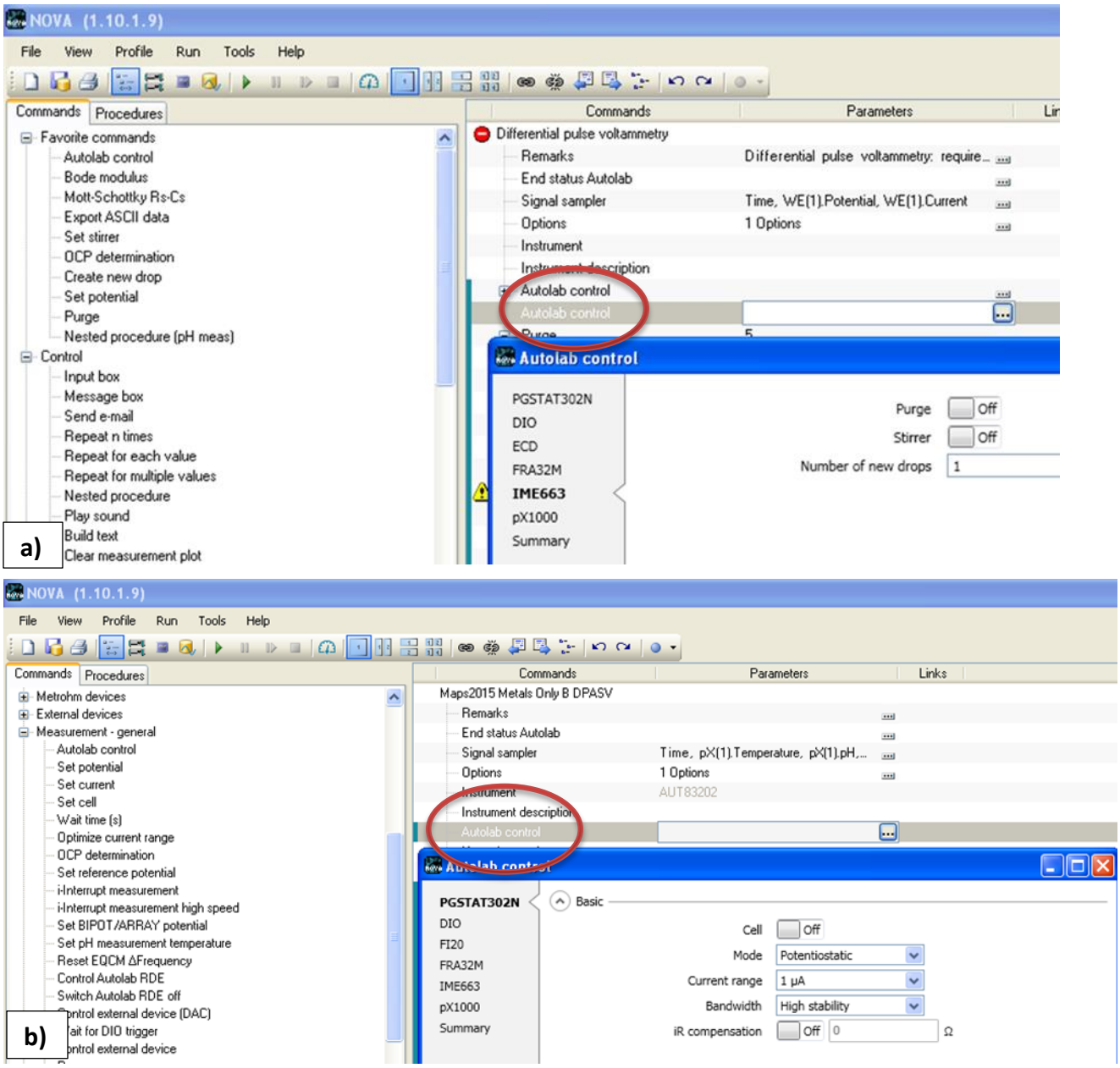


Figure 2.8: Preprogramed electrochemical methods and initial preprogramed commands.

At the beginning of every procedure there should be an *Autolab control* command, under this there are various settings. With the PGSTAT 302N (Figure 2.9a), the cell should be switched on and *mode* (either potentiostatic or galvanostatic) selected. In this work we have only used the potentiostat mode (where the voltage is applied and current measured). The *current range* is set according to the need of the experiment, e.g. if we start with low concentration solutions the range is low, however, if it is increased *current range* would be increased. The *bandwidth* was usually set to *high stability* because this minimises the noise in the voltammogram. This is displayed as “hstab” on display screen of the potentiostat itself. The iR compensation option was never used in our measurements as the ionic strength of all solutions was high. The IME663 interface can be switched on or off depending on the need of the experiment at the beginning (Figure 2.9b). The pX1 refers to the pH module installed in the potentiostat. The mode should be set to *single input* for the combination glass electrode and for the cell setup the electrodes

should be in the same cell (Figure 2.9c). The *summary* option just gives a summary of the *Autolab control* setup.



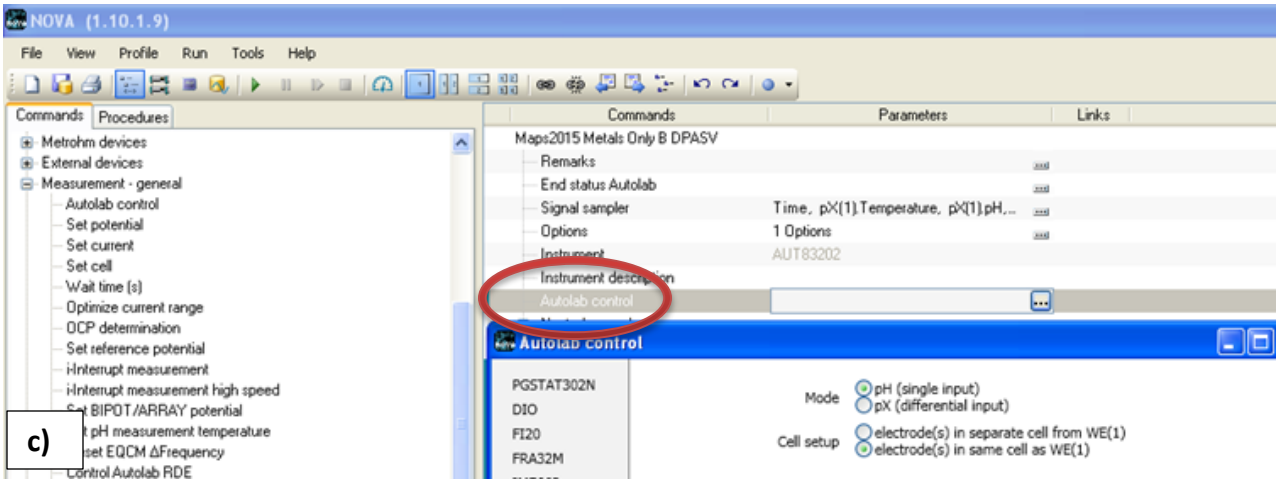


Figure 2.9: Autolab control command showing the setup for a) PGSTAT302N b) IME663 and c) pX1000 port.

At the end of the measurement, the data gets saved automatically in the database and can be analysed in the analysis window. The database saves the data according to its procedure name, time, date and also remarks. Data can also be directly exported and saved in the user's desired folder (e.g. My Documents on the PC) by using the *Export ASCII data* command. This can be found on the commands tab and dragged to the end of the procedure. For example in Figure 2.10, a DPASV measurement is done and the *Export ASCII data* command is inserted directly below the measurement parameters. The *file mode* is an option that enables the user to choose how each file should be saved. The *overwrite* option means that each measurement saved overwrites the previous measurement. There is also an option of *make unique* where every measurement gets saved with the base-file name followed by an increment number. The last option is *append* whereby all measured data are saved as one file.

The variables to be saved have to be linked to the parameters in the procedure. E.g. in Figure 2.10 the applied potential and the differential current under the DPASV procedure were linked to *Export ASCII data*. The linked variables can be seen by the presence of the square brackets on the right hand side of the page.

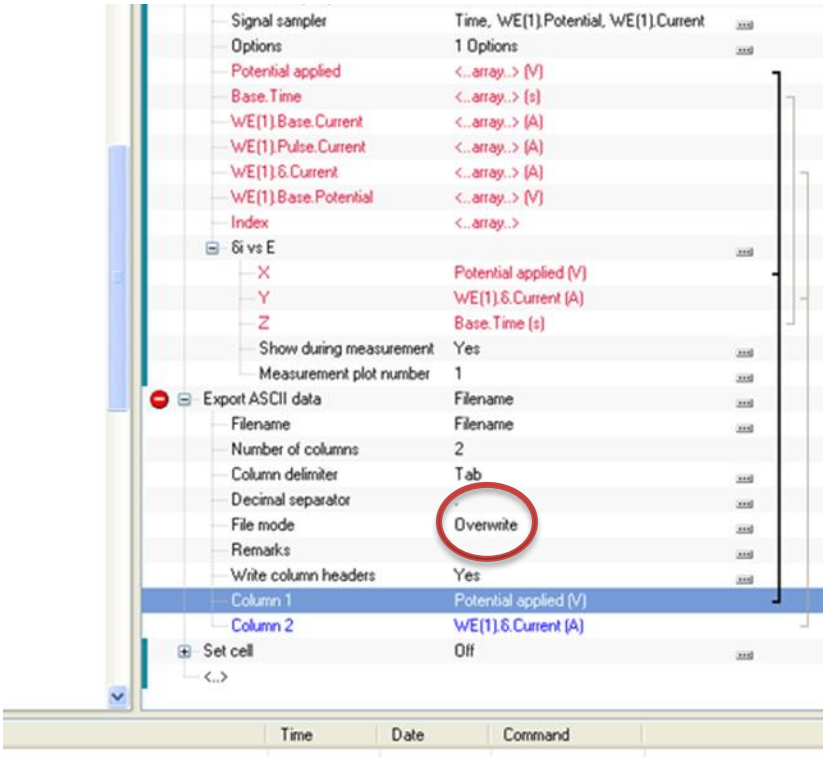


Figure 2.10: Window showing *Export ASCII data* command for saving data and linking measured data to saved data.

Amended procedures can be saved according to a given name and then be recalled at a later stage. Validation of procedures will first be done by the software to ensure that there are no errors in the procedure. To view the measurement while the procedure is running, simply go to the *measurement view* tab. A current vs potential plot is displayed by default in the measurement view. The end of a measurement is indicated by the *stop* button turning to *start*, indicating that a new measurement can be initiated.

The *analysis view* has a toolbar at the top right corner where the data stored can be viewed in different ways, i.e. as a data grid or 2D or 3D plots. To view the data simply click on the experiment and it will load onto the database screen. For peak search and analyses one can right click on the data and choose the type of analyses that is to be performed on the data as shown on Figure 2.11. The *Data grid* is a feature under analysis toolbar that tabulates all the values of each signal that was recorded in measurement. It also enables us to export all that data in a particular format to read in to other programmes such as Origin or Excel. From the *analysis view* command information such as the peak potential, peak current, peak width and peak area can be obtained.

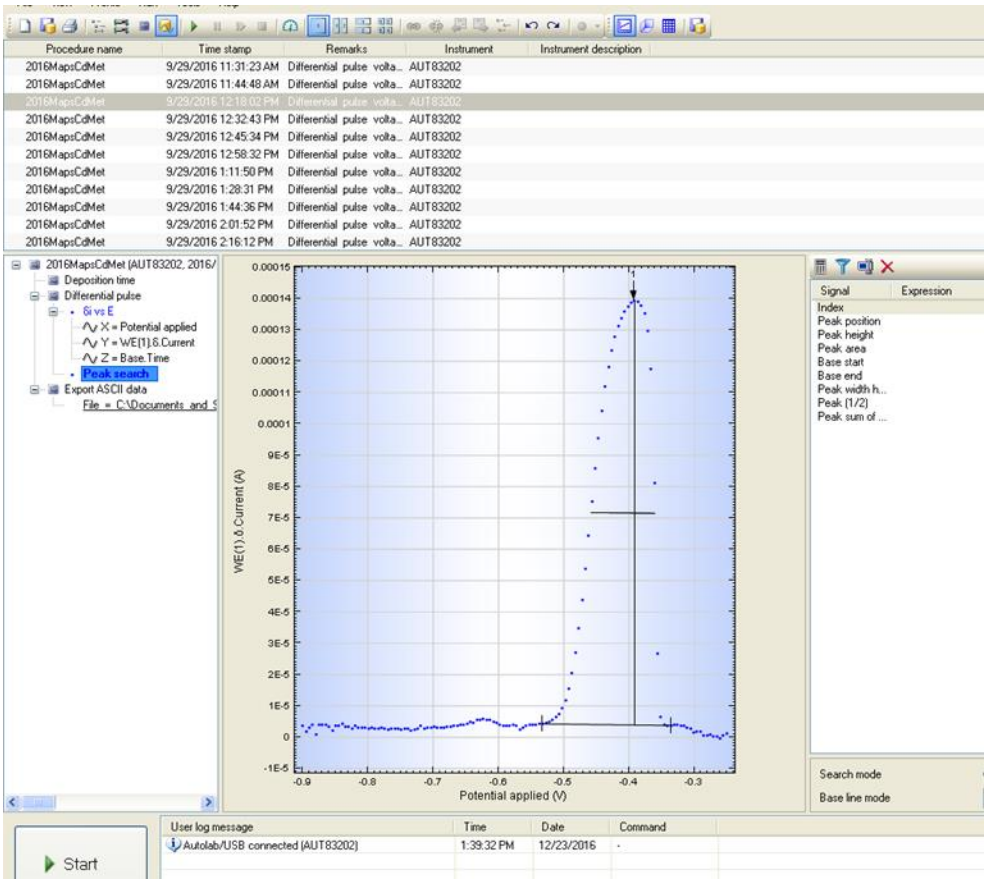


Figure 2.11: The display of the *analysis view* window and peak analysis.

2.5 NOVA Developed Procedures

2.5.1 Automated Glass Electrode (GE) Calibration Procedure

This GE calibration procedure was used mainly for the Bi^{3+} studies. It involves an acid-base titration and is more accurate than using buffers. In later work buffers were used as this lengthy calibration procedure was too tedious when using data where other issues had to be sorted out. The calibration was done by starting with 25 mL of standardised 0.1 M HNO_3 (pH 1) and to this 0.5 mL increments of standardised 0.1 M KOH was added (using the Dosino) to a final volume of 45 mL and the potential difference of the GE was recorded at each step. A calibration curve is the plot of the calculated pH against the potential difference.

The GE calibration was done at 25.0 ± 0.1 °C using a jacketed cell connected to the water bath. The calibration procedure was set up as a three part experiment on NOVA. Part A of the calibration is shown in Figure 2.12a). The *signal sampler* option in the procedure shows that the measured variables were time, temperature, pH and voltage of GE. The pH determined was found using an ideal calibration curve and is merely an estimate, it was not used to plot our actual calibration curve. The pH used for our calibration curve was calculated using exact concentrations and volumes of the reagents at each step in the titration.

The first command in Figure 2.12a) is *Dosino initialise* which registers the connection of the Dosino to the instrument and software. The magnetic stirrer was set on during initial purging (with N_2) for 30 minutes. The calibration then commenced by adding first 0 mL then 0.5 mL increments of KOH. The solution was purged and stirred during addition of the increments and also during measurements to eliminate any oxygen or CO_2 from the added KOH. For every 0.5 mL added (as shown under *repeat for each value*), there was a wait time of 30 s before measurements were taken and these were read 30 times (1 every 2 s for 60 s). This addition of 0.5 m increments carried on until a total of 24 mL of KOH was added.

Part B and C of the calibration were done in a similar manner as in part A. Part B is in the end point region so only four measurements were taken (see Figure 2.12b)). In this region, for every 0.5 mL added there was a 300 s equilibration period. This is because at this region, small additions result in large changes in the voltage. For every 0.5 mL added, each measurement was again taken 30 times at 2 s intervals for 60 s.

For part C, the equilibration time was set back to 60 s for every 0.5 ml increment added. Each signal was recorded 20 times at 2 s intervals. This was done till a total of 44.5 ml of KOH was added. At the end of the measurement the stirrer and purge were set off and the Dosino closed. All calibration data had been

saved as ASCII files for part A, B and C. The file mode under this command was set to *append* for the data from the successive repeat loops to be saved in one file.

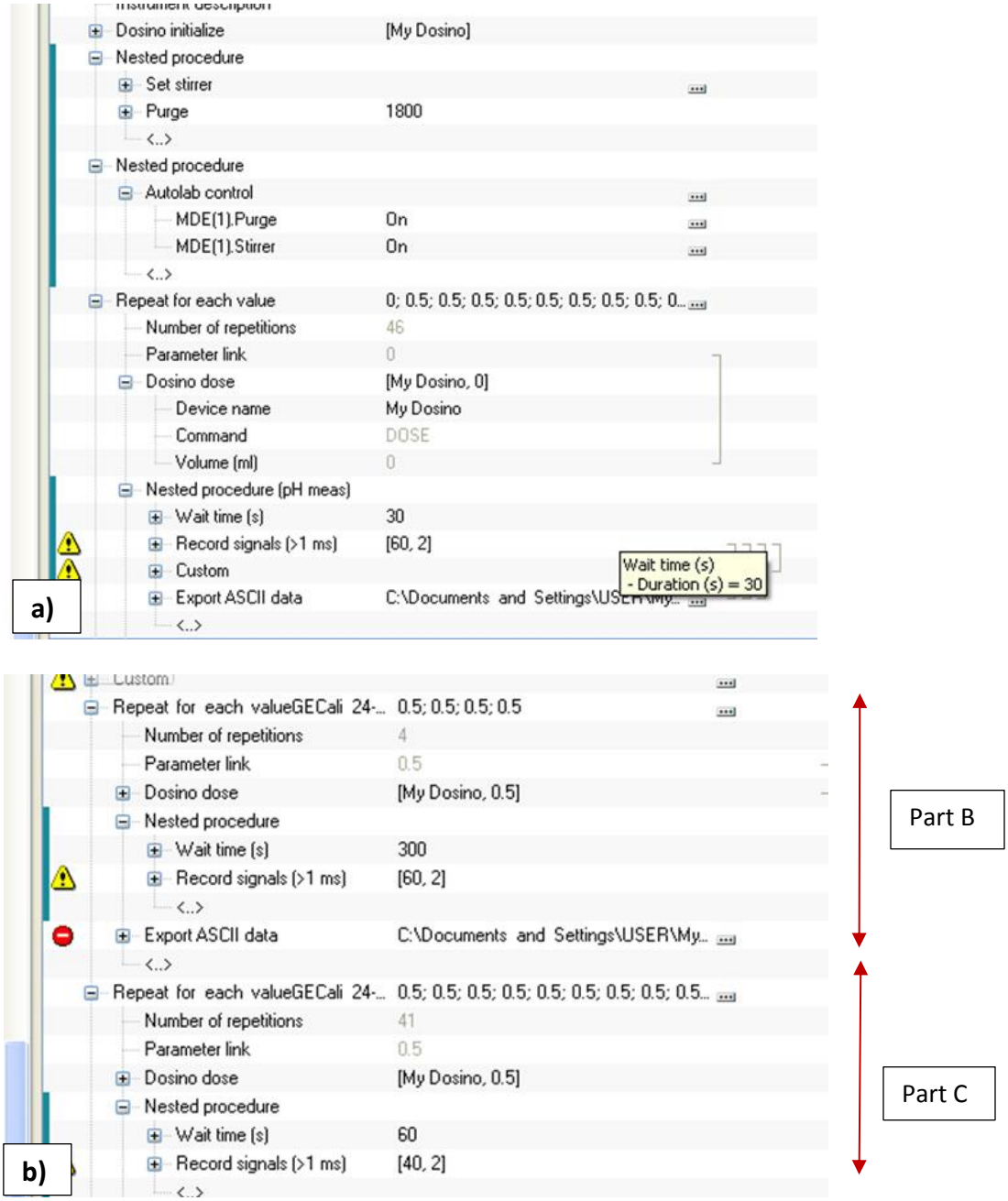


Figure 2.12: Automated calibration procedure showing a) Part A of the calibration and b) Part B and C of the calibration.

2.5.2. Automated pH titration

Acid-base titrations were used in Bi^{3+} hydrolysis studies. Before the automated procedure, an initial background solution of 0.1 M HNO_3 was measured using DPASV to ensure that there was no contamination. The metal ions were then added with the concentrations 10^{-6} M of Bi^{3+} and 4×10^{-4} M of Tl^{+}, DPASV was then run about 3 times. All other specific experimental parameters such as deposition time, deposition potential, modulation amplitude etc. are specified in Chapter 3, and the general experimental parameters are given in Table 2.1. The cell was again kept at 25.0 ± 0.1°C and purging with N_2 was done for 1800 s.

The signals sampled were the temperature, applied potential, differential current (δ current) at the working electrode, potential at the glass electrode and time. The entire titration procedure was too long and the central processing unit runs out of memory before the experiment is completed since all data gets stored in RAM while the procedure is running. It was therefore necessary to divide the experiments into part A and B. This problem has now been fixed in the newest NOVA 2.1 version.

The first command shown in part A (see Figure 2.13a) was a message box where the user can put any message that would be helpful for the setup of the procedure. The message that put here was a reminder to first prepare the Dosino. A time limit was set to 30 s meaning that the message was only displayed on the screen for 30 s after which the procedure would start automatically if no intervention occurred.

Part A of the titration was done by adding 0.2 mL increments of 0.1 M KOH until the pH changed by 0.1 pH units. The *repeat for each value* command is a loop similar to that in the calibration procedure where all actions that are under this command are repeated until the final condition is met. The first target pH value is 1, this implies that when 0.2 mL of KOH was added, the programme checks the pH to ensure that it corresponds to the target pH. If it does not correspond, another 0.2 mL KOH would be added until the pH reads 1. When the target pH value had been reached, an equilibration of 120 s takes place, thereafter the pH (and more importantly the potential of the GE) was measured every 2 s for 180 s. This gave a total of 90 measurements. A DPASV measurement was then performed and data was saved via *Export ASCII data* command. The cycle repeats itself for the next pH value. This was done till pH 2 was reached. At the end of part A, the Dosino and stirrer were closed and purge set off.

Part B commenced by initialising the Dosino and switching on the stirrer and the purge (Figure 2.13b). The titration was conducted by dosing 0.01 mL until the pH changed by 0.1 pH units. The solution was purged for 120 s before measurements were made and the GE potential measured as in part A. The pH range for

the titration in part B was from pH 2-7 and all data including DPASV data were saved in the designated ASCII files.

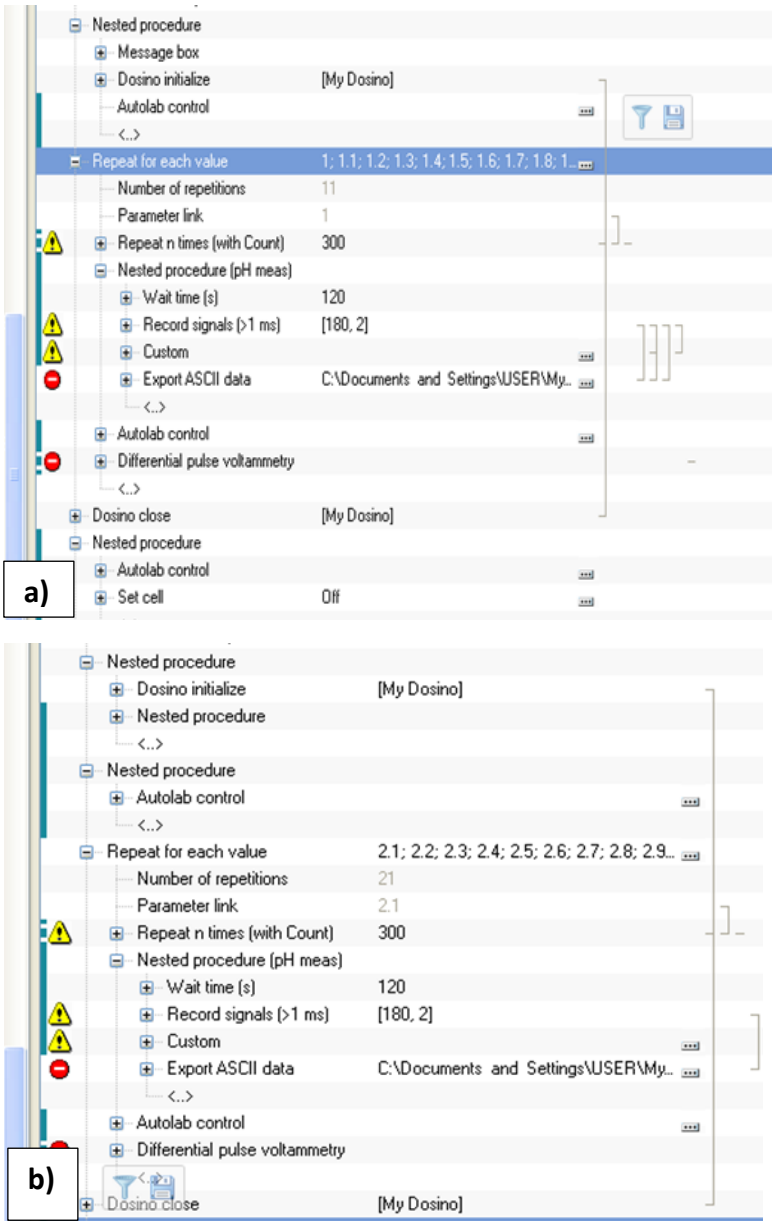


Figure 2.13: The pH titration procedure for Bi^{3+} hydrolysis studies made up of a) Part A and b) Part B.

2.5.3 NOVA Procedures for Film Formation and Analysis

The investigation of the use of the MFE to study complexation was done by both in situ and ex situ plating of the film. The ex situ study was done by first plating Hg^{2+} from a 10 mL solution containing 10^{-3} M $Hg(NO_3)_2$ and 0.01 M KNO_3. Figure 2.14 shows the plating procedure, where the plating solution was first purged with N_2 for 900 s while stirring with the RDE at a speed of 1000 rpm. The conditioning potential and time were set to clean the surface of the glassy carbon electrode before plating was done. The parameters used in Figure 2.14 are those used in this experiment and were obtained in literature.[6] The stirrer is set on during conditioning and deposition of Hg at the electrode. At the end of deposition the stirrer is set off and equilibration of 5 s was set before the cell was switched off. All ex situ film formations followed this procedure with the differences only in the parameters used and these are specified for individual experiments in the Chapter 4 (the general conditions used are given in Table 2.2). After film formation, the plated mercury film was rinsed with deionised water, the excess water was removed and transferred to the analysis solution for DPASV.

In situ film formation and analysis followed the procedure in Figure 2.15 which was similar to that in Figure 2.14 with the only difference being the DPASV measurement command directly following the plating procedure. In this case both the Hg (to form the film) and the target metal (either Cd or Pb) were simultaneously deposited. An *Export ASCII data* command is present at the end to save the applied potential and differential current data from the DPASV measurement.

The same procedure in Figure 2.15 was used for ligand titrations as this procedure was not automated. A Dosimat with a 20 ml burette was used to manually add the ligand solution with the exact volume set.

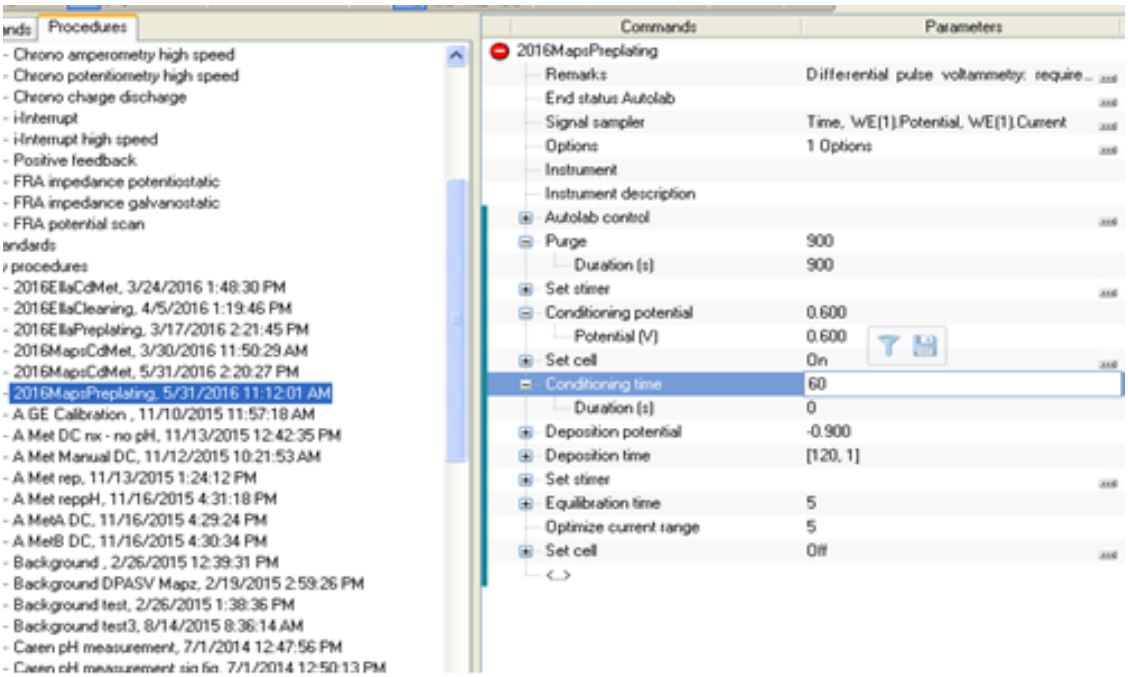


Figure 2.14: The procedure for preplating Hg at the glassy carbon electrode.

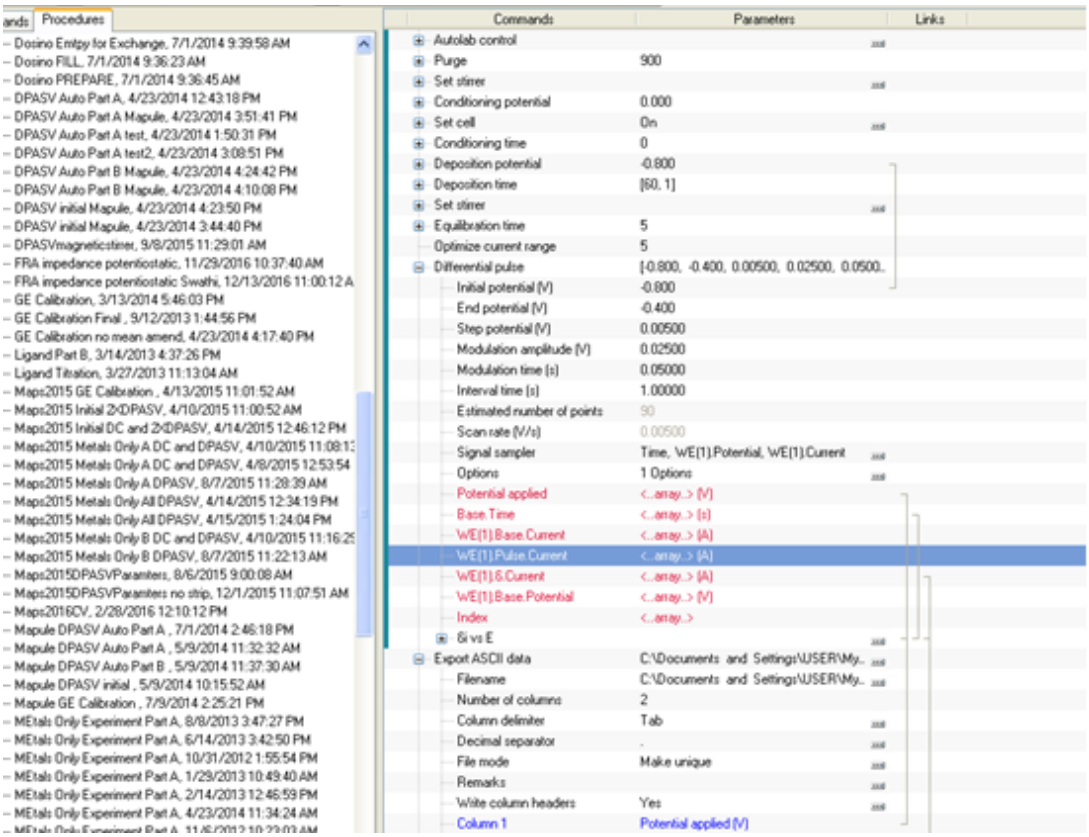


Figure 2.15. The procedure used in situ analysis and ligand titrations.

2.6 References

1. Barry, P. H. and Diamond, J. M. *J. Membrane Biol.* **3,** 93–122 (1970).
2. Billing, C., Cukrowski, I. and Jordan, B. *Electroanalysis* **25,** 2221-2230 (2013).
3. Serrano, N., Martín, N., Díaz-Cruz, J. M., Ariño, C. and Esteban, *Electroanalysis* **21,** 431–438 (2009).
4. Metrohm. NOVA Autolab Tutorial. 20–28 (2013).
5. Castro, A. A., Isa, A., Cordoves, P., Augusto, P. and Farias, M. *Anal. Chem. Insights* ***8,*** 21–28 (2013).
6. Monterroso, S. C. C., Carapuça, H. M., Simão, J. E. J. & Duarte, A. C. *Anal. Chim. Acta* **503,** 203–212 (2004).

Chapter 3 – The Study of Bi^{3+}

Stability constant determination has been widely reported using DC polarography. DPASV is a different approach which has not been used much for studying complex formation. In order to use this technique it is important to optimise parameters, in order to obtain signals of high quality for studies to be undertaken. In this work we tried to optimise the DPASV parameters E_{dep}, t_{dep} ,E_{mod} and t_{mod} so that the voltammetric peak produced would be symmetrical. For complex formation studies, the peak potentials should not be influenced by anything other than complex formation itself and ideally the reduction process should be fully reversible.

3.1. Investigating the Influence of Tl^{+} on the Bi^{3+} Stripping Peak

In this work Tl^{+} was used as an internal reference ion to calculate the diffusion junction potential, thus both Bi and Tl were accumulated at the mercury drop electrode at the same time. The first experiment conducted was to find out whether their simultaneous preconcentration affects the analysis of Bi^{3+}. This was done by running DPASV at two different deposition potentials: E_{dep} = -0.2 V for depositing Bi^{3+} only and E_{dep} = -0.75 V for depositing both Tl^{+} and Bi^{3+}, all vs. Ag/AgCl. Each of these was run at t_{dep} ranging from 5 - 120 s. Other parameters used were E_{mod} = 25 mV, step potential 5 = mV, t_{mod} = 0.05 s and interval time = 1 s. The background was 0.5 M HNO_3 and the concentrations of Tl^{+} and Bi^{3+} used were 4 × 10^{-5} M and 1 ×10^{-5} M, respectively. The solution was stirred during deposition.

Figure 3.1 shows the voltammograms at different deposition potentials. The voltammograms indicate clearly how the Bi^{3+} peak current was significantly higher at a higher deposition potential (with a difference of 232 nA), but the peak potentials (vs. Ag/AgCl) for the Bi^{3+} peaks were essentially the same (with the difference being only 1 mV). It was encouraging that the Bi^{3+} peak was not influenced by Tl^{+}.

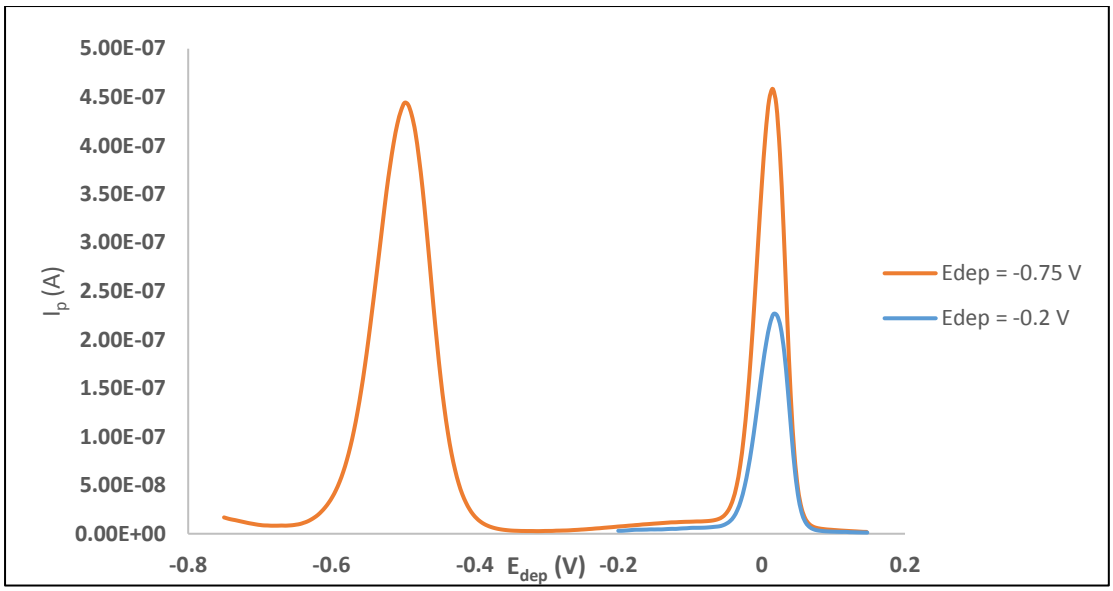


Figure 3.1: Voltammograms at t_{dep} = 60 s and different E_{dep} values. The orange curve shows the both Bi^{3+} and Tl^{+} were deposited and the blue curve shows only Bi^{3+} was deposited.

In Figure 3.2 shows the peak potentials (vs. Ag/AgCl) for DPASV measurements done at the same two E_{dep} values, but with changing t_{dep} values. It is observed that there is a slight shift in the peak potential particularly at t_{dep} = 100 and 120 s for E_{dep} = -0.2 V (vs. Ag/AgCl). This result is influenced by how the peak potential was determined. The software used to determine the peak positions is NOVA. The step potential used when collecting the voltammograms was set to 5 mV by default. The software can therefore only refine the peak potential in 5 mV steps and so takes the highest point of the voltammogram to be the peak (see Figure 3.3). From this it was observed that the I_p and E_p calculated by software is not totally accurate. An ideal analysis should analyse data by fitting an average model through the highest points that make the peak. For succeeding experiments, peak search was manually re-done by fitting the asymmetric function (to be discussed later) through the data and calculating the current at potential intervals of 0.1 mV for the data that makes up the peak.

So even though the points at t_{dep} = 100 and 120 s look like they have higher peak potentials, it is really just due to the 5 mV step potential. The same reasoning applies to the outlier point at t_{dep} 5 s. However, it can be observed that the two E_{dep} values generally gave similar potentials. This indicates that the position of Bi^{3+} is not affected by the different E_{dep} values and thus not affected by the deposition of Tl^{+}.

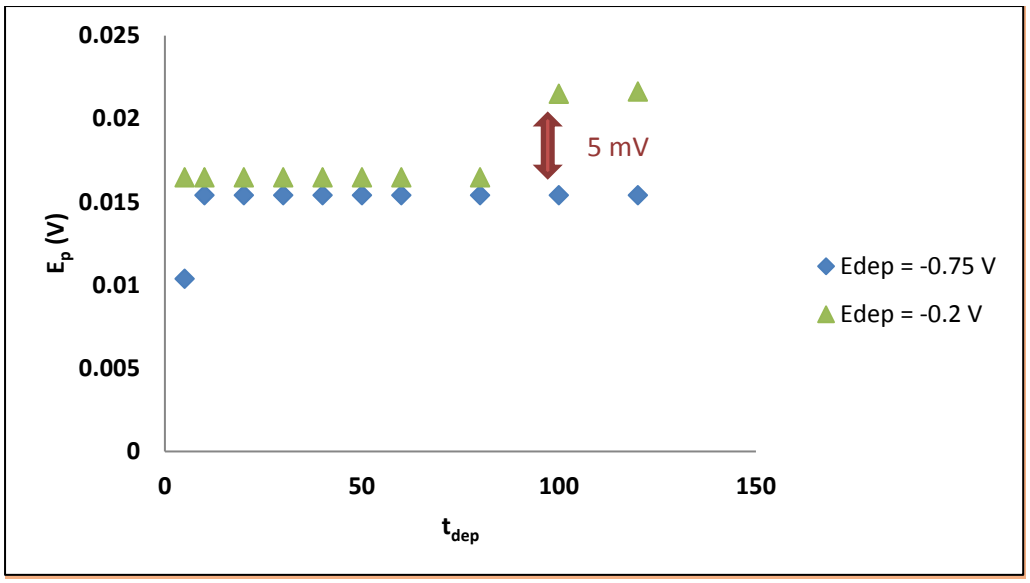


Figure 3.2: Peak potentials (vs.Ag/AgCl) at varying t_{dep} for the oxidation peaks of Bi at each E_{dep}.

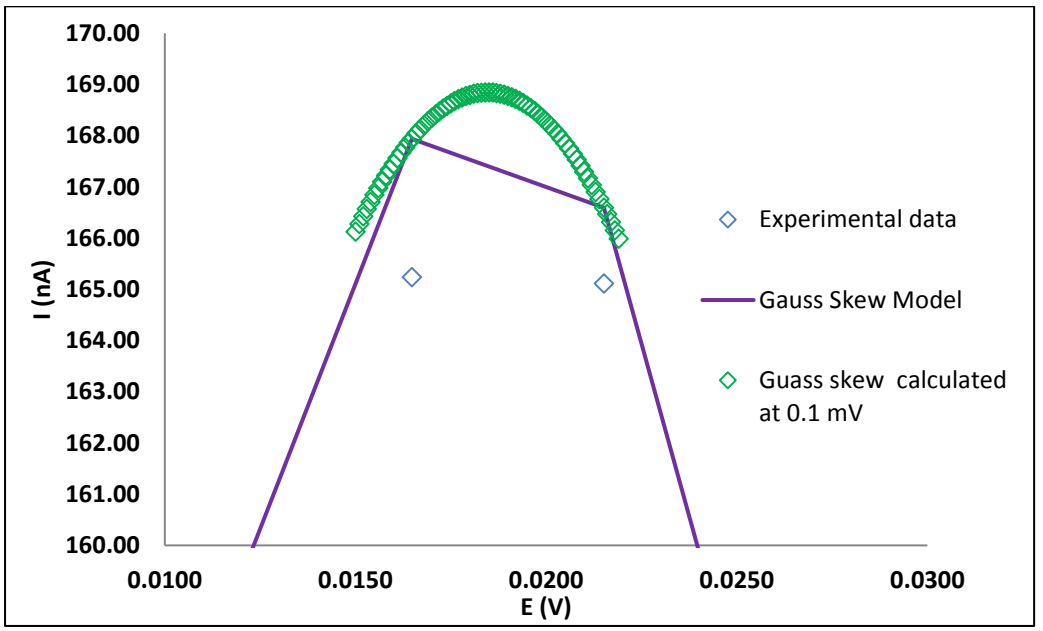


Figure 3.3: The peak of a voltammogram fitted using the Skew Gaussian model.

When comparing the peak currents for the oxidation of Bi in Figure 3.4 for the different E_{dep} values, a significant difference is observed. The current is almost double for E_{dep} of -0.75 V than it is at -0.2 V. This is not unexpected as the energy for reduction during the deposition step is greater when E_{dep} is more negative. Additionally, the solution was stirred during the deposition step, so the reaction was not diffusion controlled. Since the oxidation current depends on the amount of electroactive species

accumulated at the electrode, larger currents would be expected for the more negative deposition potentials.

Figure 3.4 also shows how t_{dep} influenced the current. A line is drawn on the data measured for E_{dep} -0.2 V to indicate the linear part of the data and where deviation from linearity begins. A t_{dep} of 60 s was taken as the optimum value because this is the t_{dep} that gave the maximum current in the linear region. At higher t_{dep} the currents deviate from the linear increase and this is due to the start of saturation effects for the Hg drop electrode. The voltammograms recorded at -0.75 V are noisy and therefore difficult to analyse. However, t_{dep} of 30 s was chosen to be the optimum t_{dep} for depositing at -0.75 V, as it gave the maximum current and t_{dep} would be expected to be lower for the more negative deposition potential.

When looking at the influence of t_{dep} on the peak current with E_{dep} = -0.75 V, we see that it is not largely influenced by deposition time because enough energy is already applied to deposit the Bi. For E_{dep} = -0.2 V, t_{dep} has more of an effect. The current keeps on increasing as t_{dep} is increased as the initial energy is not as much to deposit more electroactive species. So the more time given in the deposition step, the higher the current because more species are deposited.

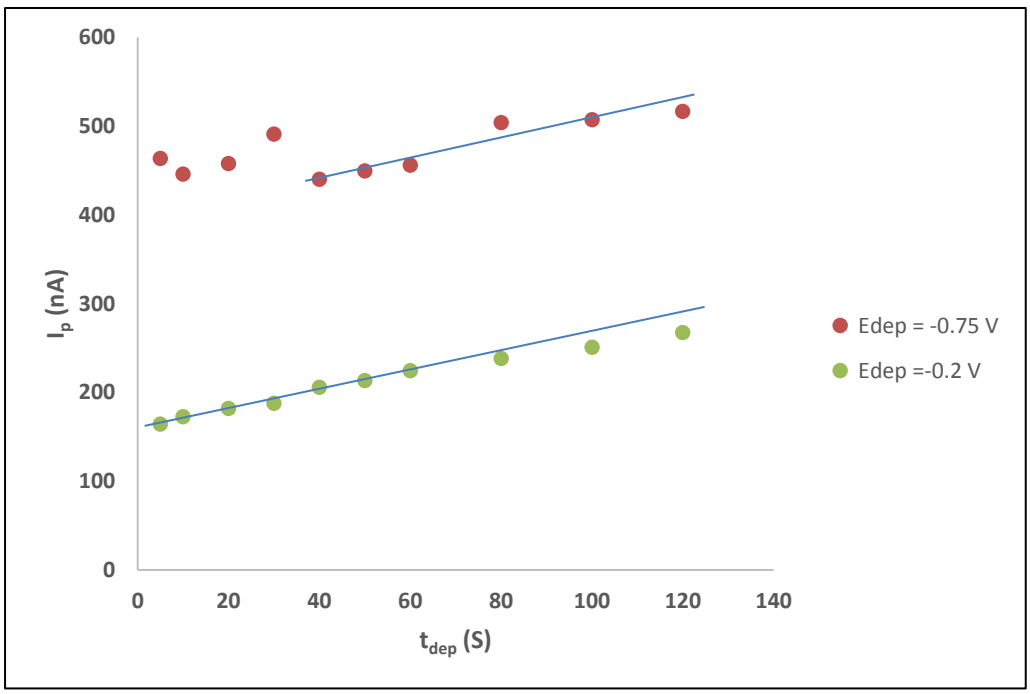


Figure 3.4: Peak currents at varying t_{dep} for the oxidation peaks of Bi at each E_{dep}.

3.2 Optimisation of E_{dep}

Figure 3.5 a) and b) show the peak potential (vs. Ag/AgCl) and peak current for the deposition of Bi^{3+} only. Deposition potentials ranging from -0.15 to -0.3 V (vs. Ag/AgCl) were applied to deposit Bi^{3+} using a 60 s deposition time. From these deposition potentials, we get a constant peak potential for deposition potentials in the range -0.2 to -0.3 V. The difference in potential between these at that obtained at E_{dep} of -0.15 and -0.2 V is 5 mV and this is once again simply due to the 5 mV step potential. Otherwise E_{dep} has very little influence on peak potential. On the other hand, at a more negative E_{dep}, higher peak currents were observed as expected because more energy is applied, but it seems to tail off from potential less negative than -0.2 V. From this, E_{dep}= -0.3 V was chosen as the optimum E_{dep} since it gave the maximum current.

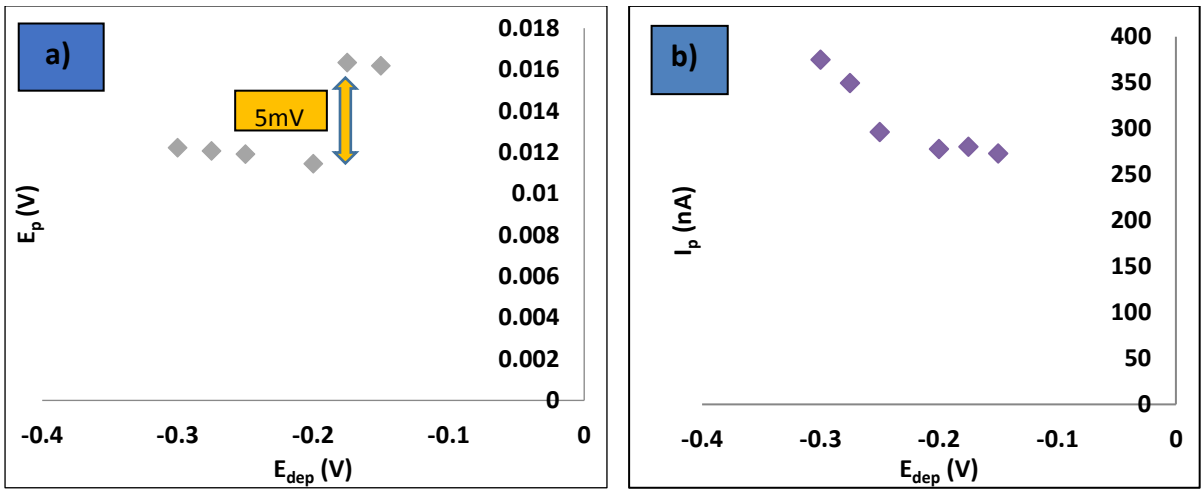


Figure 3.5: a) E_p vs E_{dep} and b) I_p vs E_{dep} for Bi^{3+} peaks without the reduction of Tl^+ in solution (t_{dep} = 60 s).

Figure 3.6 a) and b) below show the peak potential (vs Ag/AgCl) and peak current for the deposition of both Bi and Tl. Deposition potentials ranging from -0.7 to -0.8 V (vs. Ag/AgCl) were applied to deposit both metals for 30 s. The results showed that the peak potential only changed by less than 1 mV when E_{dep} was changed. However, the current changes significantly and the highest current was obtained for the most negative E_{dep}. It was decided that E_{dep} = -0.75 V would be best because H_2 evolution started occurring at -0.8 V.

At this point it appears that depositing both metals does not negatively influence the electrochemistry of Bi^{3+}. The peak position does not change and the peak current only increases due to the more negative

E_{dep} due to greater energy supplied in the reduction process. Succeeding experiments were done at this E_{dep} = -0.75 V and t_{dep} = 30 s.

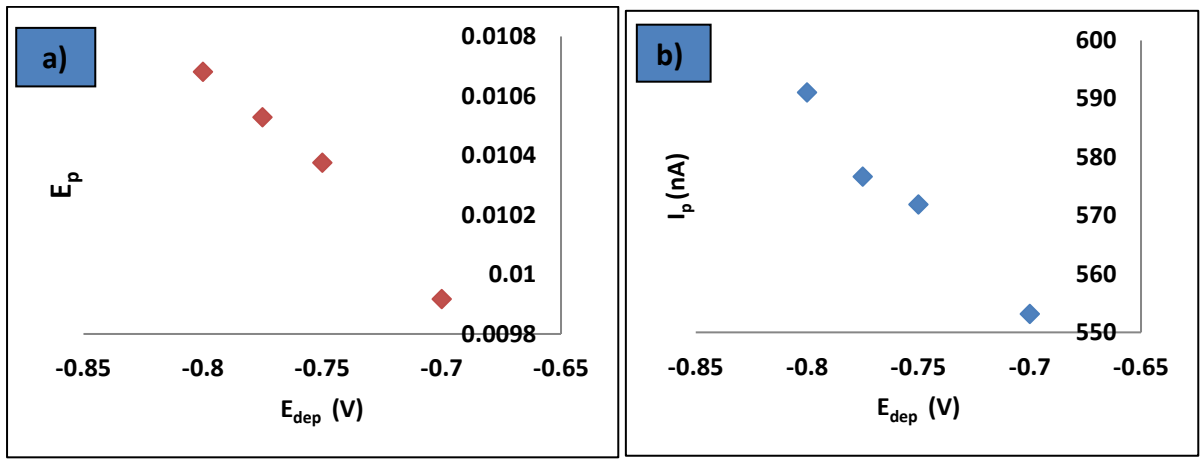


Figure 3.6 a) E_p vs E_{dep} and b) I_p vs E_{dep} for Bi^{3+} peaks when reduction of both Bi^{3+} and Tl^{+} occurred (t_{dep} = 30 s).

3.3. DPASV Reversibility

In the study of complex formation the calculation of formation constants requires that the measured peak potential be reversible. Previous studies[1–3] of Bi^{3+} formation constants study were done using DPP and DCP where Bi^{3+} behaved in a reversible manner when using a nitrate background but not reversible in perchlorate background. Since DPASV is a new approach to study Bi^{3+}, it was important that reversibility of Bi oxidation with DPASV be tested. A Gaussian distribution, also known as a normal distribution, is a common continuous probability distribution. A normal distribution is an arrangement of a data set in which most values gather in the centre of the range and the rest taper off symmetrically toward either extreme. A normal distribution is graphically represented as a symmetrical bell shaped curve. The exact shape can vary depending on the data set but the graph has to be symmetrical with the peak in the middle.[4] Because of this, it is not the best model for data that is skewed. As such, it is not a good model if there are outliers present. Below is the Gaussian function:

$$y = \mathrm{a}\exp\left(\frac{-(\mathrm{x}-\mathrm{y})^2}{2(\sigma)^2}\right) \qquad (2)$$

Where *x* is a random variable, *y* is the mean, *a* is the height of the peak, σ^2 is the variance which is related to the width at half the peak height expressed as:

$$\sigma^2 = \left(\frac{\mathrm{w}}{2.35482}\right)^2 \qquad (3)$$

Cukrowski and Luckay[5] have used the function to fit data from a reversible electron transfer process measured using DPP. Their work was focused on making Bi^{3+} complexes using various macrocyclic ligands. The Gaussian equation was modified to suit the parameters involved in the study. The function was modified as follows:

$$\mathrm{I} = \mathrm{I_p}\exp\left(\frac{-(\mathrm{E_{app}}-\mathrm{E_p})^2}{2\sigma^2}\right) + \mathrm{I_b} \qquad (4)$$

where E_{app}, I_p, E_p and I_b, are the applied potential, peak current, peak potential and background current, and σ relates to the width at half the peak height (see equation 3). I_b is a background current defined using a straight line equation $I_b = aE_{app} + b$ were a and b are constants. A very good fit between the experimental and calculated DPP peaks were obtained. Peak width is a good indication of reversibility and Cukrwoski and Luckay[5] found that the Bi^{3+} was reversible under DPP studies because the peak widths obtained were very comparable to theoretical values. A fully irreversible electron transfer should be avoided in complex formation studies. Irreversibility indicates that measurements were not done under equilibrium conditions. For DPASV if the process is not at equilibrium, the rate and probability of complexes to form is slim because the metal ion is not in the right form for complex formation to occur at the time when measurements are done.

DPASV experiments were run with Bi^{3+} and Tl^{+} concentrations of 1 ×10^{-5} M and 4 ×10^{-5} M, respectively, in 0.5 M HNO_3 with the same measurement parameters stated in section 3.1. From Figure 3.7 below it was found that the stripping peaks were asymmetrical. The figure shows how the Gaussian function does not fit the experimental data well. As such, this model cannot be used as a reliable method to accurately fit the data. These results were obtained after refinement using Excel solver.

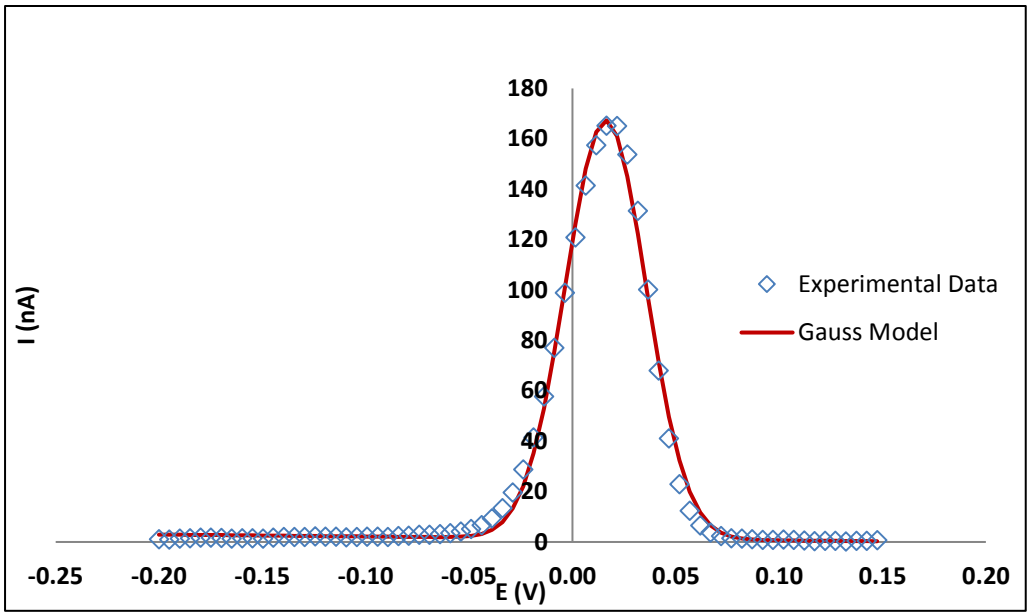


Figure 3.7: Voltammogram of Bi^{3+} data fitted using the Gaussian model.

Attempts have been made to find an asymmetric model that will better fit our data. The model below is the Gaussian function that has a complementary error function that enables it to fit asymmetric data.

$$I = I_p \exp\left(\frac{-(E_{app}-E_p)^2}{2\sigma^2}\right) \times [\text{ERFC}\,(\frac{-\alpha(E_{app}-E_p)}{\sqrt{2\sigma}})] + I_b \qquad (5)$$

ERFC is the complementary error function and the parameter α (asymmetric factor) indicates the extent of asymmetry. A zero value for α shows that the data is symmetrical. A negative α indicates that data is skewed to the left and a positive α indicates that data is skewed to the right. The skewed function in Figure 3.8 fits the data well compared to the Gaussian function. This was also seen by the difference in the magnitude of sum of squares of errors (SSE). The SSE is a measure of deviation between the data points and the calculated values, and it was calculated to be 809.25 and 52.38 for data in Figure 3.7 and 3.8, respectively. A small SSE indicates a tight fit to the model data. Therefore, it is clear that the error is significantly larger for the Gaussian function than the skewed function. However, the peak information (I_p, E_p and width) that was obtained from the skewed Gauss was significantly different from the experimental data (see Table 3.1). In fact, the Gaussian model gives peak information closer to the

visual estimate than the skewed Gaussian model. Since there is no longer a physical relationship between the data and the fitted parameters, the skewed model is not reliable when it comes to peak information. The non-zero, negative α value shows that data is asymmetric, skewed to the left.

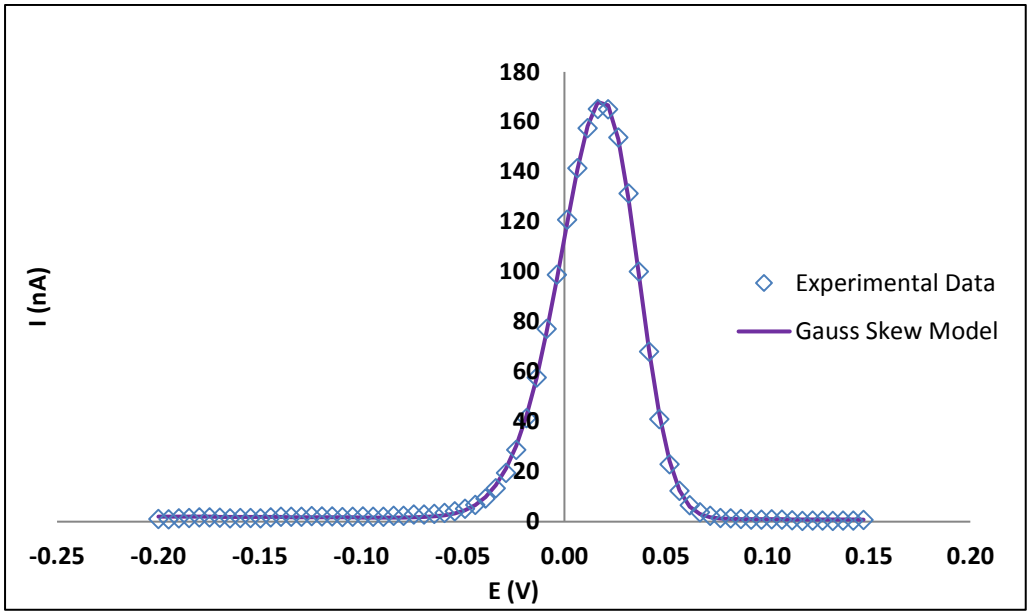


Figure 3.8: Voltammogram of Bi^{3+} data fitted using the skewed Gaussian model.

Table 3.1: Comparison of the fitted parameters for the Gaussian and skewed Gaussian models.

	Gauss	**Skewed**	**Difference**	**Visual Estimate**
E_p (mV) (vs.Ag/AgCl)	16.10	33.62	-17.52	16.5
I_p (nA)	166	116	50	165
w (mV)	46.46	66.26	-19.80	45
σ	0.01951	0.02814	-0.00863	
α		-1.8061		

From the above discussed models, the asymmetric behaviour of Bi^{3+} peaks indicates that oxidation of Bi^{3+} is not fully reversible. Since Tl^{+} was used in the experiments for evaluation of the diffusion junction potential, its reversibility when using DPASV was also studied. In theory Tl^{+} reduction is reversible and it would be expected that the oxidation is also reversible. Tl^{+} oxidation peaks were measured from a 0.5 M HNO_3 M containing 4×10^{-5} M Tl^{+} with the measurement parameters stated in section 3.1. In Figure 3.9 the Tl^{+} data fitted with a Gaussian function indicates that the Tl^{+} data is also asymmetric as the Gaussian model it does not fit well. In Figure 3.10 where the skewed Gaussian model was used, the fit

is more satisfactory. Since Tl^+ data is also asymmetric, this implies that the reduction process is not fully reversible.

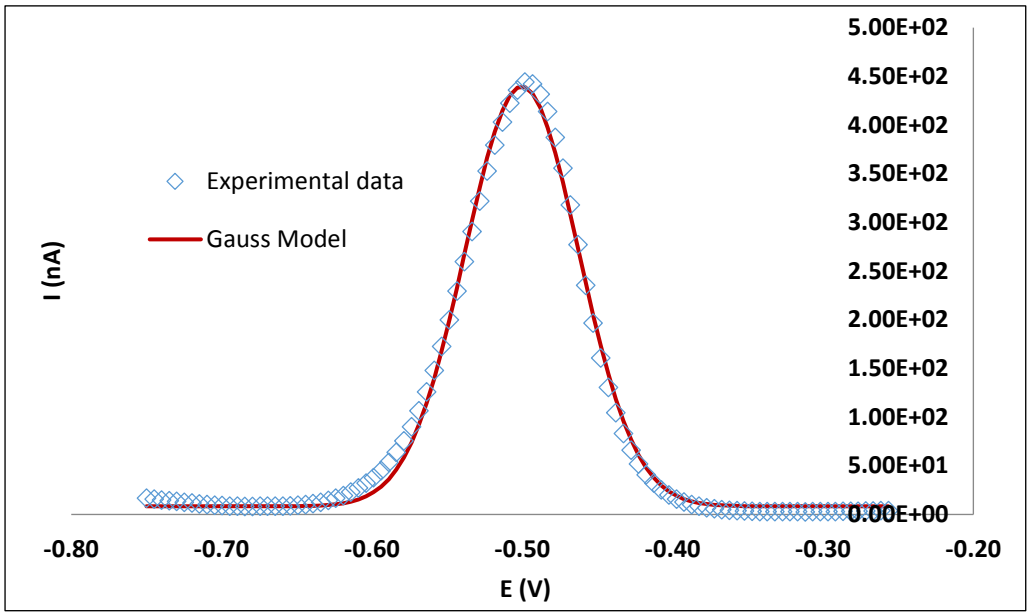


Figure 3.9: Voltammogram of Tl^+ data fitted using the Gaussian model.

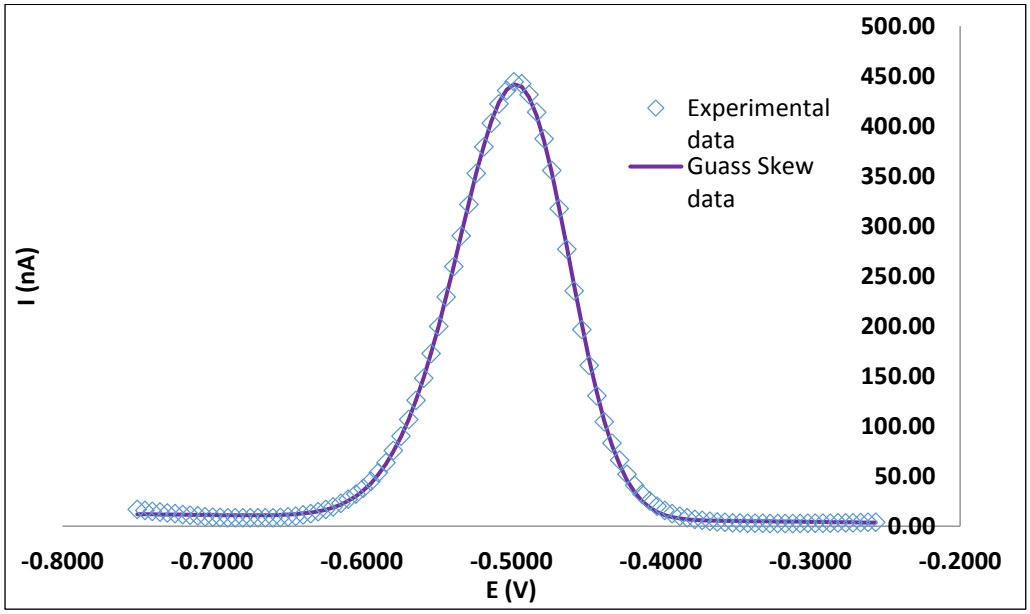


Figure 3.10: Voltammogram of Tl^+ data fitted using the skewed Gaussian model.

3.4 Optimising Parameters to Improve Reversibility

3.4.1. Optimising Parameters to Improve Reversibility of Bi^{3+}

Up until now the modelling of Bi^{3+} and Tl^{+} both indicated asymmetric responses which are suspected to be due to the DPASV technique. The problem is that as the response becomes less reversible, the peaks become broader, the peak current becomes smaller and the peak potential also shifts (more negative for reduction or more positive for oxidation). Other experimental parameters, such as modulation amplitude (E_{mod}), modulation time (t_{mod}) and interval time, were then optimsed to see if a more symmetric responses could be observed.

According to the tutorial in the NOVA software[6], increasing the modulation amplitude will give broader peaks. At high modulation amplitude, the peaks may also appear distorted as a result of non-linearity at high amplitudes. Ideally, the modulation amplitude should be between 5-100 mV and the sign of the amplitude defines the direction in which the pulse is applied. Therefore optimising modulation time, modulation amplitude and interval time should give more symmetric peaks.

This section focuses specifically on Bi^{3+} results and Figures 3.11 and 3.12 show how the Bi peak potentials (vs. Ag/AgCl) and peak currents change with modulation amplitudes at different modulation times. All the data in this section was fitted using a Gaussian asymmetric function simply for comparison purposes. Because in DPV the differential current is plotted against the base potential, the peak shifts more negative with an increase in modulation amplitude. At lower E_{mod} smaller changes in E_p occurred with changing t_{mod}. Also greater shifts in E_p with changing E_{mod} were noted for higher t_{mod}. The peak current increased with the increase in E_{mod}, as expected. The change in I_p with changing t_{mod} is smaller at the lowest E_{mod}. In general, smaller changes in E_p and I_p with changing t_{mod} are seen when E_{mod} is low (5-10 mV) indicating more reversible behaviour.

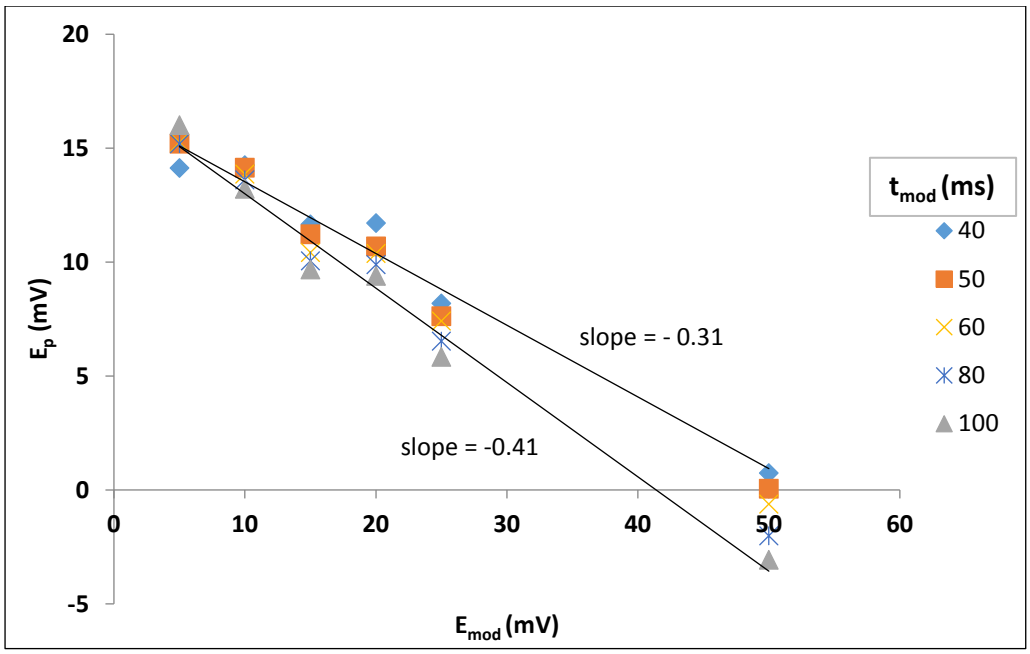


Figure 3.11. E_p (from the skewed Gaussian fit) vs E_{mod} of the Bi peaks at different modulation times using an interval time of 1 s.

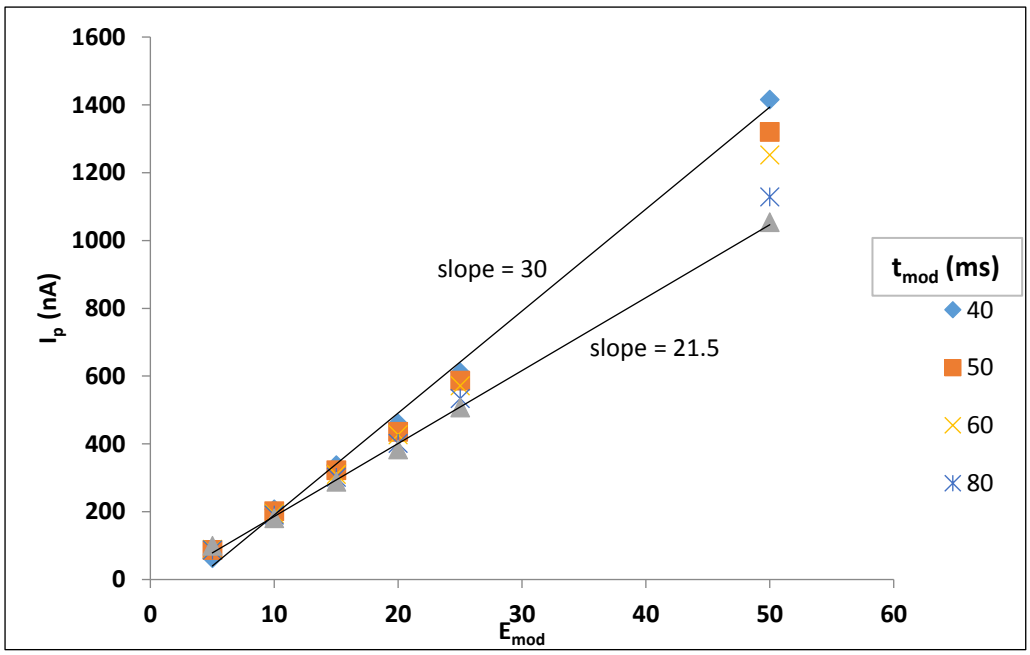


Figure 3.12. I_p (from the skewed Gaussian fit) vs E_{mod} of the Bi peaks at different modulation times using an interval time of 1 s.

Since the asymmetric factor is an indication of irreversibility, this was also investigated from the skewed Gaussian fit. From Figure 3.13 it was seen that the magnitude of the asymmetry factor increased with increasing E_{mod} and decreasing t_{mod}. Once again, the lowest E_{mod} gives the smallest magnitude of the

asymmetry factor and the smallest variation in ɣ with changing t_{mod} implying more reversible behaviours.

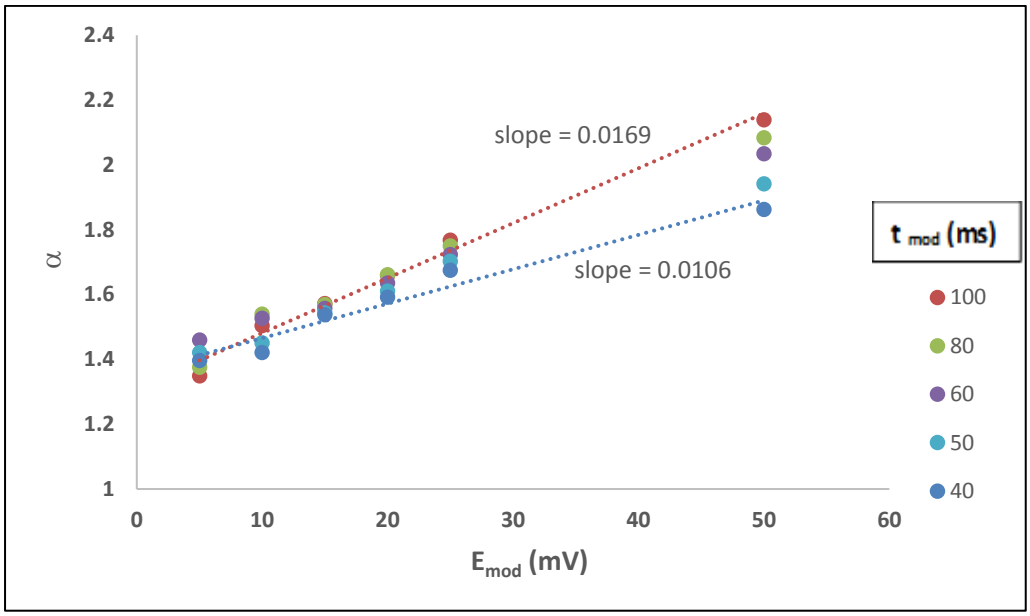


Figure 3.13: Asymmetric factor (α) vs E_{mod} at different t_{mod} using an interval time of 1 s.

From fitting the skewed Gaussian function to the oxidation peaks the width of the peaks were obtained are shown in Figure 3.14. This shows how the width of the peaks get larger as the E_{mod} increases, as expected. The variation in peak width with changing t_{mod} appears to be lower at lower E_{mod}. The width determined from the skewed model for E_{mod} of 5 mV was found to be 48.51 mV. This value was the most comparable to the Gaussian value which was found to be 46.46 mV at all values of t_{mod} and E_{mod}. The optimum E_{mod} was therefore chosen as 5 mV because it produced the narrowest peak and had the smallest asymmetry factor. This E_{mod} is not significantly influenced by t_{mod}, so t_{mod} = 80 ms was used.

Figure 3.15 shows how the area is changing with t_{mod} at different E_{mod}. Neither the Gaussian function nor the skewed Gaussian function can be used to calculate the area, so these were calculated using the NOVA software. The area decreases with a decrease in E_{mod}, but there is no big difference in the area at different t_{mod} for the same E_{mod}.

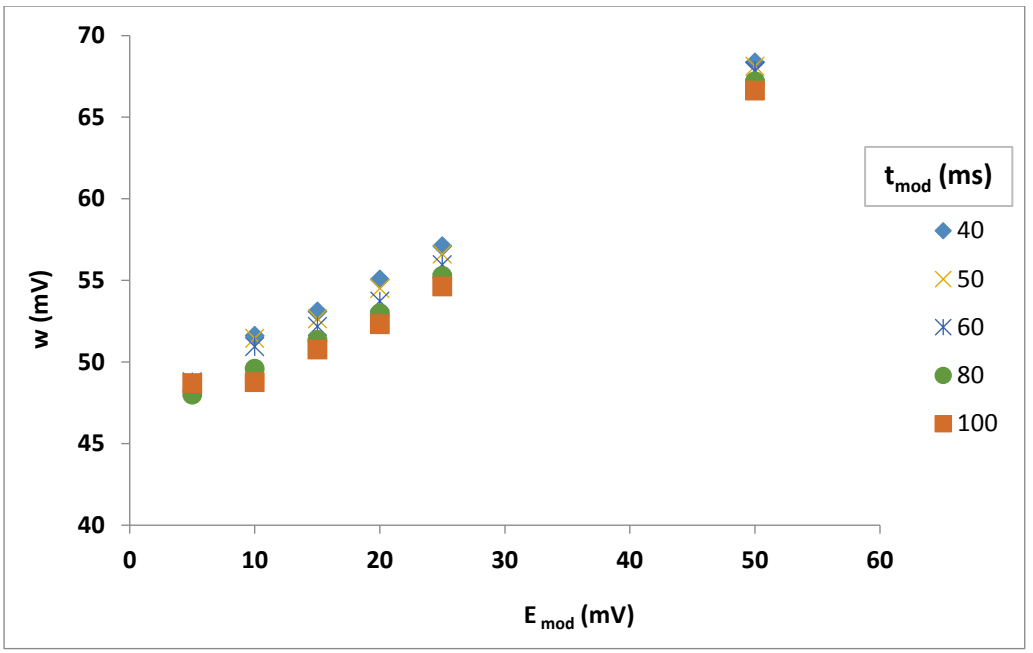


Figure 3.14: W (from the skewed Gaussian fit) vs E_{mod} of the Bi peaks at different modulation times using an interval time of 1 s.

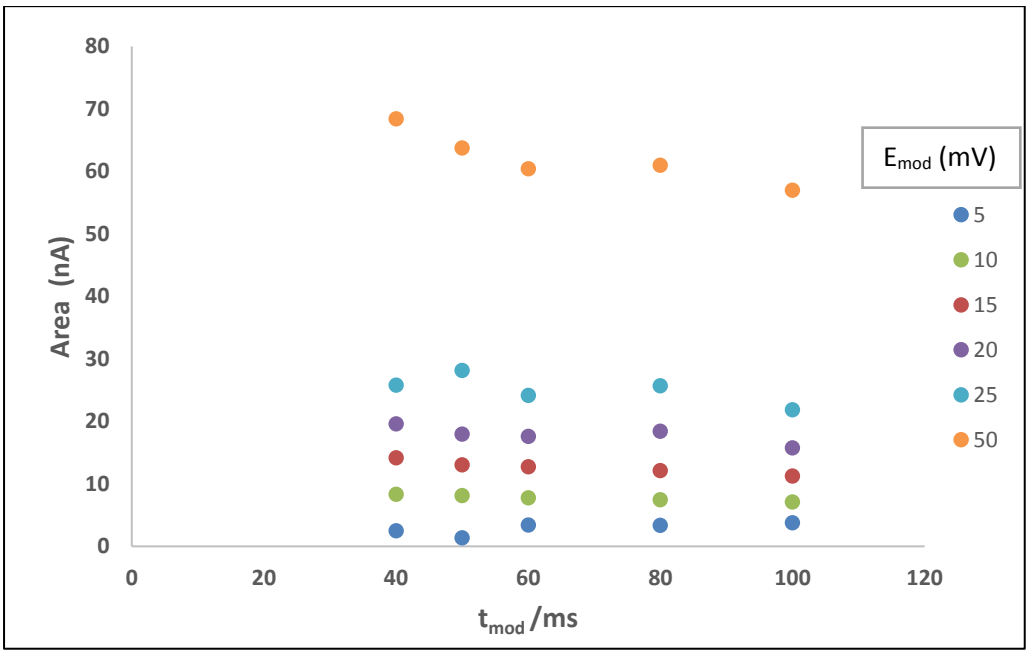


Figure 3.15: Area vs t_{mod} of the Bi peaks at different modulation amplitudes using an interval time of 1s.

The NOVA tutorial highlighted that if peak potential and peak height get lower with t_{mod}, this is a sign of irreversibility. Up until now we have seen that an E_{mod} of 5 mV gives the smallest changes with changing t_{mod}, meaning it is the E_{mod} that gives the most reversible peaks. These parameters were then used when

optimising the interval time. Figure 3.16 clearly shows that the peak potential (vs. Ag/AgCl) is independent of the interval time and from Figure 3.17 it is seen that the peak current increases as the interval time increases.

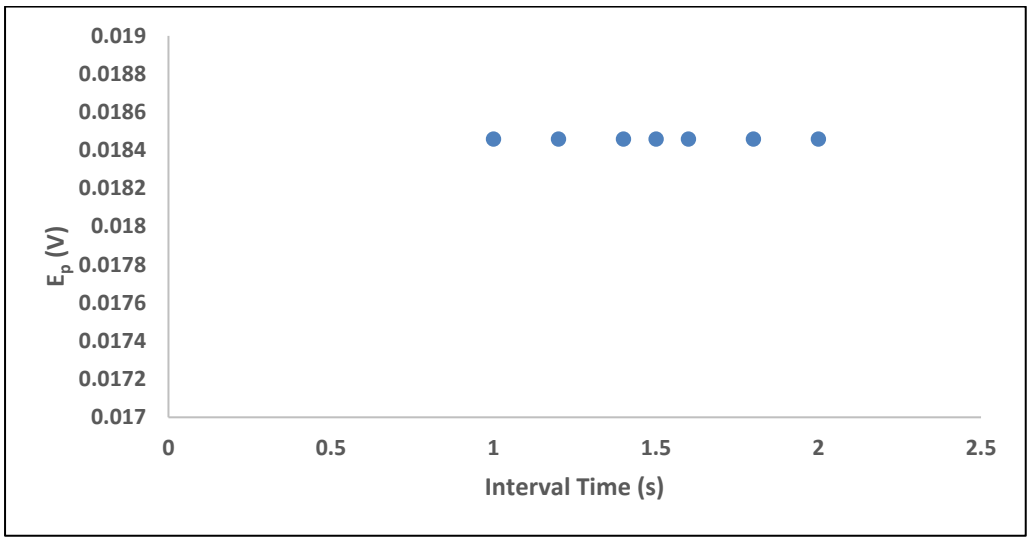


Figure 3.16: E_p (from the skewed Gaussian fit) vs interval time of the Bi peaks using E_{mod} = 5 mV and t_{mod} = 80 ms.

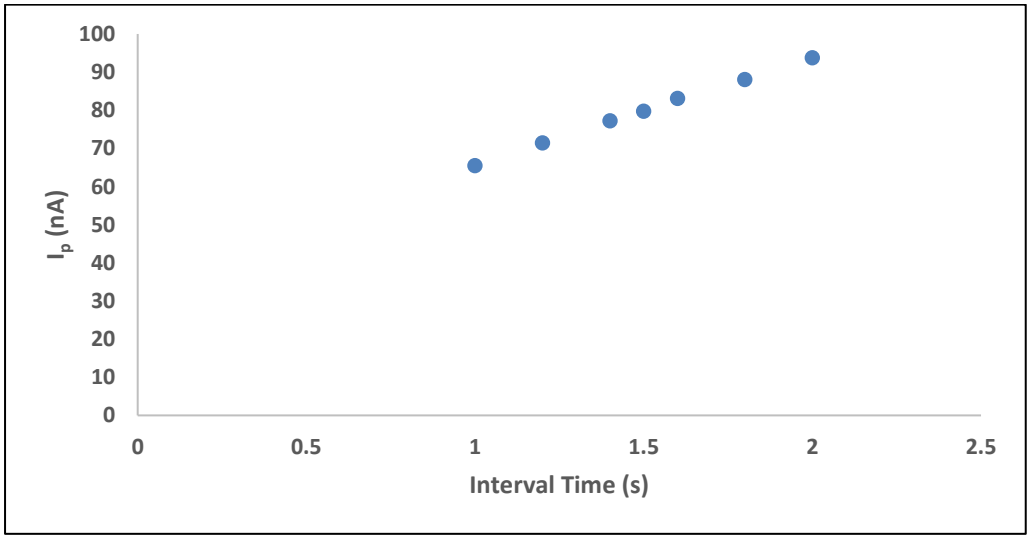


Figure 3.17: I_p (from the skewed Gaussian fit) vs interval time of the Bi peaks using E_{mod} = 5 mV and t_{mod} = 80 ms.

Figure 3.18 shows that the asymmetry factor is essentially independent of the interval time when we apply these optimised parameters and Figure 3.19 shows the peak gets narrower with an increase in interval time. An interval time of 2 s was thus taken to be the best because it has the smallest width (broad peaks indicate irreversibility) and the highest current.

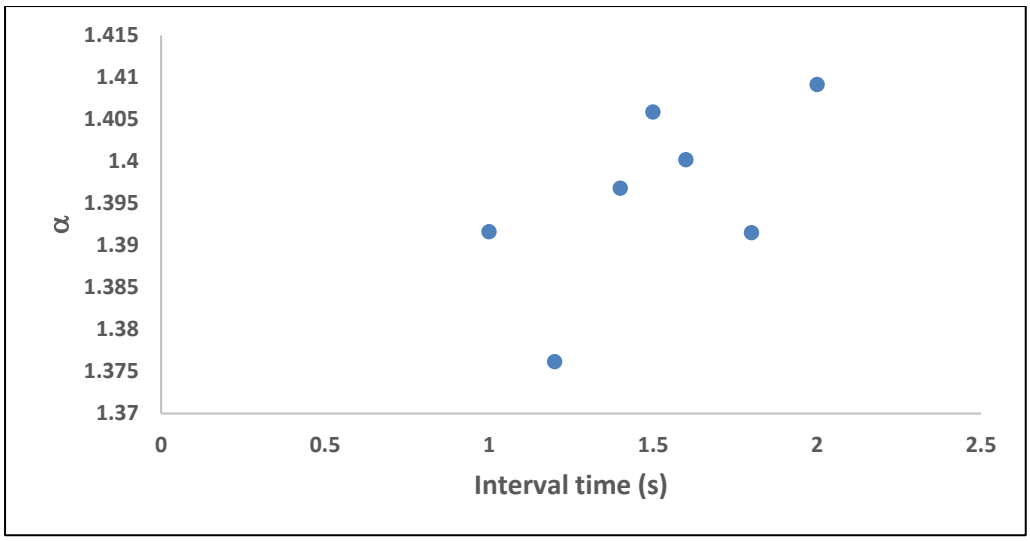


Figure 3.18: Asymmetric factor (α) vs interval time of the Bi peaks using E_{mod} = 5 mV and t_{mod} = 80 ms.

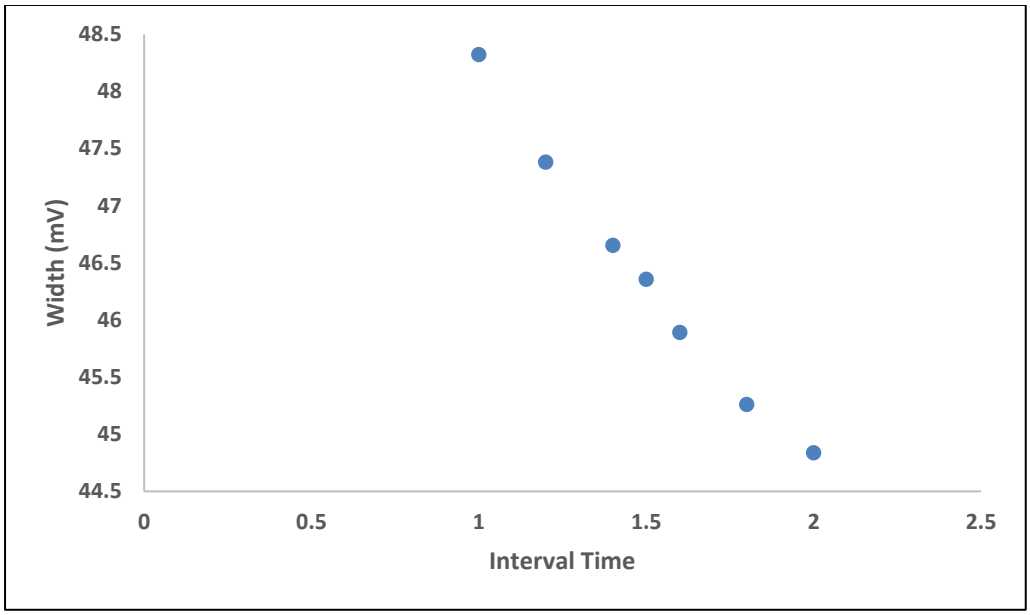


Figure 3.19: Peak width (from the skewed Gaussian fit) vs interval time of the Bi peaks using E_{mod} = 5 mV and t_{mod} = 80 ms.

In summary, from this section the peak current, peak potential, peak width, peak area and asymmetry factor were used to optimise E_{mod}, t_{mod} and interval time to get the most reversible Bi^{3+} oxidation process. The final optimised parameters at this point are listed in Table 3.2.

Table 3.2: Final optimised DPASV parameters for Bi^{3+}.

E_{dep} (vs. Ag/AgCl)	-0.75 V
t_{dep}	30 s
E_{mod}	5 mV
t_{mod}	80 ms
Interval time	2 s

3.4.2. Optimising Parameters to Improve Reversibility for Tl^{+}

The Tl^{+} data was analysed separately to determine the peak potential, peak current, peak width and asymmetry factor. Figure 3.20 shows that as the modulation amplitude increases, the Tl^{+} current increases and the current becomes highly influenced by the modulation time. A modulation amplitude of 5 mV gave the smallest change in current as the modulation time was increased. This is the same trend as seen for Bi^{3+}. However, the peak potential was not influenced by the modulation time nor the modulation amplitude. All Tl^{+} peaks had a peak potential of -489.7 mV (vs.Ag/AgCl) regardless of the modulation time or modulation amplitude. This shows that the Tl^{+} response is more reversible in comparison to that for Bi^{3+}. Figure 3.21 shows that a t_{mod} of 40 ms gives peaks with the smallest width, whereas Figure 3.22 indicates that the asymmetry factor was largely independent of the E_{mod} and t_{mod}. The optimised parameters in Table 3.2 are the conditions to give the most reversible peaks for DPASV.

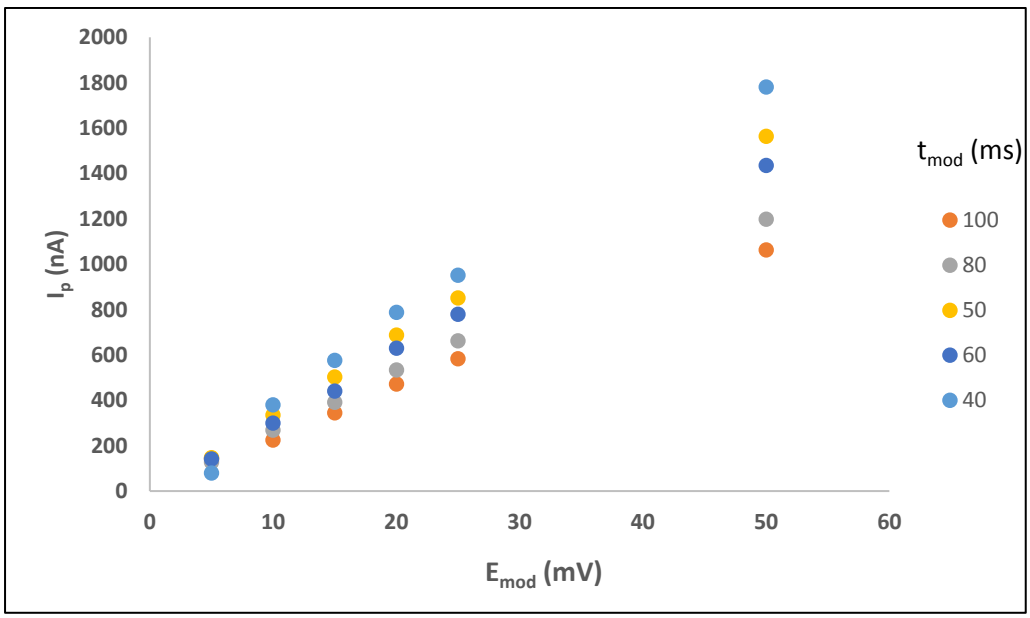


Figure 3.20. I_p (from the skewed Gaussian fit) vs E_{mod} of the Tl peaks at different modulation times.

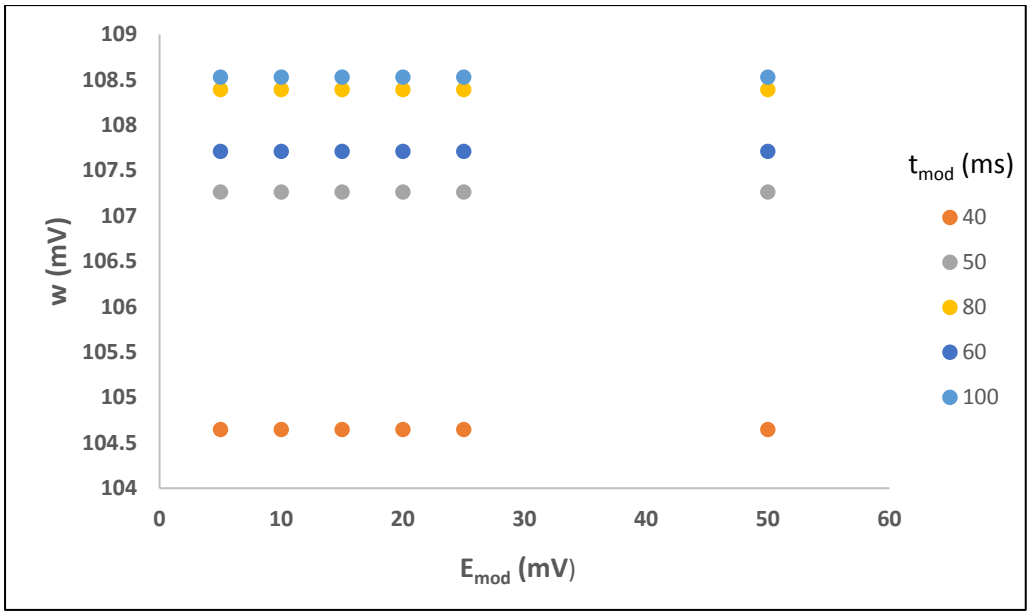


Figure 3.21: Peak width (from the skewed Gaussian fit) vs E_{mod} of the Tl peaks at different modulation times.

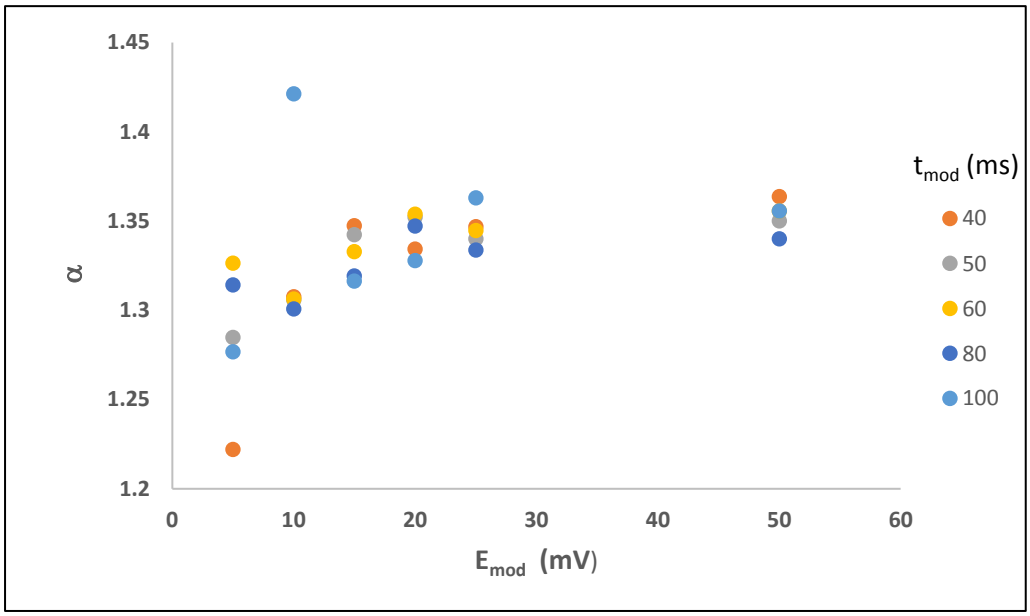


Figure 3.22: Asymmetry factor (α) vs E_{mod} of the Tl peaks at different modulation times.

3.5. Study of DPASV detection limit

DPASV is one of the most sensitive electrochemical techniques with the detection limits as low as 10^{-8} M.[7] The precipitation and hydrolysis of Bi^{3+} is a major problem in the study of Bi^{3+} complexes and has been discussed in section 1.4.1. One of the main aims of this work is to study Bi^{3+} at low concentrations to determine if this prevents or significantly postpones precipitation as suggested by the pBi vs pH diagram by Kragten *et al*.[2] (Figure 1.2b).

A study was done to determine how sensitive the analysis of Bi^{3+} is when using DPASV. Lower concentrations would require a longer deposition times because this ensures that enough electroactive species are concentrated at the electrode surface. Concentrations of 10^{-6}, 10^{-7} and 10^{-8} M were studied at different deposition times. Parameters that were used are those optimsed (Table 3.2). The concentration of Tl^{+} was four times that of Bi^{3+} in all three experiments and all solutions were stirred during deposition.

Peak current was determined using NOVA, Figure 3.23 shows that at a concentration of 10^{-6} M, a linear response was obtained up till about t_{dep} of 550 s. Deviations from linearity at higher t_{dep} indicate that saturation of the mercury is starting to play a role. At this point, the t_{dep} that come after linearity should not be used because they give longer deposition times with no significant increase in the current. From Figure 3.23, t_{dep} of 400 s was chosen as the most optimum because it gave relatively high currents and it was the last truly linear. In Figure 3.24 a concentration of 10^{-7} M had linear response at to very high t_{dep}, up until about 1000 s. A t_{dep} of 800 s was chosen as the optimum for this concentration. At an even lower concentration of 10^{-8} M (Figure 3.25) a linear response is still observed at a t_{dep} as high as 7000 s, even though it initially looked like it was deviation from linearity from about 4000 s.

As expected, the higher the concentration, the lower the required t_{dep}. At higher concentrations there is enough electroactive species in solution and hence close to the electrode surface to be accumulated at the electrode in a short space of time, even when convection is occurring and not only diffusion is relied on. The Figures 3.24 and 3.25 for concentrations 10^{-7} M and 10^{-8} M, respectively, clearly show that it is not ideal to do titration studies at these low concentrations because the experiments would be very long. Especially at the very low concentration of 10^{-8} M as this would take days and as such the reference and glass electrodes would no function properly. Studies were thus started with a Bi^{3+} concentration of 10^{-6} M as it gives a reasonable response at a reasonable t_{dep}.

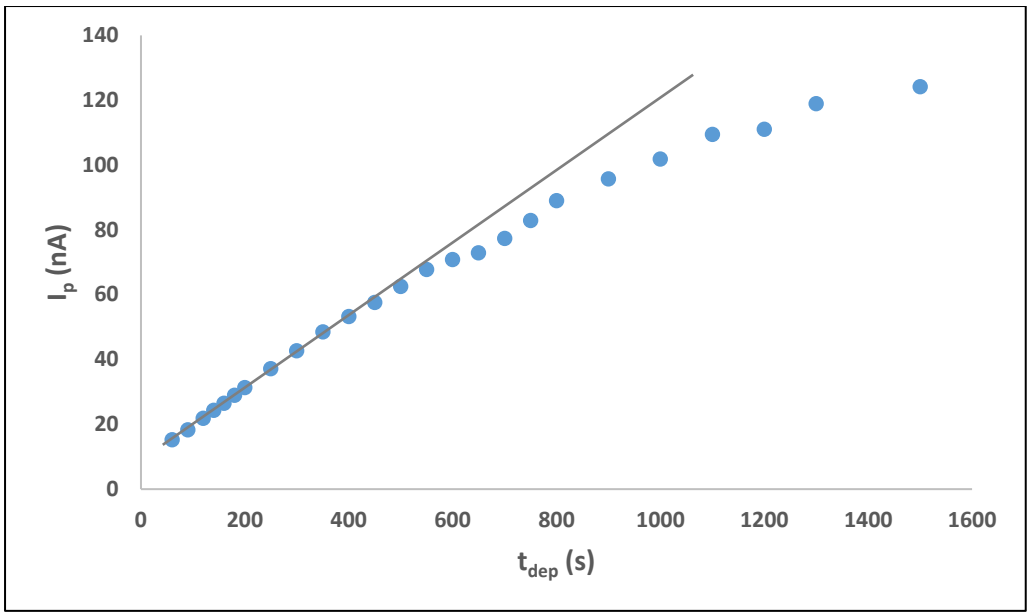


Figure 3.23: I_p vs t_{dep} for Bi^{3+} at 10^{-6} M, with the initial linear region indicated.

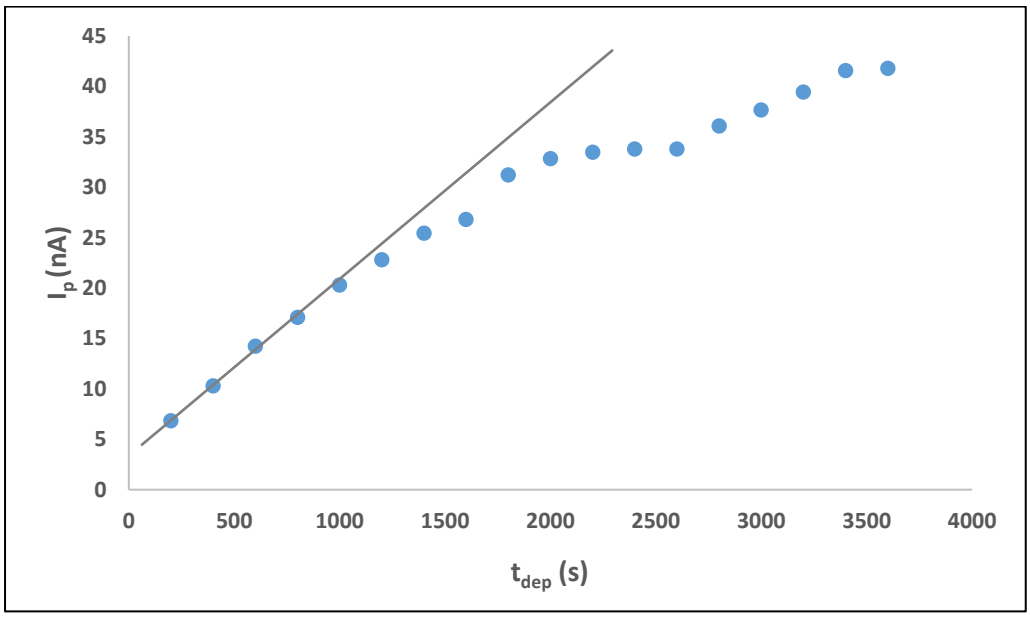


Figure 3.24: I_p vs t_{dep} for Bi^{3+} at 10^{-7} M, with the initial linear region indicated.

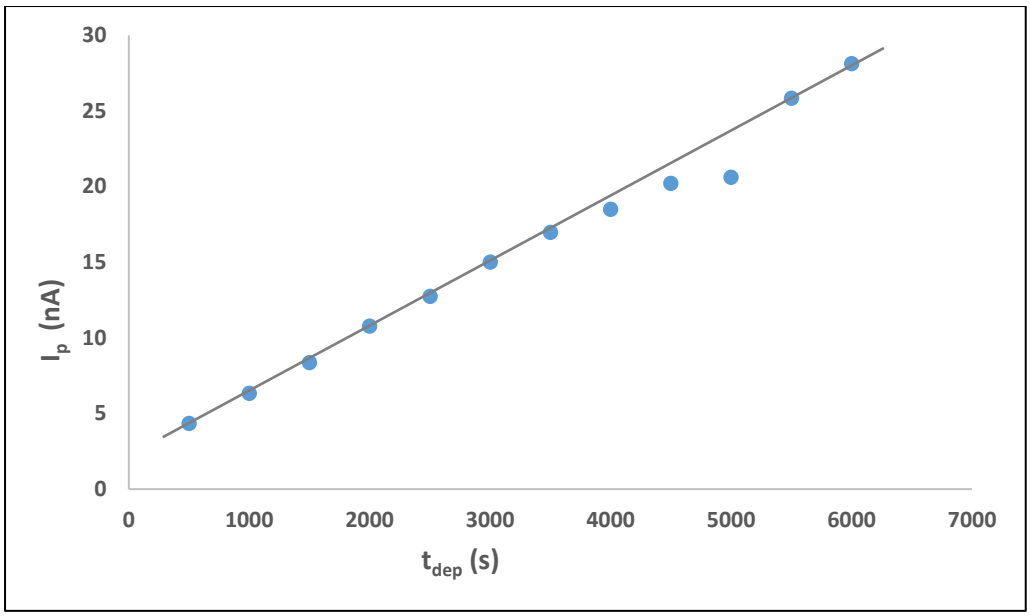


Figure 3.25: I_p vs t_{dep} for Bi^{3+} at 10^{-8} M, with the initial linear region indicated.

3.6. pH Titration at Low Bi^{3+} Concentration

3.6.1. Glass Electrode Calibration

Following the optimisation of parameters and the study of the detection limit, titrations were done at the optimised parameters and low concentration of Bi^{3+} (10^{-6} M) to investigate if this would prevent precipitation of Bi^{3+} as predicted in the pBi vs pH diagram[2] (Figure 1.2b). A pH titration was used to see what happens as the pH is increased and a glass electrode was used to probe pH.

The glass electrode (also known as a pH electrode) is a type of an ion selective electrode that is sensitive to mostly H^+. The glass electrode has a built-in silver-sliver chloride reference electrode which is filled with and stored in a 3 M KCl solution. The potential of this electrode (which changes according to the H^+ concentration of the sample solution) is measured with respect to the stable potential of the reference electrode. Unfortunately, the glass electrode is not perfect and can respond to high concentrations of other ions, especially Na^+. That is why solutions containing K^+ is used in this work. Certain substances can adsorb onto the electrode and as such the membrane could get contaminated and damaged as it ages which could lead to erroneous results.[8] It is therefore essential to calibrate the glass electrode before use in order to obtain accurate results. The calibration is often carried out using a strong acid-strong base titration or by the use of buffer solutions. The slope and the intercept of the potential vs pH calibration are close to that described by the Nernst formula.[9] The Nernst formula is temperature dependant and has a slope of -59.16 mV at 25°C.[8–10]

In our work, the glass electrode (connected to a built in pH meter in the Metrohm potentiostat) was calibrated by titration of standard 0.1 M HNO_3 with standard 0.1 M KOH at 25°C. The detailed procedure followed has been explained in section 2.4.3. The voltage measured in the titration was plotted against the pH calculated using the exact concentrations and volumes of the acid and base at each step. The resultant calibration curve is shown Figure 3.26. Extreme outlier point in the endpoint region (red curve) were removed. A slope close to the expected -59.16 mV (for blue curve) was obtained and an x-intercept close to pH 7. The R^2 value close to one indicates a linear fit. For the pH titrations of Bi^{3+}, the glass electrode calibration was done twice, before and after the titration and the calibration equations were averaged and used to calculate the accurate pH values of the Bi^{3+} titration. Figure 3.26 is simply one of the two similar calibration curves that were obtained. This is in case the properties of the electrode changes during the long automated titration experiments.

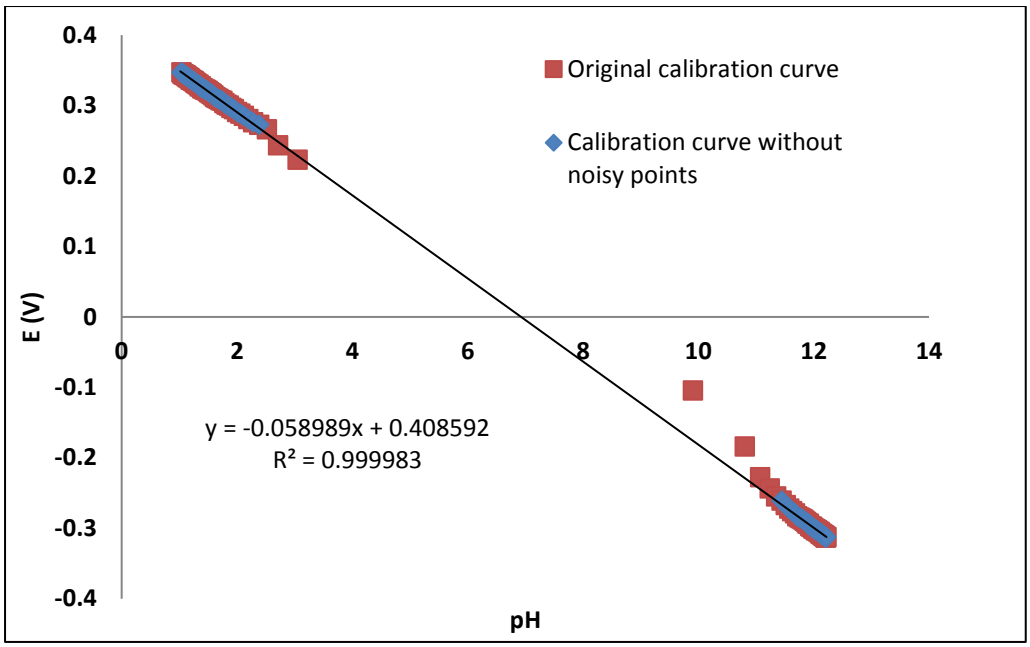


Figure 3.26: Glass electrode calibration curve obtained for the titration of 0.1 M HNO_3 with 0.1 M KOH at 25°C.

3.6.2. pH Titration

A pH titration was then done with Bi^{3+} in solution at low concentration (10^{-6} M). To evaluate the diffusion junction potential, 4×10^{-6} M of Tl^{+} was added to Bi^{3+} in the background solution of 0.1 M HNO_3 and 0.4 M KNO_3. This background was used to maintain a 0.5 M ionic strength throughout the titration. The titration was done using the optimised parameters summarised in Table 3.2. For this Bi^{3+} concentration, a t_{dep} of 400 s was used (as discussed in section 3.5). The titration was done by adding of 0.1 M KOH (in 0.4 M KNO_3) to the sample solution containing Bi^{3+} and Tl^{+} from pH 1- pH 7 in 0.1 pH steps. At each step the pH and a voltammogram were measured. The titration procedure followed was described in detail in section 2.4.3. All titration results were obtained using the Gauss asymmetric function.

Figure 3.27 shows the Tl^{+} peak potential (vs. Ag/AgCl) data from the titration. The Tl^{+} data behaves as would be expected whereby below pH 2 significant negative potential shifts are seen. Thallium complexes extremely weakly to the nitrate in the background electrolyte (log β = -0.91 for $TlNO_3$)[11] and not at all to hydroxide in this pH range, so these negative shifts are clearly due to the diffusion junction potential. As expected, above pH 2 the Tl^{+} data is linear indicating that the free Tl^{+} potential is independent of pH. The value of the free Tl^{+} potential was calculated by averaging these values and it was found to be -502.34 $\pm$ 0.36 mV. A third order polynomial was fitted to data below pH 2 to smooth

the data. The diffusion junction potential values were calculated at each pH by finding the difference between the free Tl^+ potential and the potential calculated using the polynomial. The value of the junction potential at pH 1 was very similar to that seen in previous work at the same pH.[9]

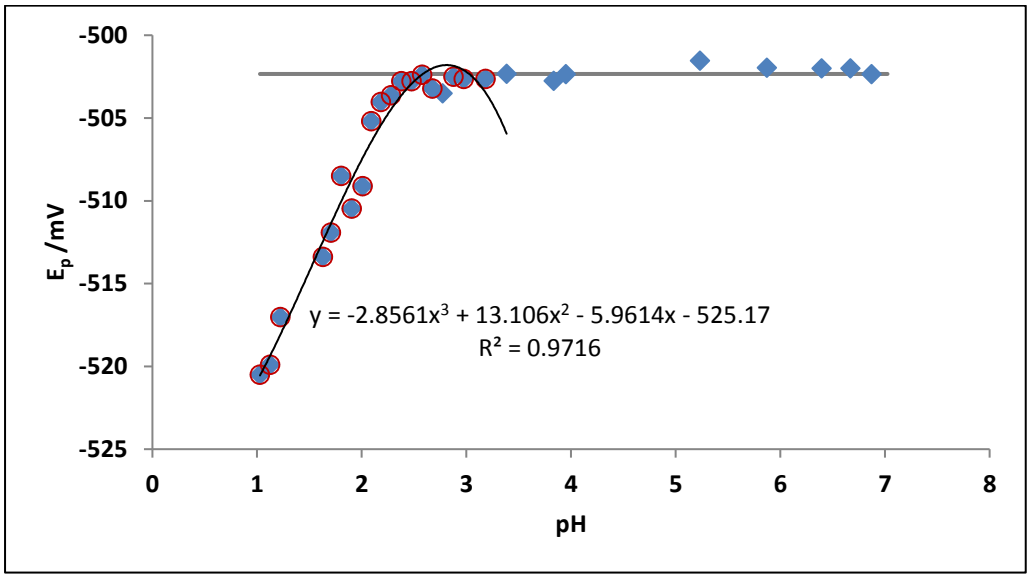


Figure 3.27: E_p vs pH for Tl^+ data obtained from the titration. The grey line shows the free Tl^+ potential and the deviation due to the diffusion junction potential below about pH 2 is fitted with a polynomial.

The peak current data for Tl^+ is shown in Figure 3.28. The decrease in current is due to dilution and the huge drop in current at low pH is because large volumes of the base are needed initially to change the pH. The observed current followed a similar trend as the expected current (calculated based on dilution) indicating that Tl^+ behaved as expected during the titration. The small discrepancy could be due to the initial voltammograms being noisier and thus less reliable. When calculating the expected currents, it is based on the current obtained for the first voltammogram. These results gave some confidence to using DPASV to measure the data.

The Bi^{3+} data on the other hand shows a different behaviour. In Figure 3.29 the observed current data does not follow the trend of the expected current. In Figure 1.2 in section 1.4, it was discussed that in theory Bi^{3+} should remain in solution if studied at 10^{-6} M for a wide range of pH.[2] This was not the case because in Figure 3.29, a slow drop in current was seen and above pH 4 the Bi^{3+} peak disappeared. This drop in current could be due to the formation of the $BiONO_3$ precipitate which is probably forming slowly. In a study by Billing and Cukrowski[3] (where the Bi^{3+} concentration was 10^{-5} M and DCP was used), precipitation occurred much faster and was seen by a huge drop in current just after pH 2. They already showed that the formation of the precipitate was kinetically slow at those concentrations. It is not

surprising that the precipitate formation is even slower at bismuth concentration that is ten times lower. In a more dilute solution the ions are further apart therefore take longer to come together and form a precipitate.

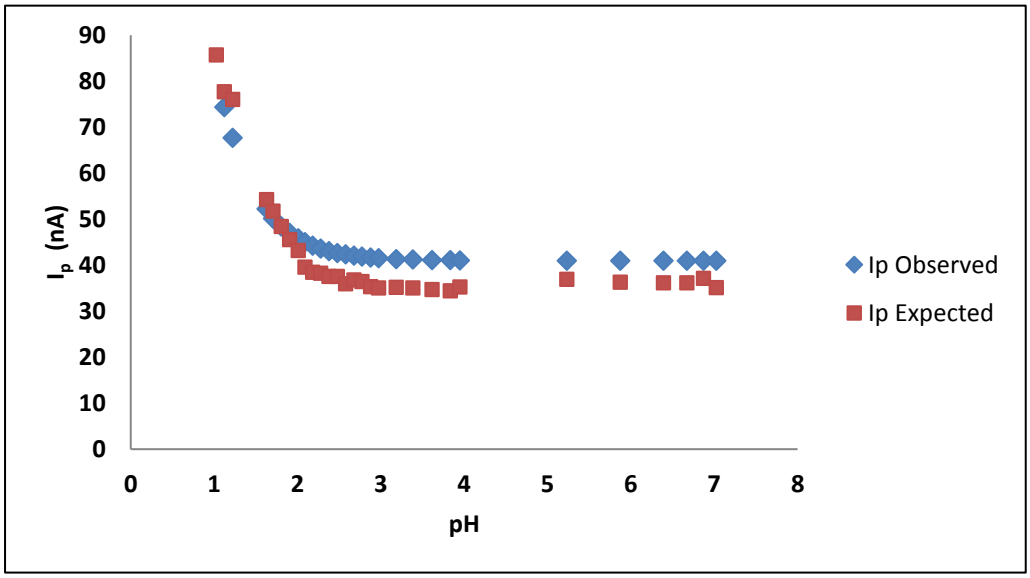


Figure 3.28: I_p vs pH for Tl^+ data obtained from the low concentration titration.

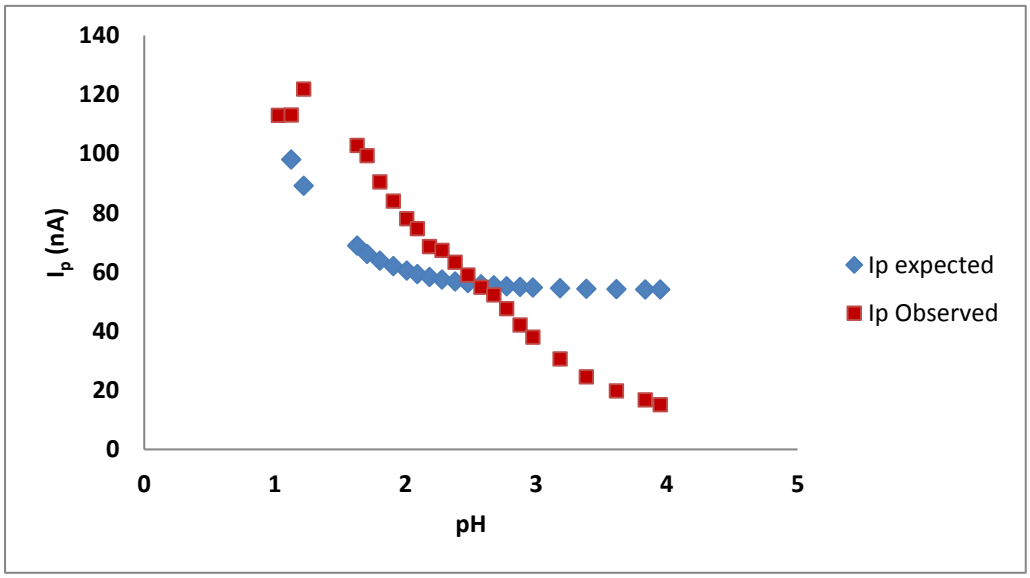


Figure 3.29: I_p vs pH for Bi^{3+} data obtained from the low concentration titration.

Figure 3.30 shows the Bi^{3+} potentials that were obtained from the titration. The titration was done from pH 1 to 7 but the voltammograms below pH 1.6 were very noisy and resulted in data which was difficult to interpret. This problematic data is circled in the figure and the missing data points were when the voltammograms could not be analysed at all. Even though the titration went up to pH 7, the Bi^{3+} data only goes up to pH 4 due to precipitation occurring thereafter.

The potential values for Bi^{3+} were corrected by adding the calculated junction potentials (Figure 3.30). In chapter 1, the hydrolysis of bismuth, which starts occurring at pH 0 already, was discussed. The background electrolyte also contained weak NO_3^- ligands. The log β values for the bismuth nitrate species (Table 3.3) are low but these complexes do form because of the excess amount of nitrate (0.5 M). Therefore the measured potentials are not for free Bi^{3+} because bismuth nitrate and hydroxide species form at very low pH. The potential shifts that are due to these species can be calculated by solving mass balance equations using their log β values (Table A1.1 of Appendix 1 for the bismuth hydroxides and Table 3.3 for bismuth nitrate). The theoretical explanation of these calculations involving mass balance equations are explained in the supplementary information by Billing and Cukrowski.[1] The species distribution diagram in Figure 3.31 shows the % of these bismuth nitrate and bismuth hydroxide species vs the pH. The shifts that are due to these species were then corrected for and the resultant bismuth potentials in Figure 3.30 (green curve) should be for the free Bi^{3+}.

Table 3.3: Log β values for bismuth nitrate species at 25°C.[12]

Species	Log β	Ionic strength (M)
$Bi(NO)_3^{2+}$	0.72	0.5
$Bi(NO)_2^+$	(0.72)	0.5
$Bi(NO)_3$	0.7	0.5
$Bi(NO)_4^-$	0.6	2.0

We expected free Bi^{3+} to have potential values that are independent of pH and therefore be linear like with the Tl^+ results in Figure 3.27, but this is not the case in Figure 3.30. The circled data was ignored because it was clearly erroneous. The data between pH 1.6 and pH 2.7 is more or less linear and the average for this data represents the free Bi^{3+} potential and can be seen by the horizontal line in Figure 3.30. The value calculated was found to be 17.9 ± 2.5 mV. Beyond pH 2.27 there are negative shifts in potential which indicate that there is complex formation which was not accounted for in the model used to correct for the potential shifts of bismuth nitrate and hydroxide species. The current data in

Figure 3.29 is consistent with the unexpected negative potentials shifts whereby beyond pH 2.7 there was a steady decrease in current. It is suspected that the $BiONO_3$ that forms remains soluble for some time before precipitation occurs. The formation of this species is then detected by the negative shifts observed.

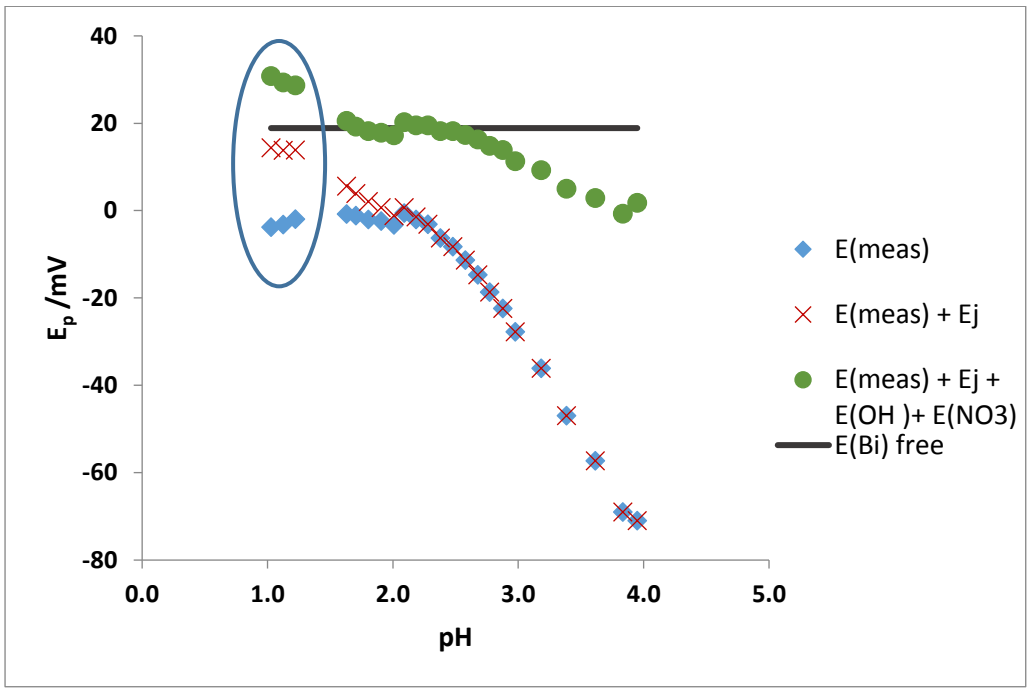


Figure 3.30: Bi^{3+} peak potentials vs pH and the values corrected for the diffusion junction potential and potential shifts due to the formation of Bi^{3+} nitrate and hydroxide species.

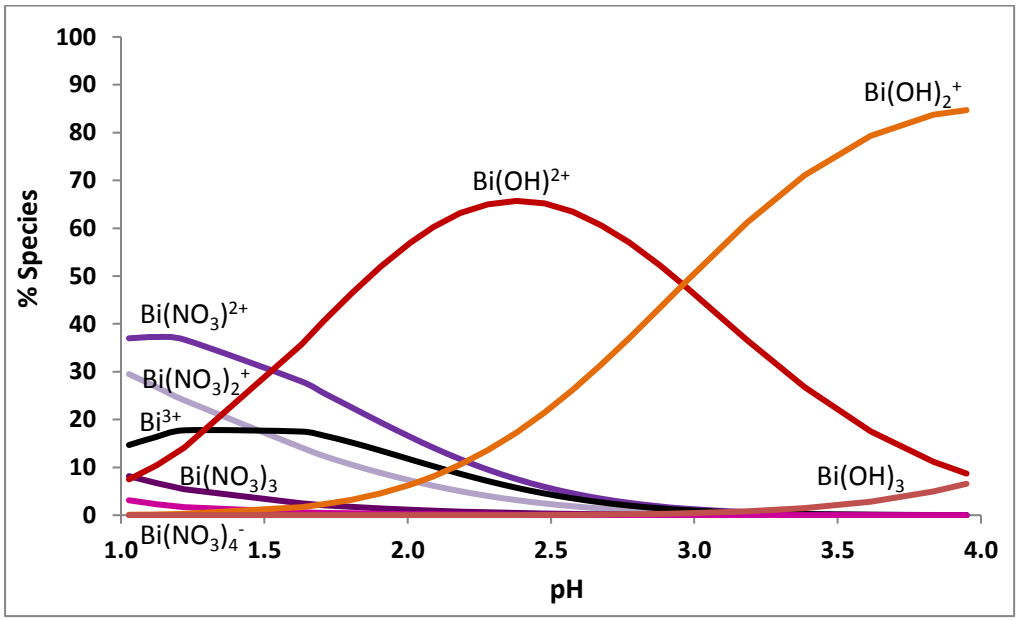


Figure 3.31: species distribution diagram of 10^{-6} M Bi^{3+} in nitrate background.

Billing and Cukrowki[3] reported that the difference between the free metal ion potential between Tl^{+} and Bi^{3+} was 495.6 ± 1.4 mV (work done at 10^{-5} M using DCP). In this work it was found to be 521.2 mV which is significantly larger. Since these potential are independent of concentration, there must be something else affecting it. It could be DPASV technique where the Bi^{3+} oxidation peaks are not fully reversible therefore the potentials shifted more positive and further away from the Tl^{+} peaks.

In literature[2] and experimentally it is known that Bi^{3+} precipitates at about pH 2 in nitrate solutions for concentrations of around 10^{-5} M and above. The aim of conducting the titration at low concentration was to investigate if precipitation could be prevented or postponed. It appears that precipitation was postponed to a small extent (to about pH 2.7), but precipitate formation still occurred even though it occurred slowly. Even though the attraction to DPASV was its low detection limit, the technique requires long accumulation times at low concentrations giving time for the kinetically slow precipitate formation. Possible issues with irreversibility also raised questions as to its usefulness in studying Bi^{3+}.

3.7. Chapter Summary

The important medicinal applications of bismuth complexes and hydrolysis and the precipitation of bismuth were extensively covered in chapter 1. This chapter aimed at investigating whether early precipitation of bismuth could be prevented if bismuth is studied at low concentration. DPASV which is a sensitive technique was used for this study. Lack of reversibility of Bi^{3+} using this technique was one of the problems encountered and attempts to optimise measurement parameters were made to improve the reversibility. The technique's detection limit was studied by studying Bi^{3+} at very low concentrations. From this, it was observed that even though very low concentrations (as low as 10^{-8} M) can be detected, the experiments become very long and therefore not practical. Kragten reported that when bismuth is studied at 10^{-6} M in nitrate solutions it would remain in solution. This work shows that when Bi^{3+} was at 10^{-6} M, the $BiONO_3$ precipitate did slowly form.

3.8. References

1. Billing, C. and Cukrowski, I. *J. Phys. Chem. B* **120,** 12972–12980 (2016).
2. Kragten, J., Decnop-Weever, L. G. and Gründler, P. *Talanta* **40,** 485–490 (1993).
3. Billing, C. and Cukrowski, I. *J. Phys. Chem. B* **120,** 4268–4278 (2016).
4. Bowling, S. R., Khasawneh, M. T., Kaewkuekool, S. and Cho, B. R. *JIEM* **2,** 114–127 (2013).
5. Cukrowski, I. and Luckay, R. C. *Anal. Chim. Acta* **372,** 323–331 (1998).
6. Metrohm. NOVA Autolab Tutorial. 20–28 (2013).
7. Kissinger, P. T. and Heineman, W. R. *Laboratory Techniques in Analytical Chemistry*. (Marcel Dekker, 1984).
8. Cheng, K. L. and Zhu, D. *Sensors* **5,** 209–219 (2005).
9. Tomi, V., Gopurenko, T., Majorinc, K. and Simeon, V. *Croat. Chem. Acta* **79,** 613–618 (2006).
10. Karlsson, A. H. and Rosenvold, K. *Meat Science* **62,** 497–501 (2002).
11. Bond, A. M. *J. Phys. Chem.* **74,** 331 (1970).
12. Martell, A. E., Smith, R. M and Motekaitis, R. J. *NIST Standard Reference Database*. Version 8,0 (2004).

Chapter 4 – Investigating the Use of MFEs for Determining Formation Constants

4.1. Preparation of the MFE

The study of the use of mercury film electrodes was first done by investigating the best experimental conditions to plate the mercury film. The ideal film would be one that has a full coverage of the mercury on the glassy carbon electrode surface and one that is robust and reproducible. This is especially important in ex situ analysis were the integrity of the film is crucial for reproducible measurements to be achieved. A number of experiments were conducted with varying conditions such as the deposition time, deposition potential and the speed of the rotating disc electrode to optimise these parameters. All the variables were very important in determining how much surface coverage is achieved and therefore how robust the film is. An optical microscope was used to view the surface coverage of the film at 12 times magnification (for a surface of 1.5 mm diameter with a naked eye). Even though the images are not of great magnification, they gave an indication of which conditions produced the most uniform surface coverage.

The plating solution was made up of 10^{-3} M of $Hg(NO_3)_2$ and 1 mL in 0.01 KNO_3.[1] Figure 4.1 shows the glassy carbon electrode surface under a microscope before mercury plating. The black area is pure carbon that does not have mercury plated on. The photos taken using the camera on the microscope were unfortunately not as clear as viewing it through the microscope, but this does give an indication of the surface quality. The surface looked smooth indicating that the electrode was adequately polished. A smooth surface is ideal because it ensures that the entire surface is active and therefore plating should result in uniform coverage.

Figure 4.2 shows the different surface coverage of the mercury films formed at three different rotation speeds, namely 500, 1000 and 1500 revolution per minute (rpm). The slight difference in colour of the images was simply due to the different lighting. These indicate that the rotation speed of the disc electrode plays a role in ensuring the full surface coverage of the film. The rotation speeds of 500 rpm in a) and 1500 rpm in c) appear to give poor surface coverage as the glassy carbon surface can be seen through the film. It appears that 1000 rpm is the optimum speed. However, this film (Figure 2 b) still showed some regions that were not well covered, so further tests were done to optimise the other parameters.

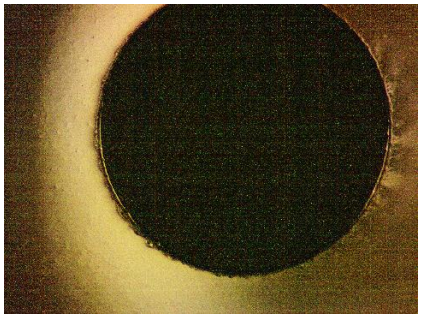


Figure 4.1. Microscopic image of an unplated glassy carbon electrode.

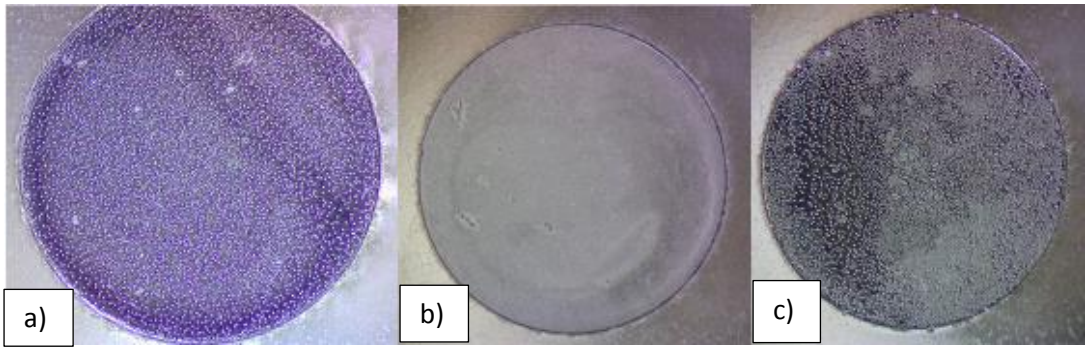


Figure 4.2. Microscopic images of the mercury film formed at rotation speeds a) 500, b) 1000 and c) 1500 rpm. The deposition potential was -900 mV and deposition time was 300 s in 10^{-3} M $Hg(NO_3)_2$.

Using 1000 rpm and a deposition potential set to -900 mV (vs. Ag/AgCl), the deposition time was tested at 300s (image in Figure 4.2b), 480 s and 600 s. The picture in Figure 4.3a) was taken at deposition time 480 s, which is a longer deposition than for the image in Figure 4.2b) (which was taken at 300 s), and the glassy carbon still showed incomplete coverage. This was not expected because the longer deposition time should result in better surface coverage. The rotator used to produce the films shown in Figure 4.3a) was somewhat problematic and it appears that that the connection was not as good as in the case of the new rotator used when forming the films in Figure 4.2.

Figure 4.3b) with a deposition time of 600 s on the other hand was plated with a proper new electrode and gave a full coverage. From this bit of work, it became quite clear that it is important to have a good connection to the rotating electrode, especially if reproducible results are to be obtained. Deposition time of 600 s was taken as the optimum deposition time due to the complete coverage and a proper film.

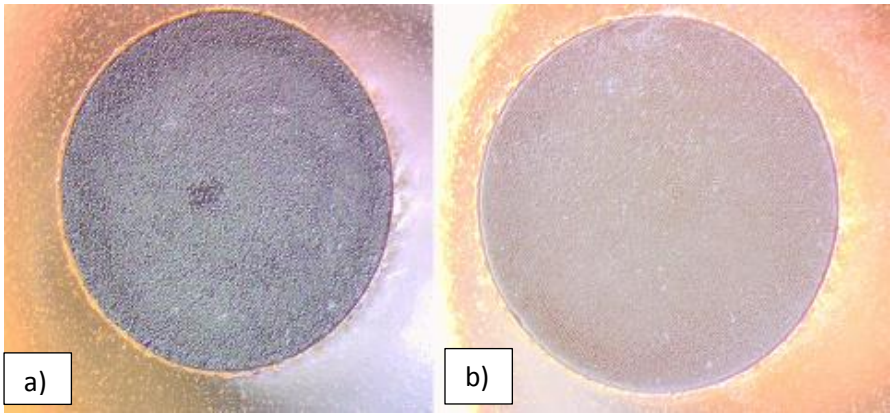


Figure 4.3. Microscopic images of the mercury film at deposition times a) 480 s and b) 600 s. The deposition potential was -900 mV and the rotation speed at 1000 rpm in 10^{-3} M $Hg(NO_3)_2$.

Deposition potential was optimised to see if a good film can be obtained at a lower energy, i.e whether a lower potential can be used for the same deposition time. Lower deposition potentials of -750, -800, -850 mV (vs. Ag/AgCl) (still at 600 s) were tested and compared against the value used in literature of -900 mV which was used up until now.[1] Figure 4.4a) is a photo taken at a deposition potential of-750 mV which shows tiny droplets of mercury, but most of the surface was still glassy carbon. This clearly shows that the potential applied was insufficient and that a mercury film is made up of tiny drops of liquid mercury starting at different nucleation sites. Even at a deposition potential of -800 mV, Figure 4.4b) shows a large area of uncovered glassy carbon. It also shows that the drops of mercury coagulate into bigger drops as more mercury is plated. Figure 4.4c) recorded at deposition potential of -850 mV shows a much better coverage. It is clear that the energy supplied for the reduction process is a determining factor in the surface coverage and any potential less negative than -850 mV does not produce a film of sufficient quality that can be used in ex situ analysis. It was decided to stick to the deposition potential of -900 mV as was used in literature.[1]

At this point the optimised conditions to plate a mercury film were deposition potential = -900 mV (vs. Ag/AgCl), deposition time = 600 s and rotation speed = 1000 rpm. The mercury concentration was increased from 10^{-3} M to 10^{-2} M to see if we could get a shorter experimental procedure. Three short deposition times of 60, 120 and 180 s were used and images in Figure 4.5 all indicate a complete surface coverage of the film. Since the images all look similar, it was difficult to tell which one was actually the best film so a deposition time of 120 s was arbitrarily chosen.

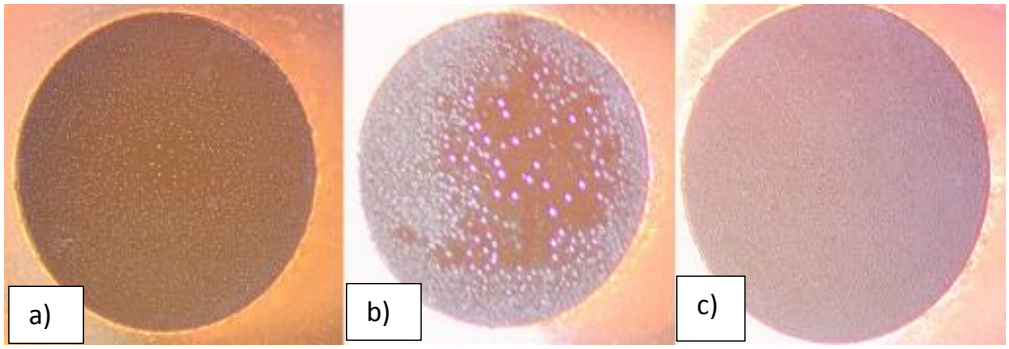


Figure 4.4. Microscopic images of the mercury film at deposition potentials a) -750 mV b) -800 mV and c) -850 mV. Deposition time was set at 600 s and the rotation speed at 1000 rpm in 10^{-3} M $Hg(NO_3)_2$.

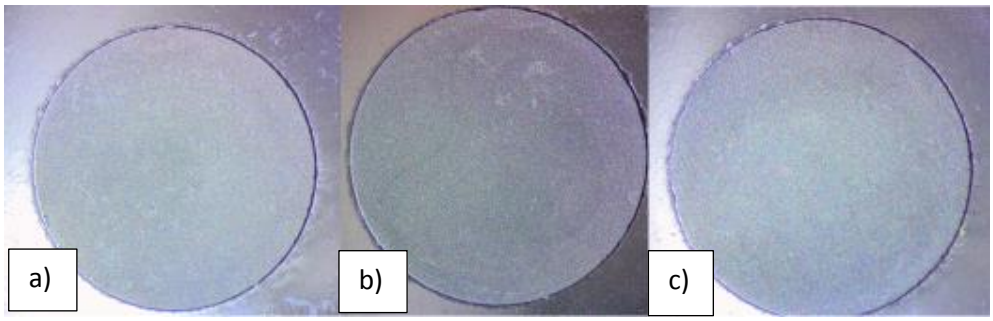


Figure 4.5. Microscopic images of the mercury film at deposition times a) 60 s, b) 120 s and c) 180 s. The deposition potential was -900 mV and the rotation speed at 1000 rpm in 10^{-2} M $Hg(NO_3)_2$.

4.2. Ex Situ Analysis of Cd^{2+}

4.2.1. Reproducibility Study

The concept of ex situ analysis has been explained in section 1.6.1. In complex formation studies, experiments should be conducted using conditions such that metal-ligand complexation of is favourable. The literature formation constants for cadmium –picolinic acid system (Cd-PA) has been studied using polarography on a dropping mercury electrode as well as other techniques.[2] Our study aimed at investigating whether those formation constants could be reproduced using a MFE. The equation 1 in section 1.5 is used to calculate formation constants. The parameters $E(M_{free})$, $E(M_{com})$, $I(M_{comp})$ and $I(M_{free})$ are obtained directly from the voltammograms measured. These values should only be influenced by metal-ligand complex formation. If for instance the film is not reproducible and its change directly influences the above values, then the calculated formation constants would not be reliable. In our laboratory, complexation experiments on MFEs were never conducted before. It was therefore crucial to investigate the robustness and reproducibility of the film electrode itself.

A reproducibility study was done by running differential pulse voltammetry (DPV) on the preplated film electrode numerous times in succession to assess whether that the voltammograms obtained were reproducible. Figure 4.6 illustrates the results obtained for the reproducibility study of Cd^{2+} on the MFE. The graph shows that the peak current decreases from one voltammogram to the next. This decrease in the current indicates a degeneration of the film electrode with use. This has been shown to be one of the major disadvantages of using the ex situ analysis.[3,4,5] It is also important to note the change in shape of the voltammograms with use. The MFE could be changing due to the accumulation of Cd^{2+} at the film because no reoxidation of Cd is done between the measurements. Even though there is a decline is peak current, the peak position remains fairly constant (apart from the last three voltammograms).

DPASV was then tested as a technique that could be more suitable for MFEs as the accumulated Cd is stripped for each measurement (and it has the added benefit of having greater sensitivity). Figure 4.7 shows the voltammograms obtained from the stripping peaks. The shape of these peaks are more well-defined than those obtained from DPV (in Figure 4.6). The background current is flatter and therefore easier to fit. However, once again the current decreases on use indicating the degeneration of the film. The current drop is quite drastic for the first few voltammograms and the change becomes less as the film is used. The peak position also shifted from one voltammogram to the next, with the change again being larger for the first few voltammograms. An ideal film should give peak currents, peak potentials and peak width that are constant throughout, so at this point it was shown that the ex situ plated film did not give reproducible results. This drastic drop in current could largely be due

to the fact that there is no significant amount of mercury in the test solution to regenerate the film for each measurement. This behaviour agrees with the already reported study of MFE robustness in literature.[3]

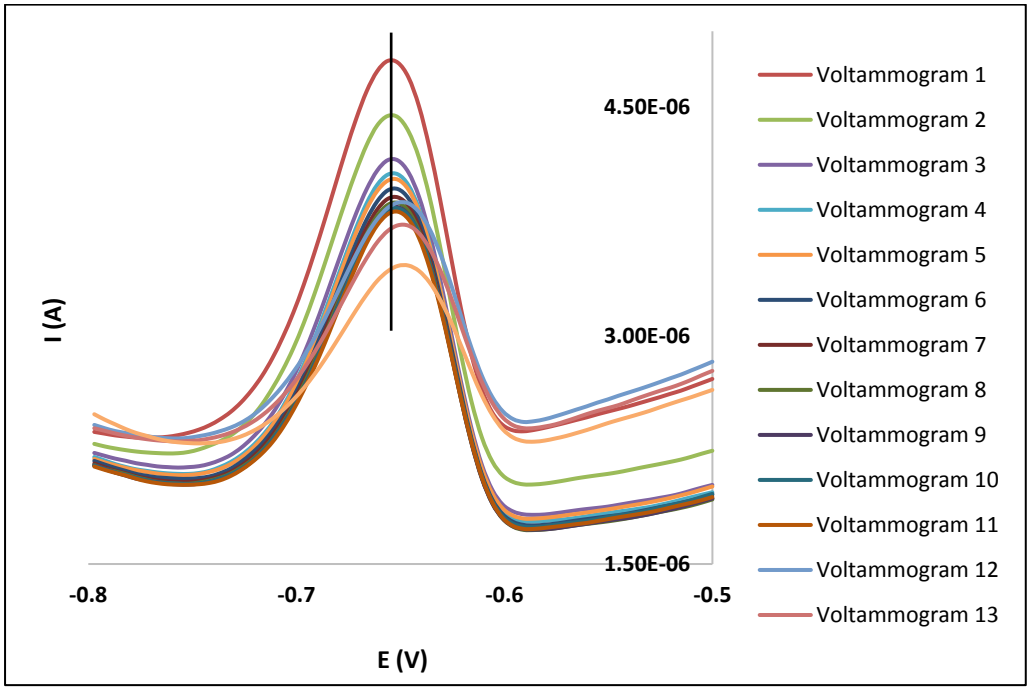


Figure 4.6. Checking reproducibility of DPV measurements for 10^{-4} M Cd^{2+} in 0.1 M HNO_3 on an ex situ plated MFE (plated at -900 mV for 120 s from 10^{-2} M $Hg(NO_3)_2$ solution). The black vertical line indicates the peak position of the first voltammogram to allow for easy comparison.

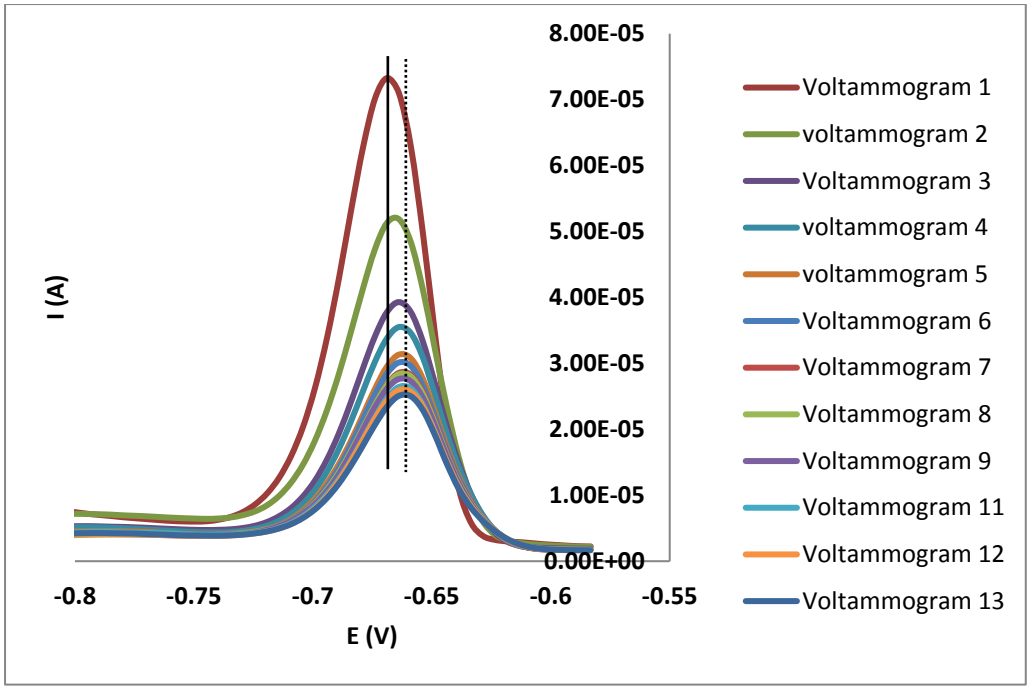


Figure 4.7. Testing reproducibility using DPASV for 10^{-4} M Cd^{2+} in 0.1 M HNO_3 on an ex situ plated MFE (plated at -900 mV for 120 s from 10^{-2} M $Hg(NO_3)_2$ solution) with Cd^{2+} deposited at -800 mV for 60 s. To allow for easy comparison the solid vertical line indicates the peak position of the first voltammogram and the dotted vertical line indicates that for the last voltammogram.

It was decided to find out by how much the peak current drops from one voltammogram to the next and to see if this drop is consistent between the experiments. This was done by calculating the % decrease in peak height. Table 4.1 shows the peak current values for a series of voltammograms recorded consecutively using DPASV on an ex situ plated MFE. The four columns indicate the experiment was repeated four times. The right side of table shows the % difference, which is a % decrease in peak height from one voltammogram to the next.

After four trials of the same reproducibility study, the average peak current and the standard deviation (SD) were calculated in each case. The standard deviations were very large due to the steady decline in the current. It was observed that the first few voltammograms were usually far off from the rest of the data set as can be seen by a larger % decrease for the first few voltammogram. The question was if the first three points were excluded when calculating the average and SD, would the results improve to give sufficient reproducibility? These new SDs were slightly smaller but still large enough to indicate insufficient consistency in the peak currents for use in experiments to determine formation constants.

Table 4.1: Peaks currents and % current decrease for consecutive DPASV measurements of Cd^{2+} solutions (deposited at -800 mV (vs. Ag/AgCl) for 60 s in 0.1 M HNO_3) on an ex situ plated MFE. The experiment was repeated four times.

	Peak current /mA				**% difference ($(n_1-n_2)/n_1*100$)**			
n	**Round 1**	**Round 2**	**Round 3**	**Round 4**	**Round 1**	**Round 2**	**Round 3**	**Round 4**
1	213.85	375.67	373.92	319.76				
2	187.77	359.27	360.92	307.16	12.20	4.37	3.48	3.94
3	169.53	343.29	349.39	293.77	9.71	4.45	3.19	4.36
4	152.57	329.18	331.40	280.68	10.00	4.11	5.15	4.46
5	135.59	319.51	320.25	271.70	11.13	2.94	3.36	3.20
6	123.25	308.09	307.45	261.30	9.10	3.57	4.00	3.83
7	115.44	300.87	292.29	251.63	6.34	2.34	4.93	3.70
8	107.12	295.50	281.50	246.58	7.21	1.78	3.69	2.01
9	102.79	286.98	274.59	238.31	4.04	2.88	2.45	3.35
10	96.59	280.42	268.10	231.94	6.03	2.29	2.36	2.67
Average	140.5	319.9	316.0	270.3				
SD	39.5	31.7	37.4	29.7				
Excluding first 3 points:								
Average	119.1	302.9	296.5	254.6				
SD	19.7	17.4	23.9	17.7				

Out of interests, it was decided to add the ligand which was picolinic acid (PA) to a solution containing Cd^{2+} to see how the resultant voltammetric response is affected. A voltammogram was collected using DPASV for the free Cd^{2+} and then the ligand added after. It was immediately picked up that the current drops drastically upon addition of the picolinic acid (see Figure 4.8). The peak current also dropped significantly from one voltammogram to the next in the presence of the ligand. This was a serious concern because it demonstrates the instability and irreproducibility of the MFE. The drop in current upon addition of the ligand could be due to the PA ligand adsorbing onto the mercury film. It has been reported before that some ligands such as picolinic acid, dipicolinic acid and quinolinic acid (all pyridine carboxylic acids) can adsorb onto and also get reduced at the mercury electrode.[6–8] In this instance if picolinic acid was adsorbing on the mercury surface then it could be possible that it led to a decrease in surface area on the film hence the drastic drop in the current of the Cd peak when PA was added. A drop in current was not observed when a dropping mercury electrode was used to study the Cd-PA system.[2]

The vertical line drawn in Figure 4.8 indicates a positive shift upon addition of the ligand. It is unclear what led to this positive shift but it could also be due to the adsorption of PA on the MFE. This shift is definitely not due to complex formation because complex formation is observed by presence of negative potential shifts. Also, from the Cd-PA species distribution diagram in Figure 4.9, it can be observed that very little complexation occurs around pH 1. In a polarographic study done by Billing *et al.*[2] only a small amount of Cd-PAH (about 10%) would formed at pH 1.

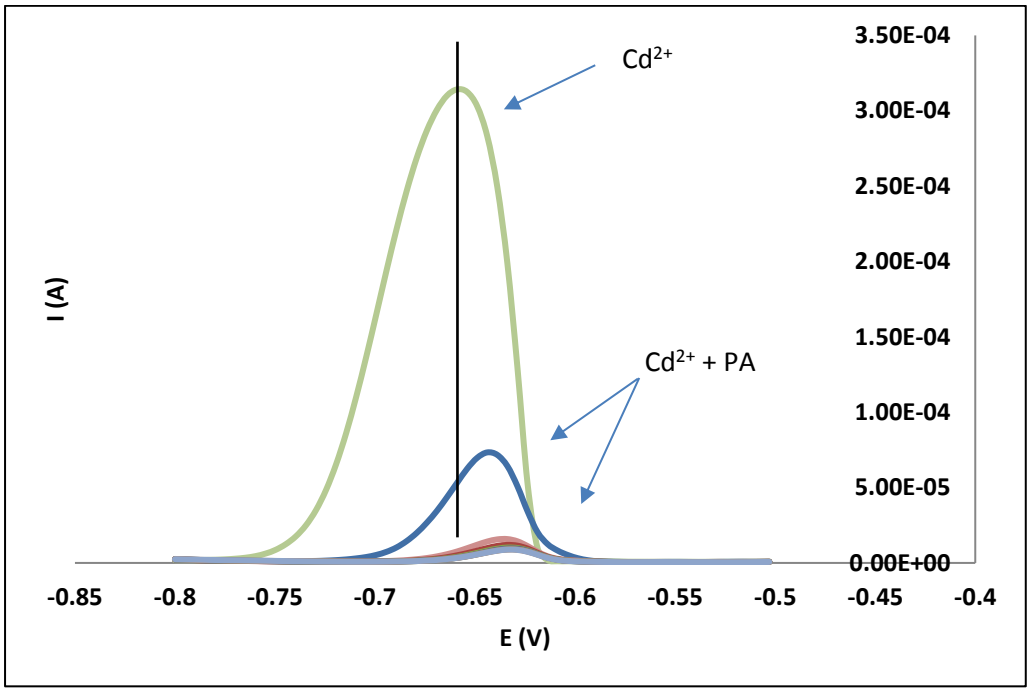


Figure 4.8. DPASV at MFE for 10^{-4} M Cd^{2+} and 0.015 M PA. The study was done in 0.1 M HNO_3 with Cd^{2+} deposited at -800 mV for 60 s.

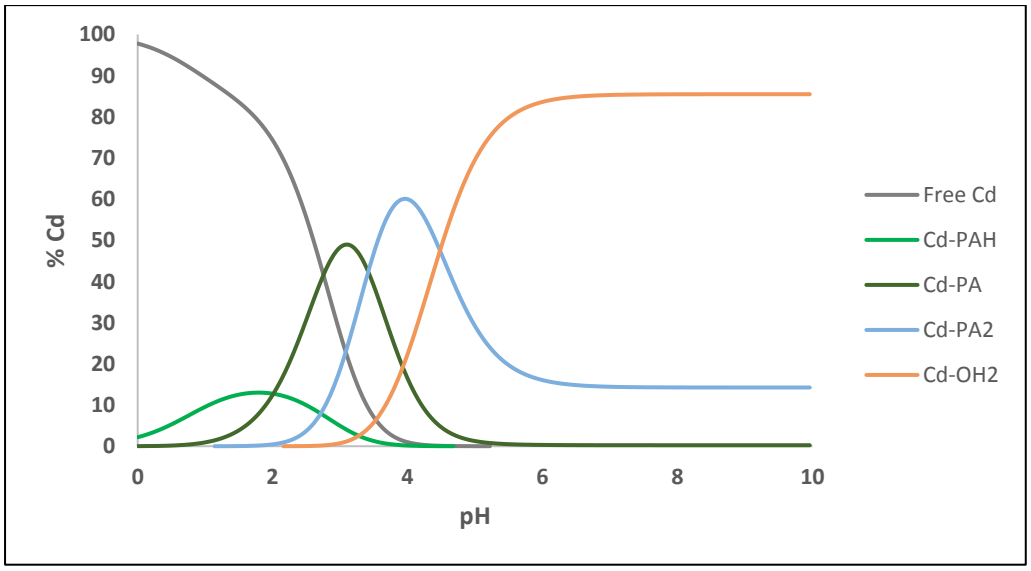


Figure 4.9. Species distribution diagram of 1×10^{-4} M Cd^{2+} and 0.015 M PA.

4.2.2. Thick vs Thin Film

Up until now, the mercury film which was used had been plated for 120 s at -900 mV (vs. Ag/AgCl). In an attempt to solve the problem of irreproducibility and instability of the MFE, a thicker film was plated and used with the hope that it will be more stable and therefore more reproducible. Ideally, a thicker film should degrade slower and last longer in solution. Figure 4.10 shows the voltammograms for free Cd^{2+} and Cd^{2+} in the presence of PA obtained at a thicker mercury film plated at 240 s. Not only are positive shifts seen again but it is clear that the problem of instability or possible adsorption of ligand persist as was observed by a huge drop in current when ligand was added to the solution. It appears that the thickness of the film electrode did not improve the stability of the film in solution. The magnitude of the current is about 100 µA less than that obtained when using a thin film. This implies that thinner films give higher currents because the volume of the mercury where Cd^{2+} is dissolved is small so there is a higher diffusion rate of the Cd^{2+} to the bulk solution. Positive potential shifts that could not be explained were still observed. This experiment was also conducted three times and the results were consistent. Succeeding ex-situ experiments were conducted using a thin film.

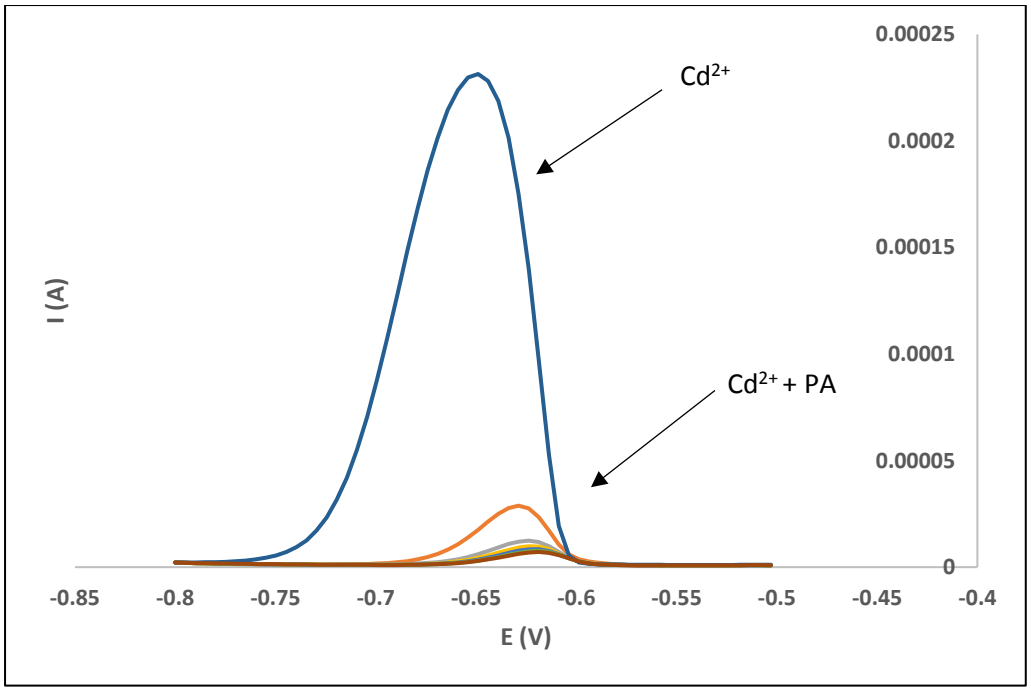


Figure 4.10. DPASV at MFE for 10^{-4} M Cd^{2+} and 0.015 M PA. The study was done in 0.1 M HNO_3 with Cd deposited at -800 mV for 60 s and with mercury preplated for a longer time (240 s).

4.2.3. An Attempt to Stabilise the Film

As seen in Figure 4.7, the first few voltammograms differ more significantly from the rest so we tried to "stabilise" the film before the ligand was added. The free Cd^{2+} measurements were run about eight times and then only was the ligand added. Figure 4.11 shows that this time the drop in current upon ligand addition is much less compared to the previous attempts. However, it then appeared that the integrity of the film is lost as can be seen by very low currents as highlighted in Figure 4.10. This indicates that the film does not last longer than 10 successive voltammograms or that adsorption of PA reduces the activity of the film significantly. Unfortunately, we did not microscopically examine the film after the measurements to see if it is there or not.

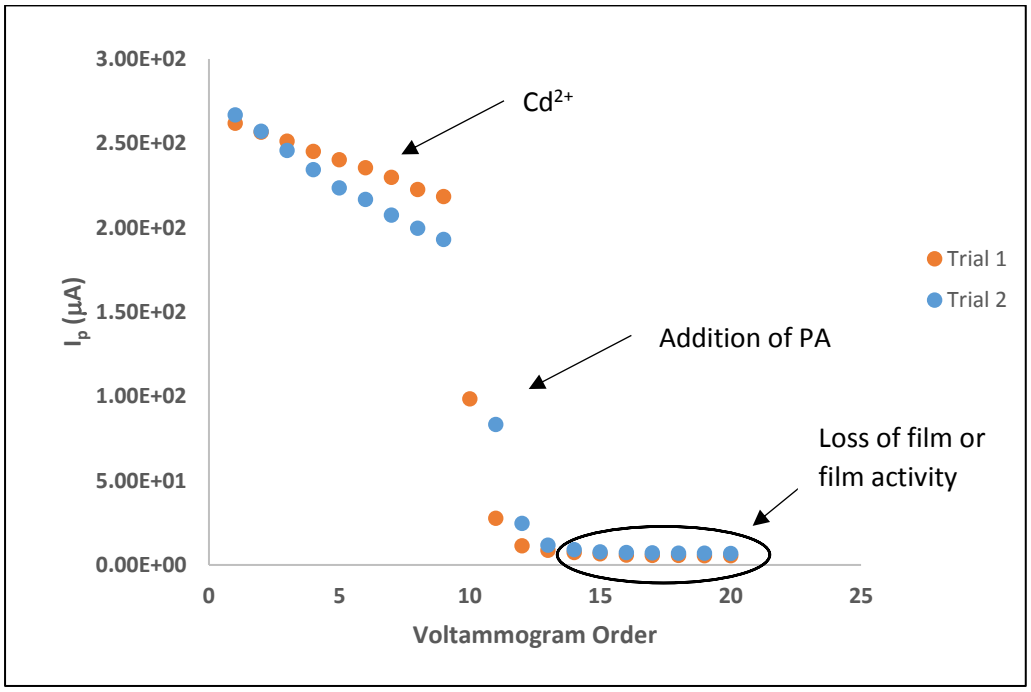


Figure 4.11. DPASV at MFE for 10^{-4} M Cd^{2+} and 0.015 M PA. The study was done in 0.1 M HNO_3 with Cd^{2+} deposited at -800 mV for 60 s and with mercury preplated at 240 s.

4.2.4 Effect of pH

As a last attempt to stabilise the film for ex situ analysis, the effect of pH was considered. With all the previous attempts the free metal measurement was done in a pH 1 solution. The ligand added was at pH 3.8 and then pH was not monitored thereafter when metal and ligand were in solution.

In this case, both the solution containing Cd^{2+} and the ligand solution were adjusted to pH 3.8 and the measured voltammograms are shown in Figure 4.12. This time a significantly smaller drop in current

was observed, but this decrease may still be problematic in complex formation studies. The voltammograms for free Cd^{2+} solution at pH 1 on a thin film gave currents above 300 µA and thick films gave above 200 µA and a pH 3.8 gave current only slightly above 100 µA (on a thin film). Even though the experiment at higher pH gave small magnitudes of the current, it is by far the most reproducible environment to carry out an ex situ metal- ligand system study. Negative potential shifts were observed this time indicating complex formation. This agrees will with the species distribution diagram in Figure 4.9 where at pH 3.8 there are various Cd-PA complexes formed.

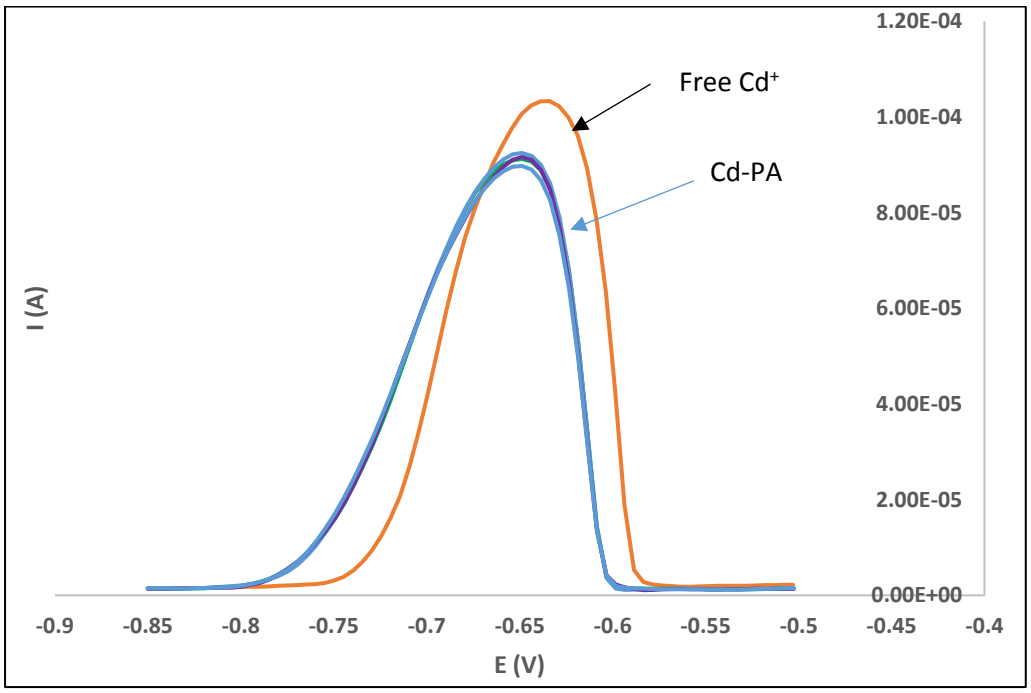


Figure 4.12. DPASV at MFE for 10^{-4} M Cd^{2+} and 0.015 M PA. The study was done at pH 3.8 with Cd^{2+} deposition at -800 mV for 60 s and with mercury preplated for 120 s.

The ex situ plating of the MFE was proven not to be the best technique to use in complex formation studies. Additionally, a pH titration cannot be used because of the significantly different behaviour of the film at pH 1 and 3.8 as shown in Figures 4.9 and 4.12, respectively. If the film stability and the extent of ligand adsorption depends on the pH then complexation has to be done at a fixed pH which means that only ligand titrations can be used for complex formation studies. Even though there are problems with irreproducibility with the film, this section has highlighted the importance of controlling the pH. We also showed the effect of ligand in Figure 4.9 where there was a huge drop in current when the ligand was added, which is suspected to be due to ligand adsorption on the mercury electrode. It was therefore decided to investigate the performance of in situ plated MFEs to see if they would be more suitable for complex formation studies.

4.3. In Situ Analysis of Cd^{2+}

4.3.1 Reproducibility Study

In situ analysis (as explained in section 1.6.1) would involves having both Hg^{2+} and Cd^{2+} present in solution. The mercury film is plated simultaneously with the reduction of Cd^{2+}. When ligand is introduced in solution, complex formation can thus occur between the ligand and both metal ions. One issue is that complexation of the mercury may change the characteristics of the film that is plated. Another issue is that competition for the ligand between Cd^{2+} and the Hg^{2+} would occur. The desired complexes to be studies in this case was the Cd-PA complexes, but PA also has a high affinity for Hg^{2+}. Formation constants (as log β values) of the Hg^{2+}-PA system are 7.70 and 15.55 for the ML and ML_2 species, respectively, The formation constants were reported at 20°C and 0.1 M ionic strength from NIST database.[9] These values are large, therefore the formation of these complexes are inevitable. In fact, the affinity of this ligand for Hg^{2+} is higher than the affinity for Cd^{2+} which has log β values of 4.26, 8.16 and 10.76 for ML, ML_2 and ML_3 species, respectively. These formation constants were also measured at 20°C and 0.1 M ionic strength from NIST database.[9]

In metal-ligand equilibria studies, it is important to know the free ligand concentration in solution and this is obtained by solving mass balance equations when determining formation constants. But in the case of in situ analysis, some ligand is involved in complex formation with Hg^{2+} as well so it complicates the calculation of the free ligand concentration hugely. To simplify this problem, large very excess of ligand was used. In voltammetric studies, generally a large excess of ligand is required, but in this case it would have an additional benefit. If the total concentration of metal ions (both Hg^{2+} and Cd^{2+}) is significantly lower than the ligand concentration, it implies that most of the ligand remains uncomplexed. The change in the free ligand concentration would therefore be negligible after any complexation to the metal ions.

The reproducibility was again tested for free Cd^{2+}, but using the in situ plated film. In the previous ex situ study, the optimised Hg^{2+} concentration for plating a film was 10^{-2} M Hg^{2+} with the deposition potential at -900 mV (vs. Ag/AgCl)for 120 s. For the in situ study, a lower concentration of Hg^{2+} (10^{-3} M) was used so that it was not significantly larger than the concentration of Cd^{2+} which was 10^{-4} M. This was to ensure that in the presence of ligand, large concentrations of ligand would not be consumed in forming Hg^{2+} complexes as compared to the Cd^{2+} complexes. However, it is required that the Hg^{2+} concentration be at least ten times higher than the Cd^{2+} concentration for in situ analyses.[10] Since this Hg^{2+} concentration was lower, a longer plating time was needed to achieve the same film coverage that was used in the ex situ analysis. Since this was an in situ study, the deposition potential and time applies to plate both Hg^{2+} and Cd^{2+}. A deposition potential of -900 mV for plating the film

would also simultaneously deposit Cd^{2+} which is reduced at about -580 mV. A DPASV experiment was run by simply measuring eight voltammograms consecutively, without cleaning the electrode in between or stripping the mercury film. Figure 4.13 shows the reproducibility at different deposition times. Initially 180s was used but it was observed that there was a constant increase in current as shown in Figure 4.13. When a deposition time of 300s was tested it was found to produce a fairly constant current throughout. This was then taken as the optimum t_{dep} for an in situ analysis. This is the most reproducible data obtained so far.

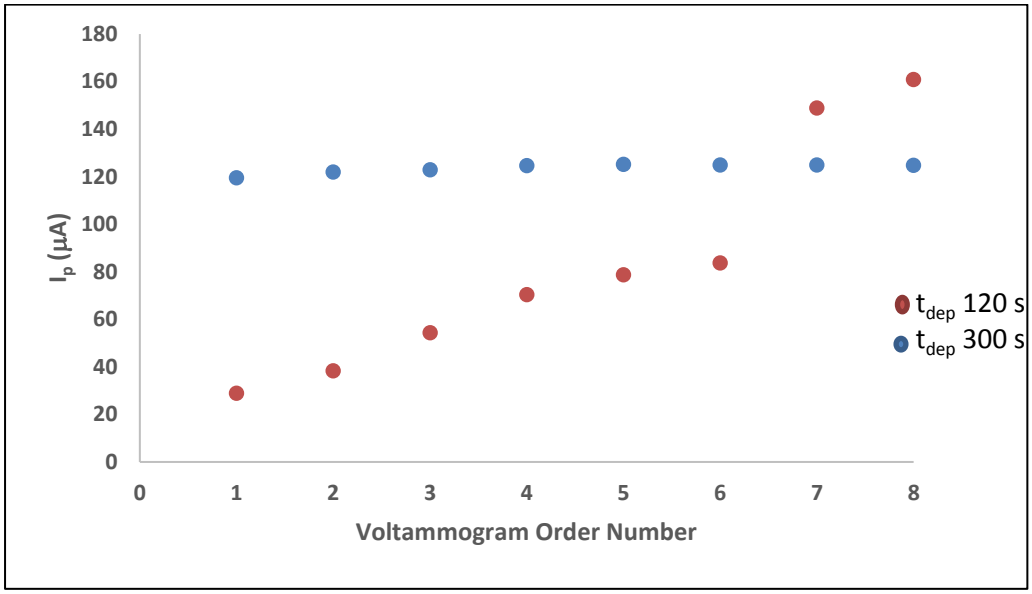


Figure 4.13. I_p from consecutive DPASV measurements at a MFE for 10^{-4} M Cd^{2+} in 0.1 M HNO_3 with 10^{-3} M $Hg(NO_3)_2$. Measurements were done at E_{dep} = -900 mV with various t_{dep}.

A reproducibility study was then done in the presence of ligand, incorporating the optimised t_{dep} value for plating both Hg^{2+} and Cd^{2+} simultaneously. The pH of the solutions were again adjusted to 3.8. Two voltammograms were first measured in a solution without ligand and the Cd^{2+} oxidation peak analysed, thereafter 150 times more ligand than Cd^{2+} was added. Although the first data point in the absence of ligand was lower than the rest, Figure 4.14 clearly shows that there was no drop in current upon addition of the ligand, unlike that observed for the ex situ analyses already discussed.

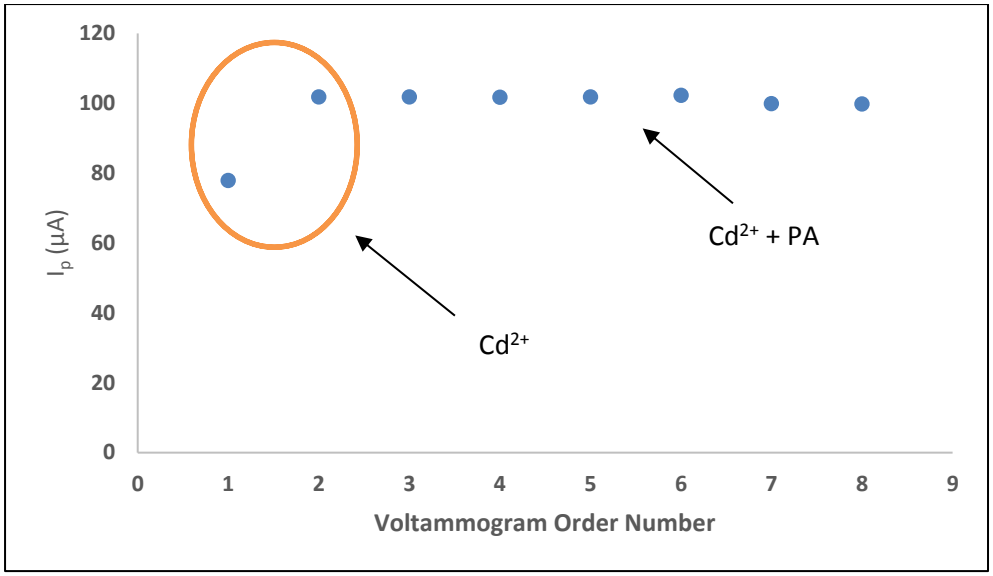


Figure 4.14. DPASV peak currents at the MFE for 10^{-4} M Cd^{2+} (with 10^{-3} M Hg^{2+}) and 0.015 M PA. The in situ study with solutions adjusted to pH 3.8 using E_{dep} = -900 mV and t_{dep} = 300 s.

4.3.2. Full pH Study of Free Cd^{2+}

The initial studies done so far, especially for ex situ analysis, have indicated that the response of the MFE seems to be dependent on pH. Formation constants can be studied by either a pH titration or a ligand titration. The latter requires that the pH be kept constant while the ligand-to-metal concentration ratio is increased. But, this also requires that the ligand titration be done at various pHs to get formation constants for various complexes formed at different pHs. A pH titration is more ideal for formation constants studies because it immediately gives an overall view of the metal-ligand system and the various complexes formed at different pH values.

To investigate whether a pH titration is feasible using in situ film formation, a pH study was done using the already optimised experimental parameters initially in the absence of ligand. The DPASVs were measured in solution at a range of pHs (from pH 1 to 7) and the voltammograms were critically analysed. An ideal pH titration should produce a response for the free metal ion, i.e. the peak current, peak potential, peak width and the overall shape of the peak that is not influenced by pH. This study would also give us some insight into which pH values would be suitable for a ligand titration. For consecutive voltammograms measured at pH 1, 1.5 and 2 in Figure 4.15 we observed a broad peak at more negative potentials than that for Cd^{2+} oxidation which increased in current with each measurement. It was initially thought that this could be caused by H_2 evolution as these humps disappeared at higher pHs, but it is not definitive. Voltammograms obtained at pH 2.5 and 3 (Figure 4.15 and 4.16) had flat baselines and showed no significant decrease in current or potential shift

(except the first voltammogram was always slightly different). The voltammograms are not symmetrical, if this remains the same throughout the titration experiment both in the presence and absence of the ligand, it should not really affect the results.

From pH 4 to 7 in Figure 4.16 we see very distorted voltammograms whereby multiple peaks were present. It was initially thought that impurities were introduced from the KOH solution that was used to adjust the pH, but when using a different source of KOH the issue persisted. These results clearly ruled out the use of pH titrations for complex formation studies using MFEs. In order to test if it was viable to do a ligand titration when using MFEs, pH 2.5 to 3 would be recommended as the initial test since the voltammograms had no double peaks, gave flat baselines and reproducible data. This work was not only for determining Cd at different pH but also mercury film being plated at different pH in situ and it was found that H_2 evolution and rapid film degradation are more pronounced at low pH.

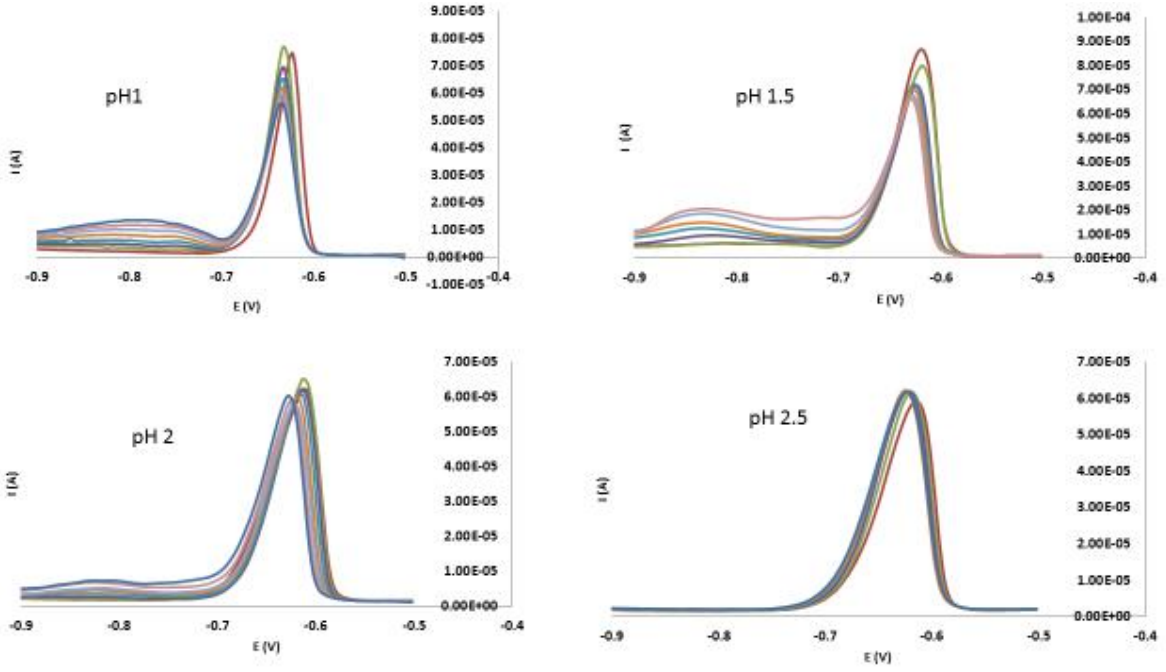


Figure 4.15: DPASVs of 10^{-4} M Cd^{2+} at a MFE obtained from solutions at pH 1, 1.5, 2 and 2.5, also containing 10^{-3} M $Hg(NO_3)_2$. The in situ study was done in HNO_3 with E_{dep} = -900 mV and t_{dep} = 300 s. The voltammograms with the highest currents were the first to be measured.

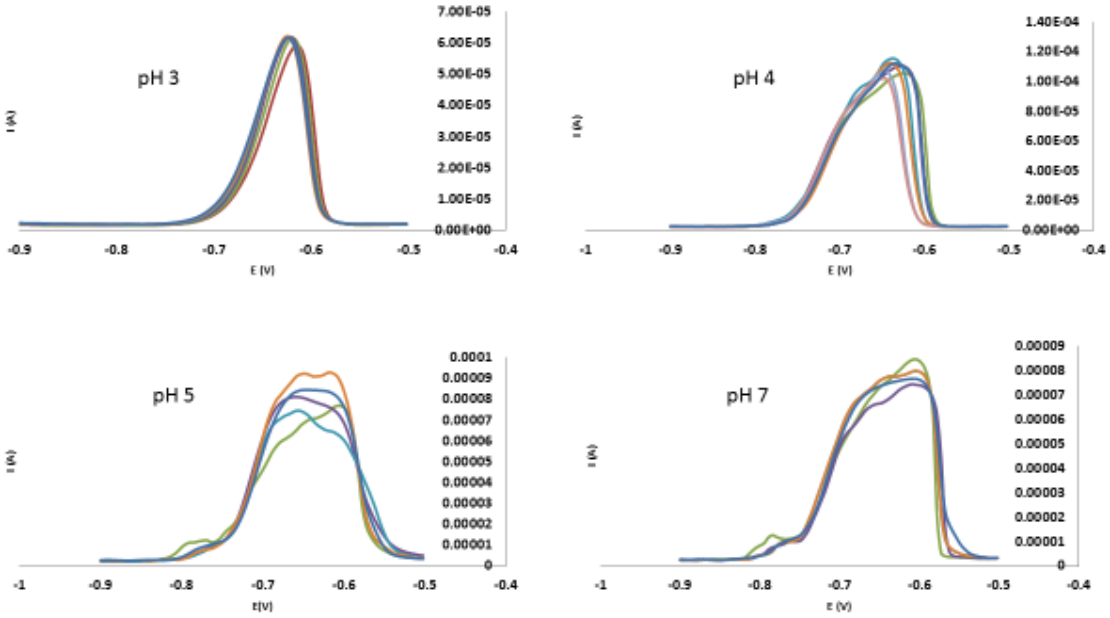


Figure 4.16: DPASVs of 10^{-4} M Cd^{2+} at a MFE obtained from solutions at pH 3, 4, 5 and 7, also containing 10^{-3} M $Hg(NO_3)_2$. The in situ study was done in HNO_3 with E_{dep} = -900 mV and t_{dep} = 300 s. The voltammograms with the highest currents were the first to be measured.

4.3.3. Cd^{2+}-PA system

The ligand titration to study the Cd^{2+}-PA system using an in situ plated MFE was attempted at pH 2.5. For the ligand titration, a very large excess of ligand was used (as explained in section 4.3) with up to 1500 times more ligand than Cd^{2+} (and therefore 150 times more ligand than Hg^{2+}). However, at this higher PA concentration, the reduction of PA itself (which has been reported before[8]) seemed to interfere with the oxidation peak of the Cd^{2+}. This can be seen by an increase in the background current during the course of the ligand titration as the ligand concentration is increased (Figure 4.17). The resulting voltammograms were extremely difficult to analyse to obtain accurate peak potentials and currents and therefore could not be used as a reliable representation of the Cd-PA system. Also the fifth voltammogram (in green) has a large increase in peak current for Cd oxidation this is not expected, there should be a decrease in current due to dilution. This must be some effect due to the film

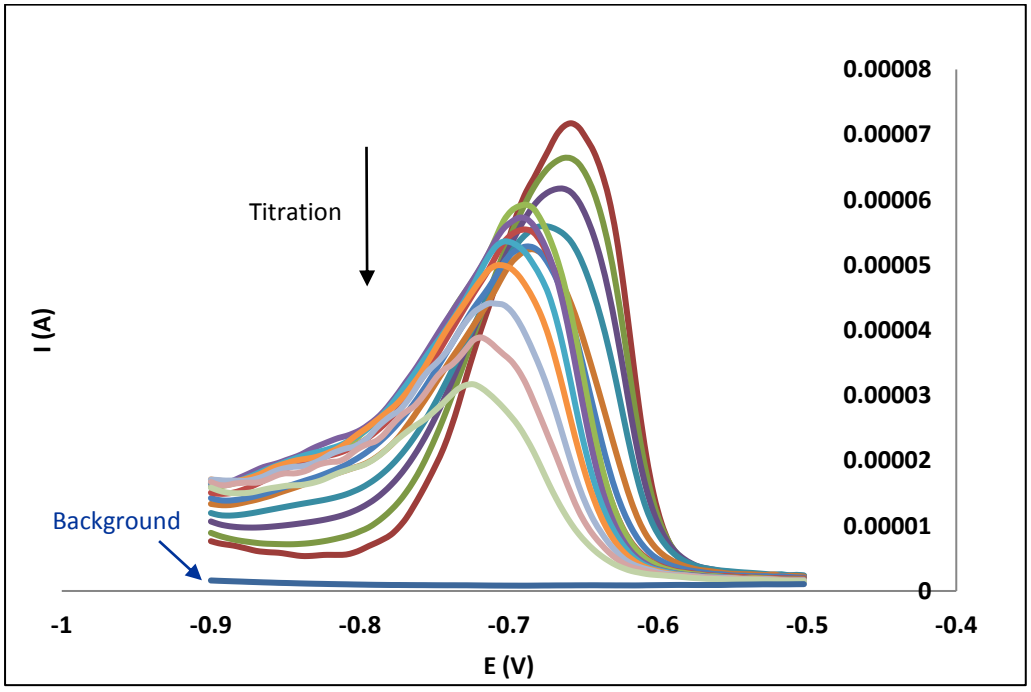


Figure 4.17: DPASVs obtained from the ligand titration at an MFE for 10^{-4} M Cd^{2+} and PA in the range [L]:[Cd] = 100-1500. The in-situ study was done in HNO_3 pH 2.5 with E_{dep} = -900 mV and t_{dep} = 300s at 0.1 M ionic strength.

We then attempted to use an alternative ligand that would not be susceptible to reduction. But, before the ligand could even be added for the ligand titration to commence, the issue of the presence of split peaks for the Cd was observed at the MFE (as seen in Figure 4.18 where the voltammograms

were measured consecutively). At this point it became clear that there are other issues associated with the study of Cd^{2+} at the MFE and therefore not the best metal ion to consider for this initial investigation. The solutions that were used were changed over and over again to eliminate any suspicions of contamination of the solutions but this did not help. Since the background produced a flat line it indicated that there was no contamination in the background that could have resulted in these double peaks.

In literature we found that similar peak splitting has been observed by Serrano *et al.*[11,12] where Pb^{2+}, Cd^{2+} and Zn^{2+} where studied ex situ on bismuth films. In their studies, Cd^{2+} produced two overlapping peaks in one voltammogram. The peak spitting was largely influenced by deposition time and concentration of Cd^{2+}. In their study, double peaks formed at higher concentrations of Cd^{2+} and when the metal ion was titrated with ligand (phthalate), the double peak would start disappearing and eventually a single peak would be observed. Also, more pronounced double peaks would form at higher deposition times. In the case of the Zn^{2+} study, an anomalous behaviour was observed during a ligand titration where positive and then negative potential shifts were seen. They reported that this could be due to two layers of the film occurring during film deposition. Zn^{2+} complexation could be occurring on the external electrode film layer and then on the internal layer hence positive and then negative shifts. This could possibly also explain some of the anomalous behaviour we saw earlier in our work (Figure 4.8 and 4.10) where positive shifts where observed upon addition of ligand. The authors concluded that a possible explanation for the peak splitting and anomalous peak shifts could be a result of the deposition step where two associative mechanisms or two layers of the films may be occurring. In their work, Pb^{2+} produced normal shaped peaks over a wide concentration range, thus we rather moved our focus to study Pb^{2+} complexation on MFE.

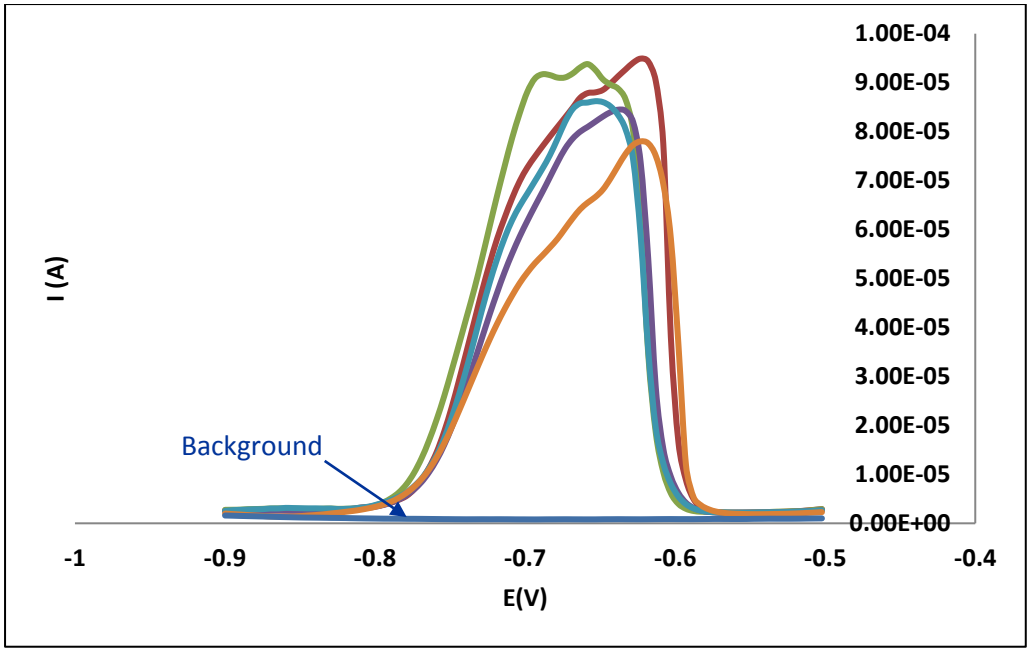


Figure 4.18: DPASVs for 10^{-4} M Cd^{2+} at a MFE. The in-situ study was done in HNO_3 at pH 2.5 with E_{dep} = -900 mV and t_{dep} = 300s.

4.4. In situ Pb^{2+} Analysis

4.4.1. Reproducibility Study

From section 4.3.3 it was discussed that Serrano *et al.*[11,12] produced single peaks for Pb^{2+} that were not split when using an ex situ plated bismuth film electrode using ASV, so we decided to see if Pb^{2+} was a better candidate to use to study complex formation on MFEs instead of the problematic Cd^{2+} that resulted in split peaks. The electrochemical response of free Pb^{2+} was studied on in situ plated MFEs at different pHs to see the reproducibility of the Pb^{2+} peak and the influence of pH using the procedure described in section 2.3. The HNO_3 background (at different pHs) contained 10^{-3} M Hg^{2+} and 10^{-4} M Pb^{2+}. The deposition potential and deposition time were -900 mV (vs. Ag/AgCl)and -300 s, respectively. The other measurement parameters used are those listed in Table 2.2. DPASV measurements were made consecutively about ten times at pHs between 1 and 4 (except at pH 5 where only 5 measurements were made) for free Pb^{2+}. It was observed that there were large drops in current and shifts in potential, usually between the first three voltammograms. Therefore, analysis was done without the first three voltammograms as in section 4.1.2. The peak potentials (vs. Ag/AgCl), peak currents and the width of the peaks at half their height (as determined using the NOVA peak analysis software) were averaged and the results are shown Table 4.2. The peak potential obtained by this process is not the most accurate (because a 5 mV step potential was used, as explained in section 3.1) but it does give us an indication of whether the peak potential is shifting significantly. The standard deviation of the peak potential at most pH values is 4-8 mV (except pH 4 where it is 13 mV). Although this is only an indication, a standard deviation of at most 2 mV would be ideal. Even though the actual value of the peak potential is slightly different at each pH, the average value is 395 ± 4 mV. Also, the actual value of the peak potential can change slightly if the reference electrode system changes slightly (this could explain why the value at pH 5 is small). Also, below pH 2 the diffusion junction potential affects the potential reading.

The magnitude of the peak current increases with increasing pH. The slight variation in the peak current between experiments could be expected due to the mercury film not always being the same. The fact that we generally see lower peak currents at lower pHs probably indicates faster film degradation especially with the higher standard deviation (16 µA) at pH 1. The relatively higher film degradation at pH 1 due to the acidity can also be seen in the voltammograms in the Appendix A4.1 at pH 1. It is also possible that at acidic pH the very negative deposition potential (-900 mV) could have resulted in a small amount of hydrogen evolution. The increase in the magnitude of the peak current with increasing pH indicates that pH has an influence on the voltammograms measured thus a pH titration would not be feasible.

Table 4.2: The average and corresponding standard deviation for the peak potentials, peak currents and peak widths of 7 voltammograms measured consecutively at various pHs. The solution contained 10^{-4} M Pb^{2+} and 10^{-3} M Hg^{2+} and E_{dep} = -900 mV and t_{dep} = 300 s.

pH	**E_p (mV) (vs. Ag/AgCl)**	**I_p (μA)**	**$W_{1/2}$ (mV)**
1	-392.8 ± 3.8	128 ± 16	48.5 ± 0.9
1.5	-395.7 ± 4.5	118.0 ± 1.1	60.4 ± 2.5
2	-397.1 ± 4.5	133.8 ± 1.6	70.0 ± 6.2
2.5	-394.2 ± 8.2	140.9 ± 3.5	76.3 ± 8.2
3	-402.9 ± 3.8	146.5 ± 1.8	67 ± 26
3.5	-396.4 ± 6.4	152.4 ± 2.9	76.8 ± 8.8
4	-395 ± 13	154.7 ± 3.9	78 ± 17
5	-388.7 ± 5.7	152.4 ± 3.6	84.7 ± 3.5

The peak width increases quite significantly as the pH is increased. This shows that the electron transfer process becomes less reversible with the increasing pH. From the graphs in Appendix 2(see Figure A2.1) it also became clear that the peaks become more asymmetric as the pH increases, again indicating a decrease in reversibility. The dilemma is that more reversible peaks are at lower pH where film degradation is more rapid as seen by the drop in current.

Figure 4.19 shows the fifth voltammogram selected at each pH. Here it can clearly be seen that there is an increase in peak current and width with increasing pH as well as a slight negative shift. A pH titration is thus not feasible to use in an experiment to determine stability constants because these parameters are influenced by the pH; a ligand titration will thus be used. The voltammograms for all pHs can be found in Appendix A2.1. A general observation in these voltammograms is the small negative current that is seen just after the Pb^{2+} peak in some cases. It is unclear what causes this but the suspicion is that it could be caused by the film. Fortunately, these negative currents do not affect peak analysis because they did not overlap with the peak of interest. At pH 5 some peak splitting was seen and hence only five voltammograms could be recorded. From this initial work it would be recommended that the ligand titration experiments not be done at pH 1 because of the significant film degradation or at pH 5 because of peak splitting. Ligand titrations were thus carried out at pH 4 and will be discussed in the following section.

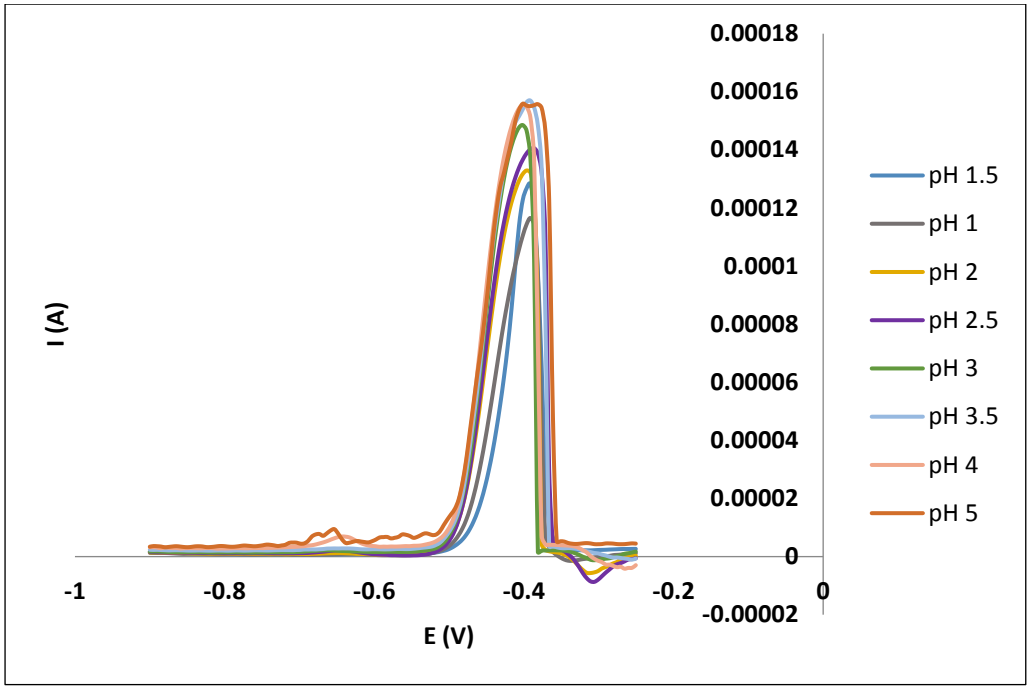


Figure 4.19: The fifth voltammograms of 10^{-4} M Pb^{2+} (and 10^{-3} M Hg^{2+} in situ plated) at different pHs (E_{dep} and t_{dep} at -900 mV and 300 s, respectively).

4.4.2. In Situ Lead-Glycine (Pb-Gly) Complex Formation Studies

Following insights gained from the reproducibility studies at different pHs, a ligand titration for the Pb-Gly system was done at pH 4.01. The detailed description of the procedure followed for a ligand titration is as explained in section 2.3. The initial solution consisted of 10^{-4} M Pb^{2+} and 10^{-3} M Hg^{2+} adjusted to pH 4.01. The deposition time and deposition potential was set at -900 mV (vs. Ag/AgCl) and 300 s, respectively, as before (other parameters as tabled in Table 2.2). DPASVs for free Pb^{2+} was measured about three times before ligand was added to ensure that the free metal current and potential was reproducible. The titrant consisted of 1 M glycine solution (also at pH 4.00) and the titration commenced at [L]:[Cd] = 47 and ended at [L]:[Cd] = 14 375. At each step in the titration a DPASV was measured and the NOVA peak analysis software was used to analyse the voltammograms. Since NOVA peak search does not accurately determine peak potential (as explained in section 3.1), a derivative plot was used to determine the peak potentials. Figure 4.20 shows an example of the derivative plot where the x-intercept gives the peak potential and this was found by fitting a straight-line through data points close to the intercept (Figure 4.21) and using the equation to find the x-intercept.

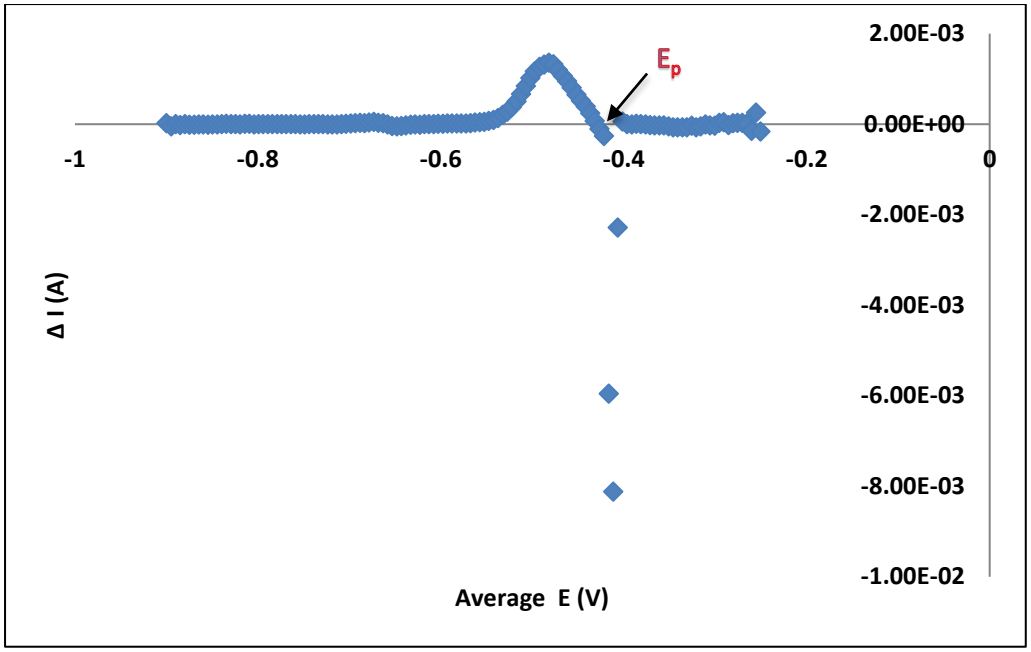


Figure 4.20: Example of a derivative plot of change in current vs average potential for a voltammogram obtained from the Pb-Gly titration.

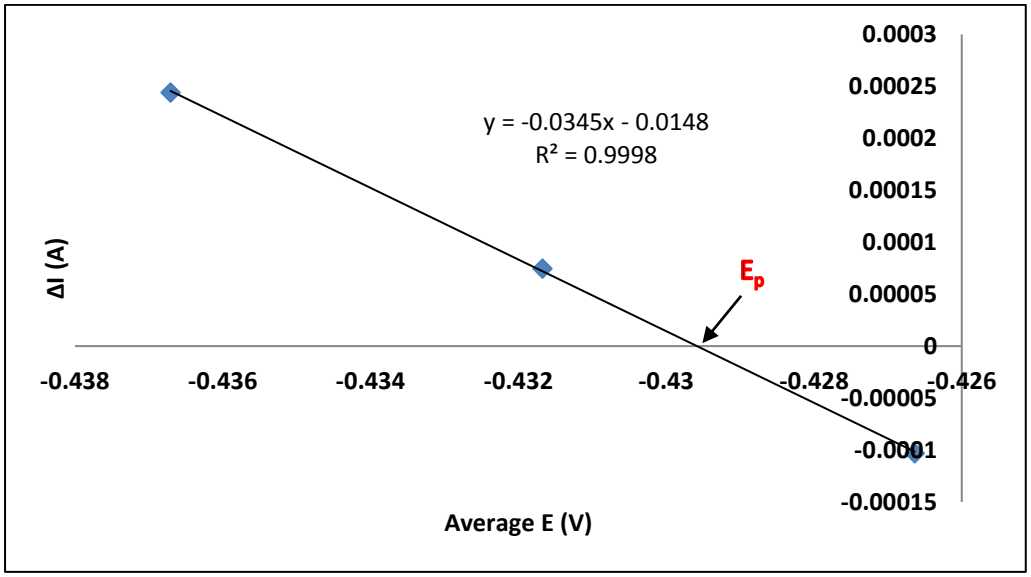


Figure 4.21: The straight-line graph fitted through the points close to the x-intercept (from Figure 4.20) to calculate the peak potential.

Figure 4.22 shows the resulting experimental complex formation curve (ECFC) for this ligand titration. The increase in the corrected potential shift with increasing ligand concentration indicates complex formation. The ECFC data had some noise where in some cases the points that were out could be due to shape of the voltammograms that were obtained (see Appendix A2.2) where some peak splitting had occurred.

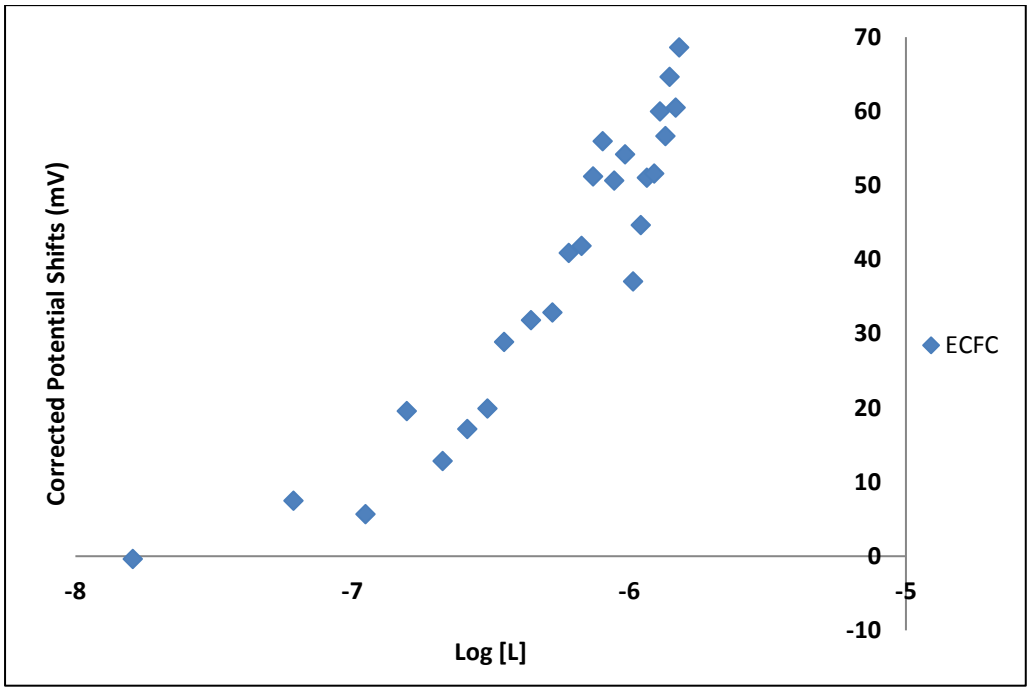


Figure 4.22: Experimental complex formation curve for the Pb-Gly ligand titration at pH 4.01 in the range [L]:[Cd] = 47-14 375 on the MFE.

Figure 4.23 shows both the observed and expected peak currents vs log [L]. The decrease in current in is expected due to dilution when the ligand solution is added. The expected peak currents are calculated from the peak current obtained from the voltammogram for free Pb^{2+} and this is then multiplied by the dilution factor. The fact that the observed currents are similar to the expected currents shows that there was not a bigger than expected decrease in the currents due to the degradation of the mercury film. The ratio of the two currents (I_{obs}/I_{exp}) was calculated at each step in the titration and the average value for all data was 1.07 ± 0.05. Since this ratio is the same as $\frac{I(MComp)}{I(Mfree)}$ in equation 1.1 (section 1.5), this ratio of approximately 1 indicates that the correction term is close to zero as is the case for the formation of the labile species[13] and the potential shift is thus mainly used to calculate the formation constants.

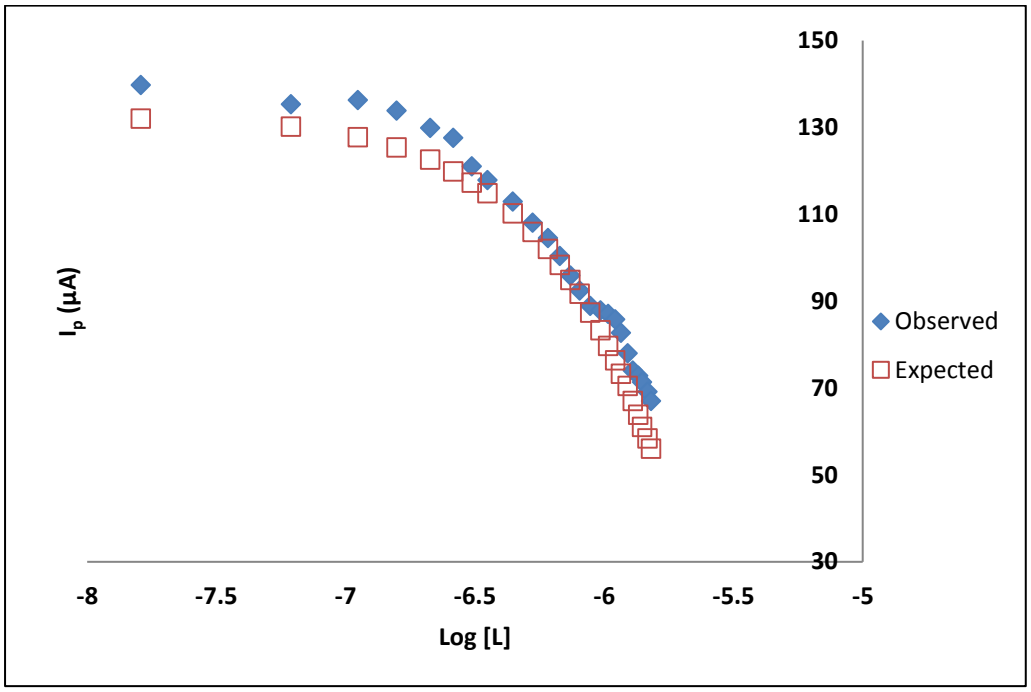


Figure 4.23: Peak current vs log [L] for the Pb-Gly ligand titration at pH 4.01 in the range [L]:[M] = 47-14 375 on the MFE.

Slope analysis is a method of predicting the type of species formed in solution, and it is based on the Nernstian slope which is approximately 60 mV at 25 °C (the temperature at which our experiments were run). The equation for the slope is as follows:

$$\text{Slope} = \frac{\text{Number of ligands} \times 60 \text{ mV}}{\text{number of electrons transferred}} \quad (6)$$

ASV involves the oxidation of the metal from the electrode followed immediately by the complexation process (discussed in section 1.4.2). When doing slope analysis we thus look at this overall process. For example if the process is:

$$M_{Hg} + L \rightarrow ML + 2e^-$$

there is one ligand and two electrons involved, thus the slope would be 30 mV. Similarly, for the formation of ML_2 and ML_3 the slope would be 60 mV and 90 mV, respectively. If the ligand is protonated at the pH at which the ligand titration is is being done, the reaction could be either:

$$M_{Hg} + HL \rightarrow MLH + 2e^- \quad \text{or}$$

$$M_{Hg} + HL \rightarrow ML + H^+ + 2e^-$$

In both cases the slope is also 30 mV. Thus slope analysis is merely a guide to predict which species are formed. Since mass balance equations are simultaneously solved for the free metal ion and free ligand concentrations, and the free hydrogen ion concentration is determined from the measured pH

of the solution, when the actual formation constants are determined using the 3D-CFC software, the difference between ML and MLH species are realised. If there is mixture between two species in solution, for example ML and ML_2, the slope will lie somewhere between the two predicted slopes i.e. between 30 and 60 mV in this case and so on.

Figure 4.24 shows the slope analysis for the Pb-Gly titration. The extreme outliers have been deleted (as indicated on the graph) and a straight line was fitted in three different regions on the graph. According to the species distribution diagram in Appendix A1.5 at pH 4, the dominant form of glycine is the singly protonated form, LH. So the first slope of 15 mV in Figure 4.24 indicates that there is very little complex formation and therefore a small amount of the MLH species could be formed. The second slope of 67 mV could indicate a mixture of ML_2H_2 and ML_3H_3 species because the slope is between 60 and 90 mV, but ML_2H_2 would be dominant in this region. The last slope of 131 mV is abnormally high. Formation of ML_4H_4 and ML_5H_5 would give slopes of 120 and 150 mV, respectively. A mixture of these two would thus be predicted for the high slope. These two species have not been predicted in literature before. The large slope could be due to the very large excess of ligand in this region (as high as [L]:[M] =14 375) or the very noisy data, or it could be due to anomalous film effects.

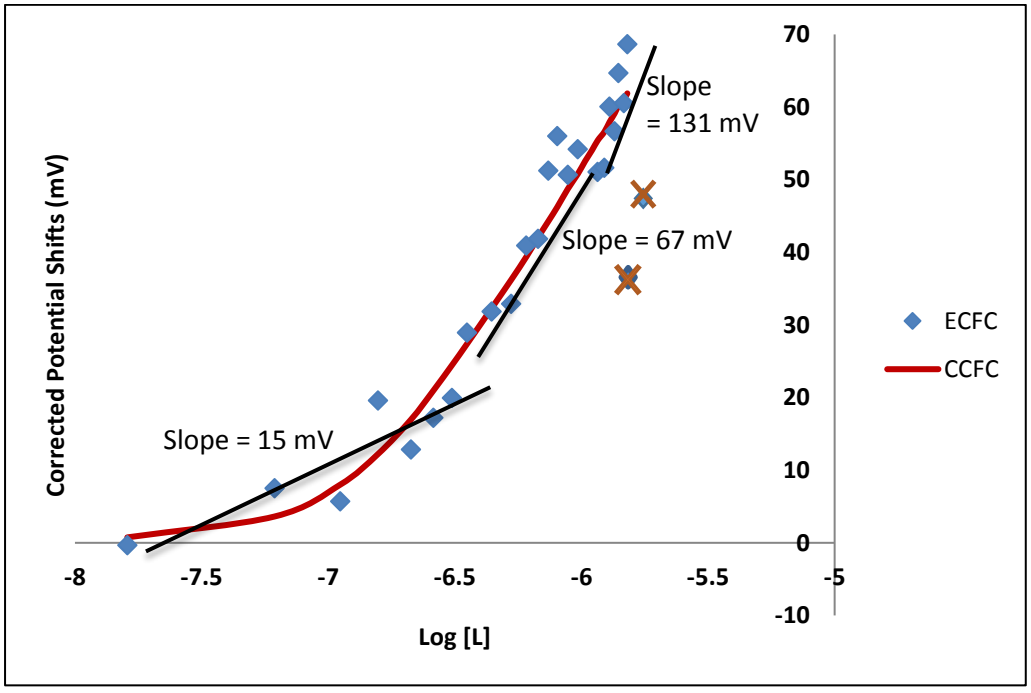


Figure 4.24: Slope analysis of the ECFC for the Pb-Gly ligand titration, also showing the deleted points. The CCFC is also shown.

The ECFC was fitted using the species model MLH, ML_2H_2 and ML_3H_3, giving the CCFC in Figure 4.24 with an overall fit of 31.2. The overall goodness of fit is calculated using equation 5 below.

$$s_{yx} = \sqrt{\frac{\sum_{i=1}^{N} \left(y_i(obs) - y_i(calc)\right)^2}{N - p}} \qquad (6)$$

Where N is number of data points, p is number of fitting parameters and y= corrected potential shifts. This value was fairly large due to the noisy data. The ML_4H_4 species was then added but a model containing both ML_3H_3 and ML_4H_4 could not be refined. It is thus suspected that the high slope is due to noisy data. Table 4.3 shows the refined formation constants that were calculated from this work and these were compared to those reported in literature. The ML_2H_2 value was slightly higher and the MLH and ML_3H_3 values were slightly lower but these formation constants were quiet comparable to the literature values, despite having to deal with the issues of peak splitting that was sometimes seen and some instability of the film. It should also be noted that this titration was done over a range of ionic strengths whereas formation constants are generally reported at a constant ionic strength. In our experiment, a very high concentration of ligand was important to force complexation and simplify mass balance equations (as discussed in section 1.2), but this also changed the ionic strength during the titration (in the range of 0.011 M – 0.578 M). Usually in titration experiments, KNO_3 at high concentration (e.g 0.5 M) is added to keep the ionic strength constant but in this case it would not have been sufficient to keep a constant ionic strength because of the need for a high concentration of ligand.

Table 4.3: Experimentally determined formation constants for the Pb-Gly system at pH 4.01 and 25 °C (0.011 M – 0.58 M ionic strength) together with the literature formation constants[9] at the ionic strength stated in brackets.

Species	**Experimental Values (Log β)**	**Literature Values (Log β)**
MLH	10.61 ± 0.14	11.07 (0.1 M)
$M(LH)_2$	21.67 ± 0.06	20.64 (1 M)
$M(LH)_3$	30.30 ± 0.06	30.78 (0.1 M)

When using Cukrowski's equation (equation 1 in section 1.5) to calculate formation constants, it applies to fully reversible systems. When considering the reversibility of the Pb^{2+} process, it appeared to be not fully reversible at higher pH due to the broader peaks. However, the peaks remained broad

throughout the titration (with the width not changing significantly) and they were similar in the presence and absence of ligand. Also of importance is that when comparing the observed vs the expected currents, they were largely comparable indicating that the extent of the peak broadening and reversibility largely remained the same throughput the titration. Therefore, as in there are no change in the extent of reversibility (and hence changes in the potential shift) and the current ratio used in the calculation is not affected by this, the use of Cukrowski's equation should be acceptable.

A duplicate ligand titration experiment at pH 4.01 was done using the same experimental conditions and parameters as in the first titration above. The data trend in Figure 4.25 is similar to that in Figure 4.24. The overall fit was found to be 27.4 which is slightly lower than the fit if 31.2 found in the first titration. Although this duplicate experiment is less noisy, it also has extreme outlier points. These points were deleted (indicated by red crosses) to avoid them affecting the fitting process. Slope analysis was done and the first region of 13 mV corresponds to a small amount of the MLH species and the 71 mV slope corresponds to a mixture of ML_2H_2 and ML_3H_3 species. The last slope of 108 mV corresponds to the ML_3H_3 species and the fact that its magnitude is not above 120 mV (which was considered as abnormally high in Figure 4.24), indicates that this titration data was less noisy. With the duplicate titrations, , all 3 species are present in significant amounts Figure 4.26 shows the expected peak currents and the observed peak currents which again follow the same trend. The ratio of the two currents was calculated and the average for the ratios was found to be 1.099 ± 0.064 which also indicates that there were no significant decreases in current due to film degradation and gives confidence in the measured data.

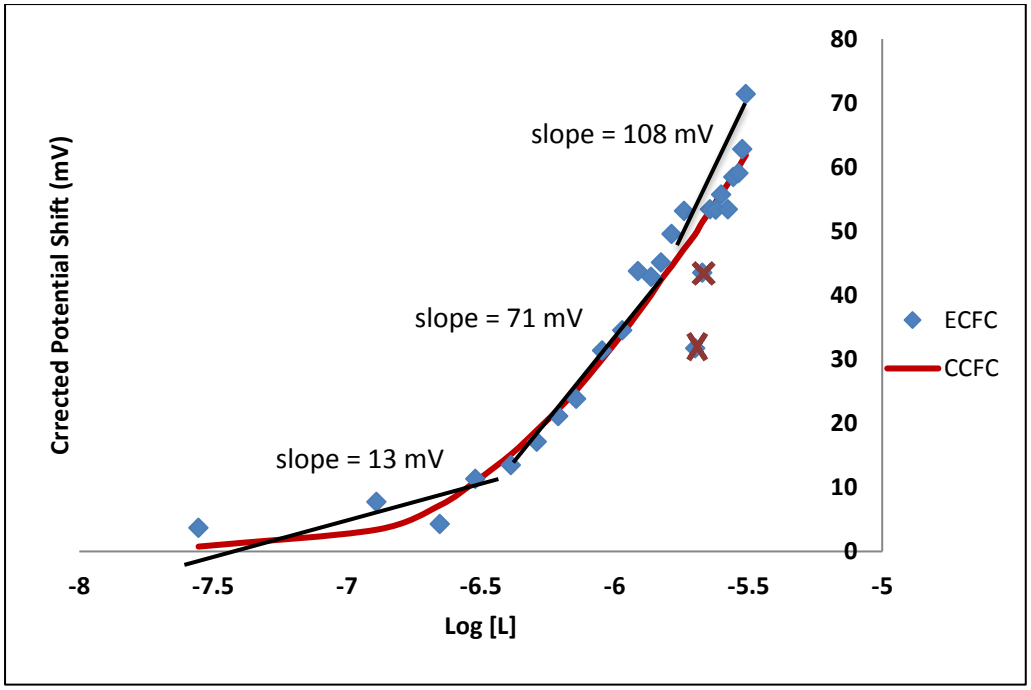


Figure 4.25: Slope analysis of the ECFC and the CCFC for the duplicate Pb-Gly ligand titration.

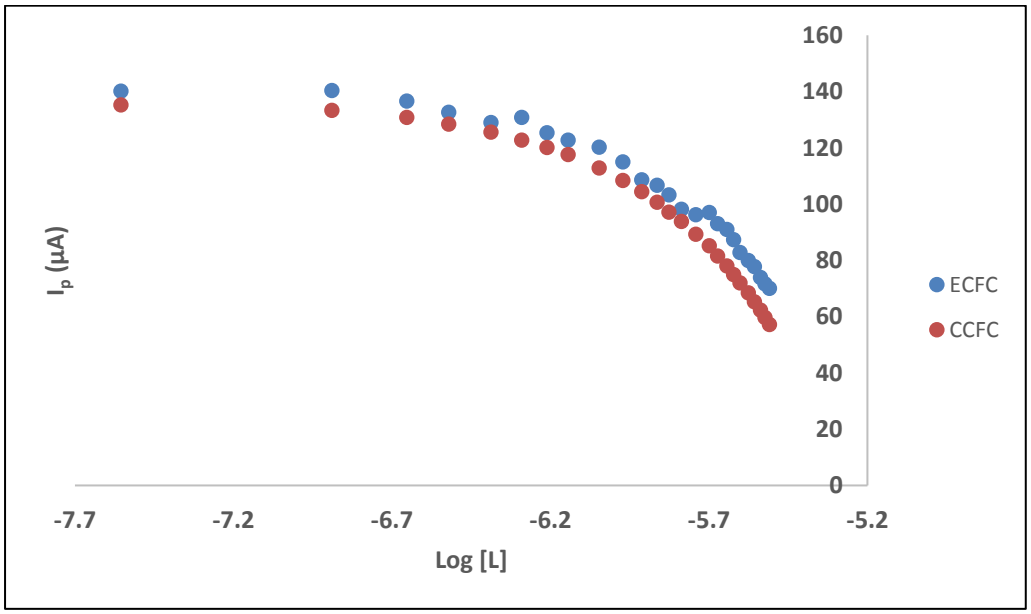


Figure 4.26: Peak current vs log [L] for the duplicate Pb-Gly ligand titration at pH 4.01.

The formation constants for this titration were calculated and are given in Table 4.4 (the column highlighted in red) along with the already reported constants from the first titration, the average of the two titrations and the literature values. These results showed the same trend as the 1st titration with the value for ML_2H_2 slightly higher and the MLH and ML_3H_3 values slightly lower than literature values. The data for the second titration was somewhat lower than the first titration and there is no

real indication in the actual data to indicate why the values were lower. The average values of the two titration experiments was compared to the literature values and the difference can be attributed to factors already discussed such as the fact that the titration was done at a range of ionic strength due to the need of excess ligand and other factors such as less reversibility at high pH (pH 4 in this case) and the sometimes observed split peaks.

Table 4.4: Pb-Gly experimentally determined formation constants at pH 4.01 and 25 °C (0.011 M – 0.578 M ionic strength) and literature formation constants[9] at ionic strengths indicated in brackets.

Species	**Experimental Values (Log β)**	**Experimental Values (Log β) (duplicate)**	**Average of the two titration experiments.**	**Literature Values (Log β)**
MLH	10.61 ± 0.14	10.03 ± 0.21	10.31 ± 0.41	11.07 (0.1 M)
$M(LH)_2$	21.67 ± 0.06	21.02 ± 0.05	21.35 ± 0.46	20.64 (1 M)
$M(LH)_3$	30.30 ± 0.06	30.14 ± 0.15	30.22 ± 0.11	30.78 (0.1 M)

4.5. Ex situ Pb^{2+} Analysis

4.5.1. Optimisation

The in situ Pb^{2+} analysis done in the previous section was demonstrated to be somewhat useful for the determination of formation constants. However, there were problems encountered with the use of film electrodes that could limit their potential use in formation constants determination. These include the inability to do the titration at a constant ionic strength due to the need of a very large excess of ligand and a somewhat unstable film as noticed by the noisy data. Another problem encountered was peak splitting which was observed largely in the Cd^{2+} study and some minor splitting was observed in the Pb^{2+} study (studied in situ). It was then decided try an ex situ analysis study to investigate if the peak splitting would still be observed and also find out how the data for formation constants would compare to those reported using in situ analysis. The film reproducibility study for ex situ analysis had been previously done for Cd^{2+} in section 4.2.1 where it was observed that the film was largely unstable as seen by the large changes in the current and the slight shifts in the potential for consecutive measurements. The degradation of the film was expected for ex situ analysis and has been reported in literature[3] to be a major disadvantage of using ex situ analysis.

The preplating solution used for film formation was 10^{-2} M $Hg(NO_3)_2$ in 0.01 M $KN0_3$ and a deposition potential of -900 mV (vs. Ag/AgCl) and deposition time of 120 s was used. These preplating conditions and parameters were optimised before in section 4.1 and have thus been used in all preplating methods for this ex situ study. The first experiment conducted with the use of ex situ analysis for Pb^{2+} was the optimisation of deposition time and deposition potential. The detailed procedure, conditions and parameters used for this experiment is as described in section 2.3 and 2.4 but in summary, 10^{-4} M Pb^{2+} was added to 0.1 HNO_3 and a DPASV was measured at different deposition potential and deposition time.

In a study by Serrano *et al*.[12], the Pb^{2+} position on a voltammogram was about -650 V on a MFE (using Ag/AgCl reference electrode) for a deposition potential of -950 mV. As a starting point we used deposition potential of -750 mV (at deposition time of 90 s chosen arbitrary) to find the position of Pb^{2+} on our MFE which was found to be at about -450 mV (Figure 4.27). From this, it was also observed that for the -750 mV deposition potential, H_2 evolution occurred from -700 mV. It was then decided that deposition potential of -650 mV (vs. Ag/AgCl) would be used to avoid H_2 evolution. This was then used to optimise the deposition time in the range 90 - 180 s. From Figure 4.28, it was noted that the peak current for Pb^{2+} did not change significantly with deposition time, this could suggest that saturation was reached. On hindsight we should have tested lower deposition times. The width increased as the deposition time was increased and since increase in width is associated with reduced

reversibility, a lower deposition time (90 s) was almost chosen as the optimum because it has the narrowest width, but, it had a more asymmetric and an almost split peak so deposition time of 120 s was instead chosen.

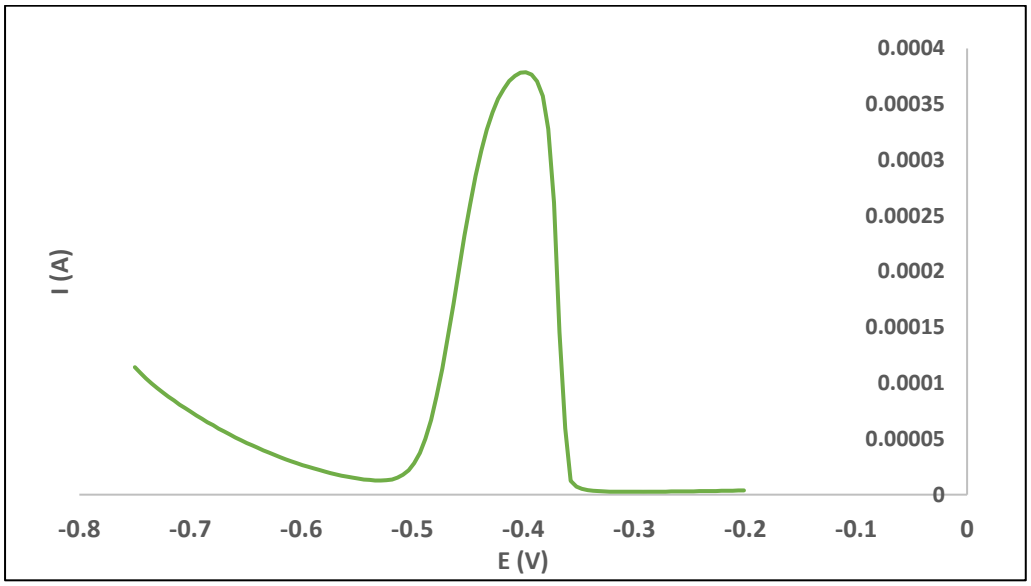


Figure 4.27: DPASV recorded with E_{dep} = -0.75 V and t_{dep}= 90 s showing the position of Pb^{2+} on a MFE.

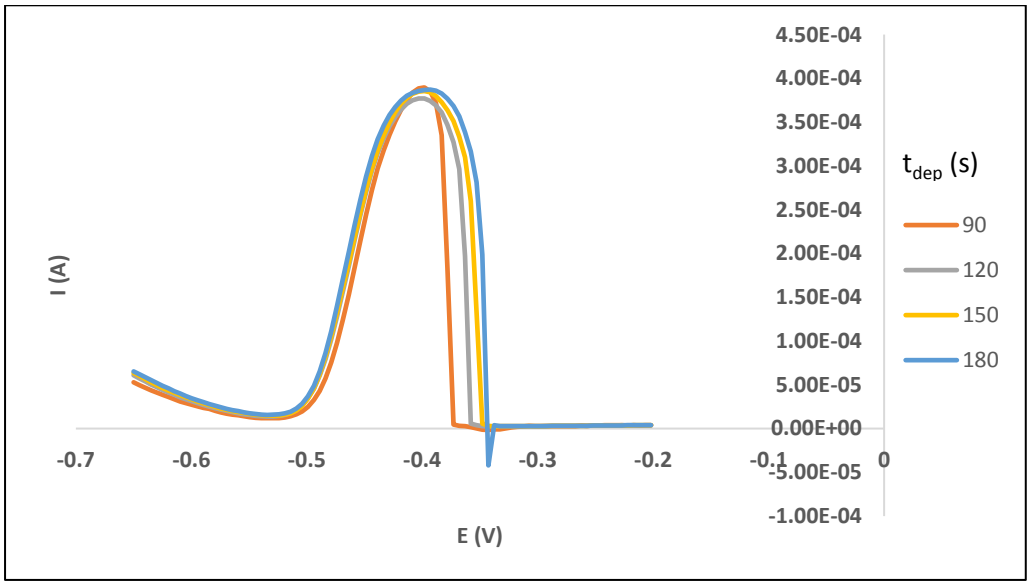


Figure 4.28: DPASV recorded at E_{dep} = -0.65 V of Pb^{2+} at different t_{dep} values.

4.5.2. Reproducibility Study

The reproducibility of the film was studied at various pHs (between 1 and 5). The film was first preplated and then transferred in a solution containing 10^{-4} M Pb^{2+} in HNO_3 which had been adjusted to the pH under study. Voltammograms were then measured consecutively about 15 times (for each pH) using the optimised parameters (deposition potential of -0.65 mV (vs. Ag/AgCl) and deposition time of 120 s). NOVA software was used to determine the peak potential and current and for each voltammogram and the average values are given in Table 4.5. A general observation is that the standard deviations for the peak currents are larger relative to those found in the in situ study (Table 4.2) discussed earlier. This was not unexpected because ex situ plated films degrade rapidly as mentioned earlier.

From pH 2-5, the voltammograms appear broader indicating a less reversibility (Appendix A2.3). There is no observable trend in the peak potential or peak current with pH. One thing that can be picked up from this table is that for pH 1, the standard deviations for the average peak potential and current is the smallest compared to that at other pHs. Peak splitting was observed in voltammograms at pH 2, 3 and 4 (voltammograms in the Appendix A2.3) and it appeared that this was occurring randomly since some voltammograms had split peaks and some did not. In this case, not all the voltammograms could be analysed (with the value of n in Table 4.5 indicating how many were analysed at each pH). At this point it had become clear that peak splitting is not an issue that only occurs for in situ analysis, it is also observed for ex situ analysis. This points to it being an issue that is probably associated with the use of film. It is difficult to predict when peak splitting would occur because it occurs randomly and it is also generally difficult to relate it to pH. However, at this point it appeared that at pH 1 and 5 the least amount of peak spitting occurred and were thus used for further analysis.

Table 4.5: The average and corresponding standard deviation for peak potentials and peak currents of consecutively measured voltammograms at various pHs. The solution contained 10^{-4} M Pb^{2+} and E_{dep} = -0.65 V and t_{dep} = 120 s.

pH	**E_p (mV) (vs. Ag/AgCl)**	**I_p (µA)**	**n***
1.09	-396.5 ± 0.2	325.0 ± 1.3	15
2.07	-370.2 ± 4.6	106.6 ± 0.9	9
3.14	-379.1 ± 8.7	93.1 ± 7.1	8
4.23	-366.0 ± 2.5	99.2 ± 9.5	9
5.18	-382 ± 12	96 ± 35	12

* Although 15 voltammograms were measured at each pH, only n voltammograms could be analysed.

4.5.3. Ex situ Pb-Gly Complex Formation Studies.

Studies of Pb-Gly complexation was done via a ligand titration at pH 1 and 5. Unfortunately no complexation occurred at pH 1 because the ligand is in its fully protonated state at this pH (see species distribution diagram Figure A1.5 in Appendix 1). A ligand titration was done at pH 5.12 following the procedure described in section 2.3 and section 2.4. Ex situ preplating of the film was done as described earlier and then the ligand titration was carried out in HNO_3 containing 10^{-4} M Pb^{2+} at pH 5.12. A 1.0 M glycine solution was titrated to achieve [L]:[M] in the range 47 -14 375. The optimised deposition potential and deposition time used were at -0.65 V (vs. Ag/AgCl) and 120 s, respectively. Figure 4.29 below shows the selected voltammograms that were obtained from the titration. The voltammograms were generally noisy and it appears that severe peak splitting occurred. This type of data would make analysis too difficult and results unreliable.

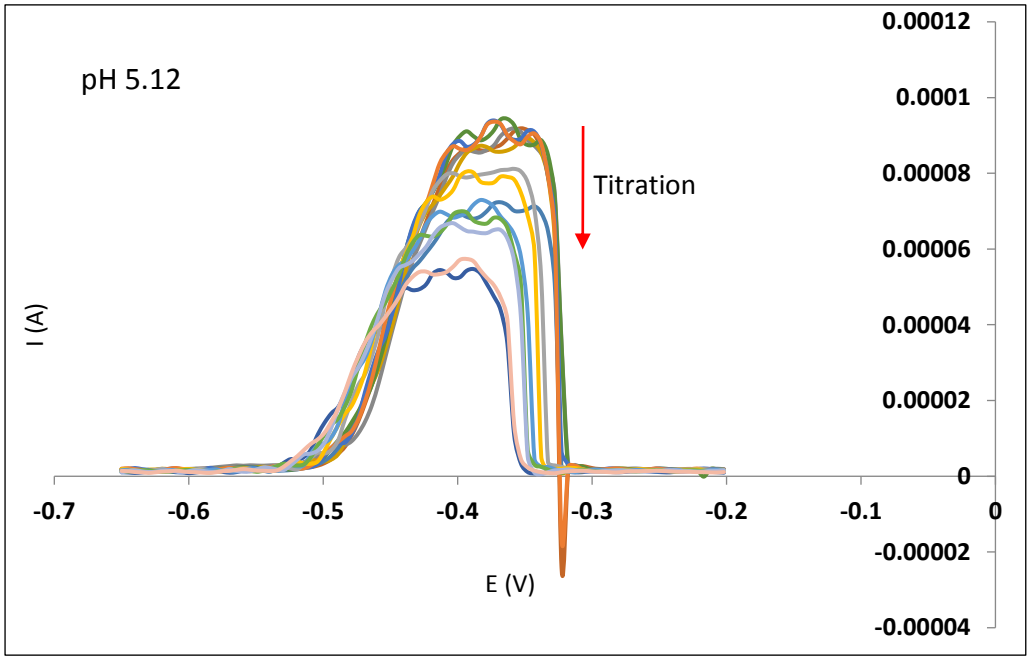


Figure 4.29: Ex situ Pb-Gly titration with 10^{-4} M Pb^{2+} showing peak splitting.

In previous reports[11,12] it was indicated that a high concentration of the metal ion could be a reason for peak splitting because when they lowered the concentration of the metal ion, there was a decrease in peak splitting. We then decided to follow the same idea and lowered the Pb^{2+} concentration from 10^{-4} M to 10^{-5} M. A titration of 10^{-5} M Pb^{2+} at pH 5.12 was done using the same procedure as that used for the higher concentration with the difference being that [L]:[M] was in the range 95 - 12 577. The selected voltammograms shown in Figure 4.30 show a reduced amount of peak splitting compared to

those obtained in Figure 4.29 with the higher Pb^{2+} concentration. This data was much more usable and thus analysed further.

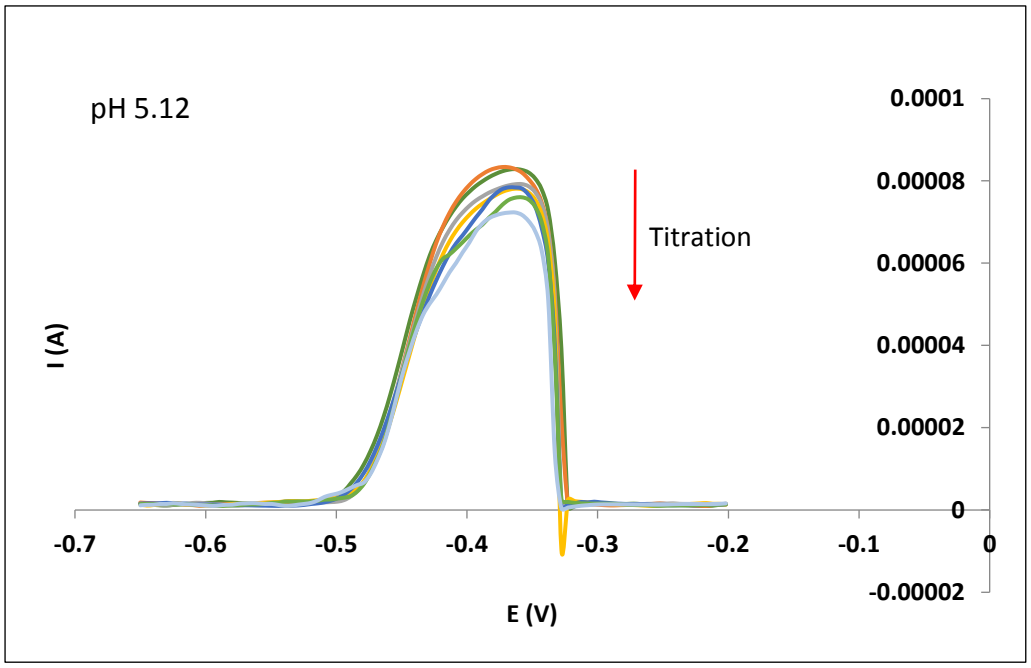


Figure 4.30: Ex situ Pb-Gly titration at lower concentrations (with 10^{-5} M Pb^{2+}) showing a reduced amount of peak splitting.

Figure 4.31 shows the corrected potential shift vs log of the free ligand concentration for this titration. Even though the amount of peak splitting was less in this low concentration titration, the presence of some peak splitting resulted in noisy data and some outlier points were deleted as shown in Figure 4.31. Slope analysis was done on the data and the MLH and ML_2H_2 species were predicted, although the noisy data made this very difficult. The slope of 47.2 mV predicts a mixture of these two species. However, the ML_2H_2 species from the species distribution diagram (Appendix A1.6) is predicted to be below 10% (at [L]:[M] =12 577)so at this point it is difficult to know exactly if ML_2H_2 species did form in this titration. If it did form it would be the minor species and thus the formation constant would not necessarily be accurate.

Figure 4.32 shows that the observed and expected peak currents follow the same trend. The ratio of the currents, I_{obs}/I_{exp}, was calculated to be 1.08 ± 0.05. This again indicates that the correction term in the Cukrowski equation used to calculate formation constants is small and that the shift in potential is the most important parameter in these calculations. Recall that for ex situ analysis film degradation occurs and that is seen by drops in current. Additionally, the reproducibility test at pH 5 gave a very

high standard deviation for the peak current (see Table 4.5). The ratio of observed and expected peak currents being close to 1 is thus a positive results because it indicates ex situ analysis could possibly be used for formation constant determination. In this case, the fact that the observed current is very close to the expected current implies that film degradation is probably not occurring at a significant rate.

The formation constants were calculated for this titration and the results are given in Table 4.6 (highlighted in red). For this titration, only the MLH species is detected when fitting the data for formation constant determination. This is consistent with the species distribution diagram in Appendix A1.6 which shows that MLH is present in 70 % and ML_2H_2 only 8% for the conditions used for the titration. The ML_2H_2 species either did not form or was present in very small amounts to be detected. The MLH value obtained is more comparable to the literature value than those reported using in situ analysis.

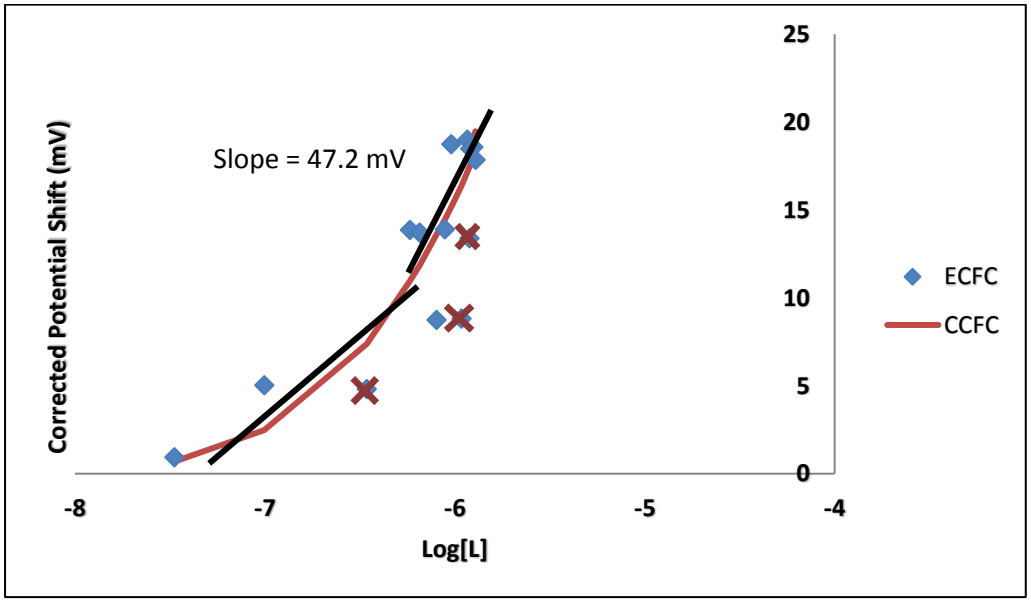


Figure 4.31: The ECFC and CCFC for the Pb-Gly titration at pH 5.12 with 10^{-5} M Pb^{2+}, together with the slope analysis.

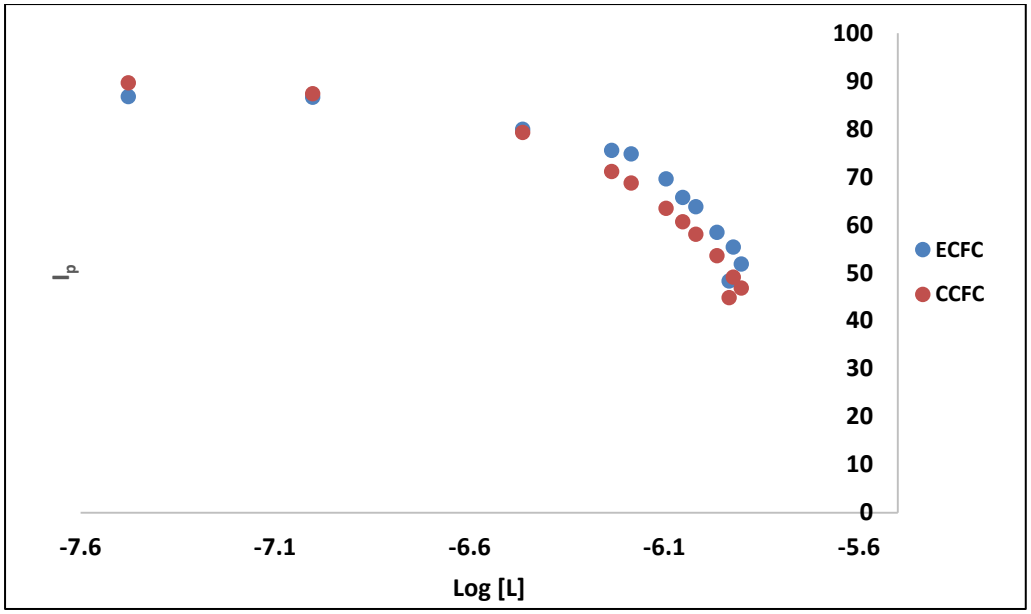


Figure 4.32: Peak current vs log [L] for the Pb-Gly ligand titration at pH 5.12 on the ex situ plated MFE.

Table 4.6: Pb-Gly ex situ experimentally determined formation constants at pH 5.12 and 25 °C (0.001 M – 0.061 M ionic strength) and literature formation constants[9] at ionic strengths indicated in brackets.

Species	**Experimental Log β (In situ, pH 4, [L]:[M] = 46 - 14 375)**	**Experimental Log β (ex situ, pH 5, [L]:[M] = 94 - 12 577)**	**Literature Values (Log β)**
MLH	10.31 ± 0.41	11.33 ± 0.014	11.07 (0.1 M)
$M(LH)_2$	21.35 ± 0.46	—	20.64 (1 M)
$M(LH)_3$	30.22 ± 0.11	—	30.78 (0.1 M)

4.6. Chapter Summary

This chapter focused on the properties and the use of mercury film electrodes. Microscopic analysis revealed the surface morphology of the film and this enabled us to get the optimum conditions to plate a homogenous film. Cd^{2+} and Pb^{2+} were studied on the film and important factors such as instability, effect of pH, lack of reversibility and ligand adsorption on the film were observed. The Cd^{2+} study was largely unsuccessful and therefore discontinued before formation constants could be determined. But, it gave enough insight into the film since most of the preliminary tests were done using Cd^{2+}. In situ and ex situ analysis methods were both used and although both methods have pros and cons, they also have similarities that determine the reliability of MFEs. Peak splitting was seen in both and this became a factor in the complexation study of Pb^{2+}. Nonetheless, formation constants for Pb-Gly were calculated using both in situ and ex situ analysis and the results were fairly comparable to the literature values.

4.7 References

1. Castro, A. A., Isa, A., Cordoves, P., Augusto, P. and Farias, M. *Anal. Chem. Insights* **8,** 21–28 (2013)

2. Billing, C., Cukrowski, I. and Jordan, B. *Electroanalysis* **25,** 2221-2230 (2013).

3. Wu, H. P. *Anal. Chem.* **6,** 3151–3157 (1994).

4. Monterroso, S. C. C., Carapuça, H. M., Simão, J. E. J. and Duarte, A. C. *Anal. Chim. Acta* **503,** 203–212 (2004).

5. Maleki, N., Absalan, G., Safavi, A. and Farjami, E. *Anal. Chim. Acta* **581,** 37–41 (2007).

6. Hoyer, B., Florence, T. M. and Batley, G. E. *Anal. Chem.* **59,** 1608–1614 (1987).

7. Pintado, S., Montoya, M. R. and Mellado, J. M. R. *Electrochim. Acta* **74,** 87–92 (2012).

8. Harrison, J. A. and Sastry, K. S. *Electroanal. Chem. Interfacial Chem* **58,** 387–391 (1975).

9. Martell, A. E., Smith, R. M and Motekaitis, R. J. *NIST Standard Reference Database*, Version 8.0 (2004).

10. Economou, A. *Analyst* **24,** 334–340 (2005).

11. Serrano, N., Alberich, A., Diaz-Cruz, J. M., Arino, C. and Esteban, M. *Electrochim. Acta* **53,** 6616–6622 (2008).

12. Serrano, N., Martín, N., Díaz-Cruz, J. M., Ariño, C. and Esteban, M. *Electroanalysis* **21,** 431–438 (2009).

13. Cukrowski, I. *Anal. Chim. Acta* **336,** 23–26 (1996).

Chapter 5 – Conclusion

The aim of this work was to investigate alternative methods to study complex formation and the focus was on the two methods: Bi^{3+} study and the use of MFE. The study of bismuth at low concentration was expected to prevent early precipitation of bismuth but this was not the case. Formation and precipitation of $BiONO_3$ species still occurred although this happened at a slightly higher pH (about 0.5 pH units higher) and at a slower rate than work done by others[1] with a bismuth concentration 10 times higher than was used in this work. If no precipitation occurred for Bi^{3+} data, we hoped to obtain Bi^{3+} data in the wider pH range. Necessary corrections would be made to determine free Bi^{3+} potential (i.e pH independent potential values as seen with Tl^{+} data) more accurately. But, data was only obtained up to pH 2.7 before $BiONO_3$ was detected. Optimisation of measurement parameters was done to get more reversible Bi^{3+} measurements when using DPASV but this only improved the reversibility to an extent. Bi^{3+} is not fully reversible on DPASV, this was noticed by significantly larger difference between $E(Bi_{free})$ and $E(Tl_{free})$ as compared to previous work[1].

Even though the use of DPASV to study Bi^{3+} was not fully successful, the peak potentials and peak currents vs pH for Tl^{+} data followed trends similar to what was expected hence this technique was not dismissed but used in the second part of the project (MFE work).

Although mercury film electrodes are attractive possible replacements for mercury drop electrodes from an environmental aspect, this study revealed that they are not as robust as the mercury drop electrodes. The study showed that there were limitations in the choice of ligand that could be studied, as some ligands (for example picolinic acid) were found to adsorb on the surface of the film and this had major consequences on the shape of the voltammograms (and hence the peak currents and potentials of these) especially as the ligand concentration was increased. The degradation of the film and peak splitting were the major factors that influenced the study but optimising experimental conditions minimised these challenges faced. For example, the film was more robust at less acidic pH and peak spitting was less pronounced at low concentrations of metal ion.

The study also showed that measurements on the film are pH dependant because the pH affected the shape of the peak. This restricted us to ligand titration which is a problems that was not there with mercury drop electrodes. The in situ and ex situ methods of analysis were compared and it was found that in situ has a more reproducible film and although ligand titrations were done at different pHs, the in situ ECFCs were less noisy. This is because with ex situ method, a single film is used throughout the titration whereas with in situ, the film is replenished at each step when deposition occurs. The problem with in situ is that the ligand complexes with both Hg^{2+} and Pb^{2+} in solution therefore a very

large excess of ligand is needed such that most remains uncomplexed. This simplifies the mass balances equation calculations, drives complexation to Pb^{2+} but, it also significantly changes the ionic strength. Also, since large amounts of ligand is needed, this restricts which ligand be studied (e.g picolinic acid adsorbs to the MFE surface).

Broad asymmetric peaks indicating lack of reversibility were also observed in this part of work. The fact that the peak width remained fairly constant throughout the titration, including for the free metal ion, seems to indicate that when calculating the potential shift these effects are largely cancelled out and therefore does not affect the formation constants determined significantly. Despite the all the challenges faced, formation constants for Pb^{2+}glycine system were determined and are surprisingly comparable to the literature values. This work gave insight into the use of these methods but more work still needs to be done before MFEs can be used to study complexation of unknown systems.

References

1. Billing, C. & Cukrowski, I. *J. Phys. Chem. B* **120,** 4268–4278 (2016).

Appendix 1 – Species Distribution Diagrams

All species distribution diagrams were plotted using the Sol-Eq software.[1]

Table A1.1: Formation constants for the Bi^{3+} hydroxide and Bi^{3+} acetate (Ac) systems as well as the protonation constants for acetate at 25 °C and the given ionic strengths.

	Log β	Ionic strength (M)
$H^+ + OH^- \rightleftharpoons H_2O$	13.78 [a]	0.1
$Bi^{3+} + OH^- \rightleftharpoons Bi(OH)^{2+}$	12.4 [a]	0.1
$Bi^{3+} + 2OH^- \rightleftharpoons Bi(OH)_2^+$	23.5 [a]	1.0
$Bi^{3+} + 3OH^- \rightleftharpoons Bi(OH)_3$	31.9 [a]	0.1
$Bi^{3+} + 4OH^- \rightleftharpoons Bi(OH)_4^-$	33.6 [a]	0.1
$6Bi^{3+} + 12OH^- \rightleftharpoons Bi_6(OH)_{12}^{6+}$	165.3 [a]	0.1
$9Bi^{3+} + 21OH^- \rightleftharpoons Bi_9(OH)_{21}^{6+}$	10.6[a]	0.1
$9Bi^{3+} + 22OH^- \rightleftharpoons Bi_9(OH)_{22}^{5+}$	11.1[a]	0.1
$Bi^{3+} + Ac^- \rightleftharpoons BiAc^{2+}$	1.04 [b]	
$Bi^{3+} + 2Ac^- \rightleftharpoons Bi(Ac)_2^+$	1.81 [b]	
$Bi^{3+} + 3Ac^- \rightleftharpoons Bi(Ac)_3$	4.20 [b]	
$Ac^- + H^+ \rightleftharpoons AcH$	4.56 [a]	0.1

[a] Values obtained from the NIST database[2]

[b] Values obtained from work by Shock and Koretsky[3]

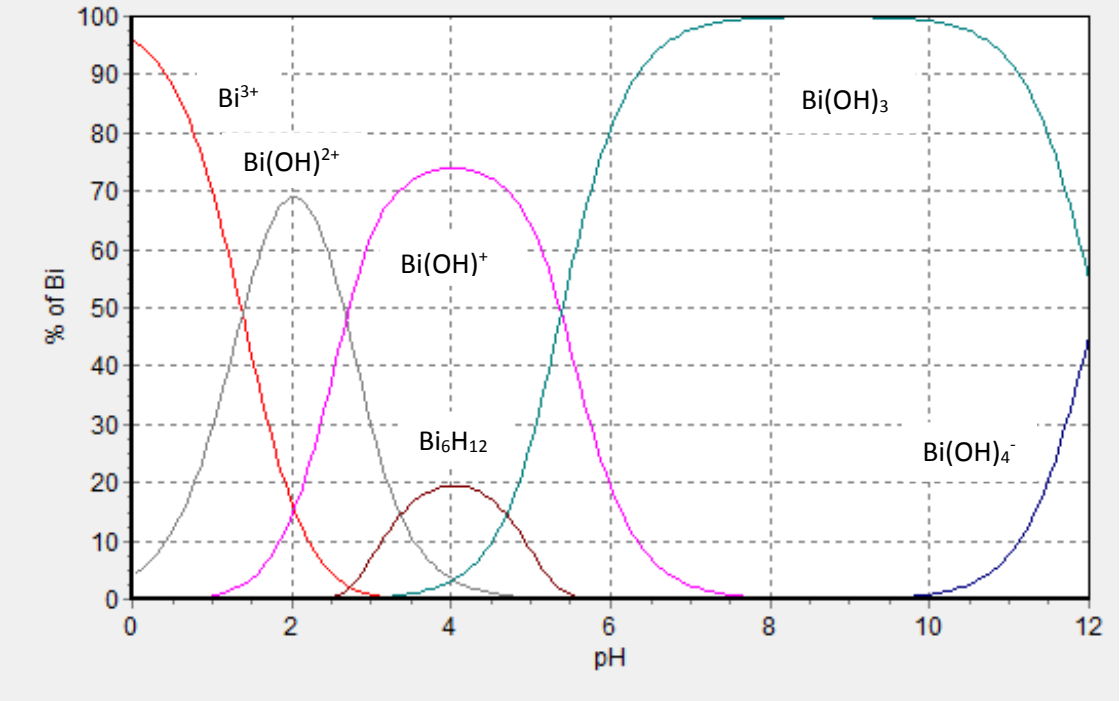


Figure A1.1: species distribution diagram for 10^{-5} M Bi^{3+} in water medium. The diagram was plotted using formation constants in Table A1.1.

Table A1.2: Formation constants[1] for the Hg^{2+} hydroxide and Hg^{2+} glycine (Gly) systems as well as the protonation constants for glycine at 25 °C and the given ionic strengths.

Equilibrium	Log β	Ionic strength (M)
$H^+ + OH^- \rightleftharpoons H_2O$	13.78	0.1
$Hg^{2+} + OH^- \rightleftharpoons Hg(OH)^+$	10.20	0.1
$2Hg^{2+} + 2OH^- \rightleftharpoons Hg(OH)_2$	21.20	0.1
$2Hg^{2+} + OH^- \rightleftharpoons Hg_2(OH)^{3+}$	11.3	0.3
$3Hg^{2+} + 3OH^- \rightleftharpoons Hg(OH)_3{}^{3+}$	4.20	0.3
$Hg^{2+} + Gly^- \rightleftharpoons HgGly^+$	10.3	0.5
$Hg^{2+} + 2Gly^- \rightleftharpoons HgGly_2$	19.2	0.5
$Gly^- + H^+ \rightleftharpoons GlyH$	9.57	0.1
$Gly^- + 2H^+ \rightleftharpoons GlyH_2{}^+$	11.9	0.1

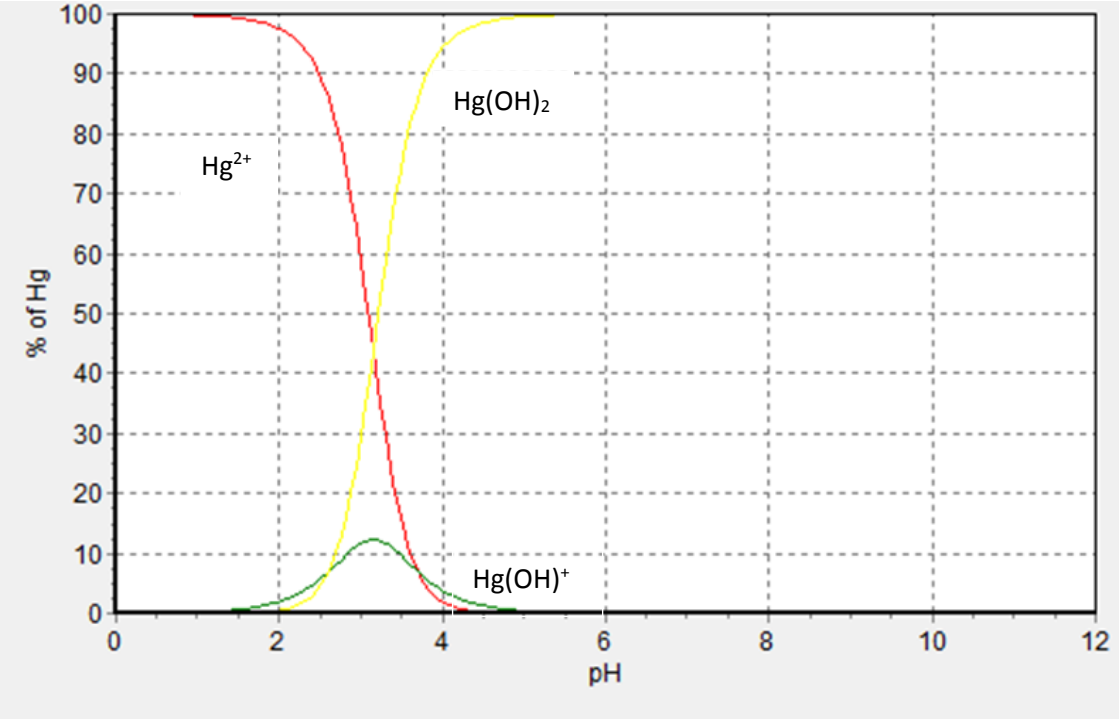


Figure A1.2: Species distribution diagram for aqueous solutions of Hg^{2+} (1×10^{-4} M) plotted using formation constants in Table A1.2 at 25°C and the indicated ionic strength.

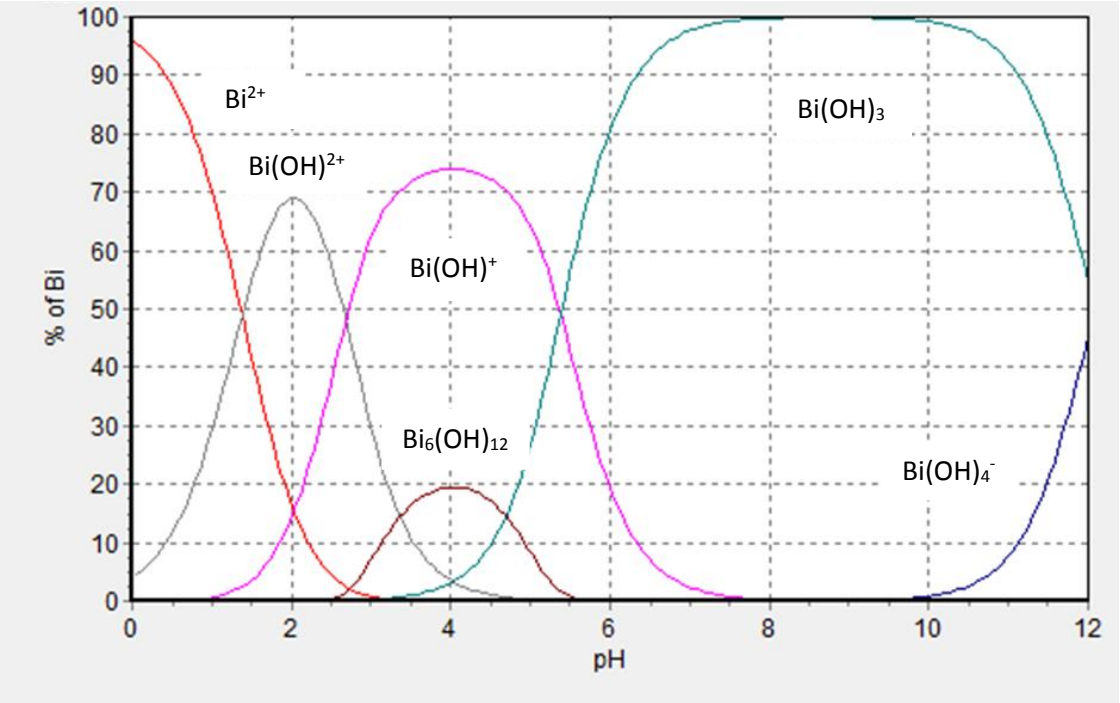


Figure A1.3: Species distribution diagram for aqueous solutions of Bi^{3+} (1×10^{-5} M) in acetate medium (0.1 M) plotted using the literature formation constants in Table A1.1 reported at 25 °C and the indicated ionic strength.

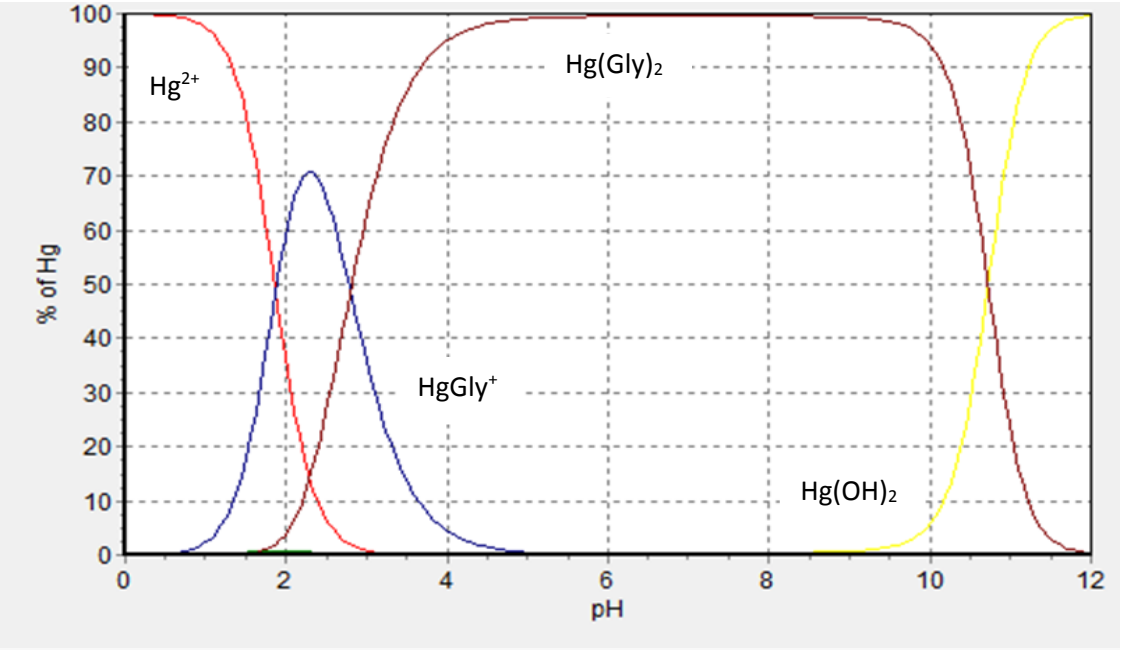


Figure A1.4: Species distribution diagram for aqueous solutions of Hg^{2+} (1×10^{-4} M) in glycine medium (0.1 M) plotted using formation constants in Table A1.2 at 25°C and the indicated ionic strength.

Table A1.3: Formation constants[1] for lead hydroxide, lead glycine systems and protnation constants for glycine at 25°C and the given ionic strengths.

Equilibrium	Log β	Ionic strength (M)
$H^+ + OH^- \rightleftharpoons H_2O$	13.78	0.1
$Pb^{2+} + OH^- \rightleftharpoons Pb(OH)^+$	5.9	0.1
$Pb^{2+} + 2OH^- \rightleftharpoons Pb(OH)_2$	7.8	3.0
$2Pb^{2+} + OH^- \rightleftharpoons Pb_2(OH)^{3+}$	7.0	1.0
$4Pb^{2+} + 4OH^- \rightleftharpoons Pb_2(OH)_4^{4+}$	34.7	0.1
$6Pb^{2+} + 8OH^- \rightleftharpoons Pb_6(OH)_8^{4+}$	66.9	0.1
$Pb^{2+} + Gly \rightleftharpoons Pb(Gly)$	11.07	0.1
$Pb^{2+} + Gly \rightleftharpoons Pb(Gly)_2$	20.64	1
$Pb^{2+} + Gly \rightleftharpoons Pb(Gly)_3$	30.03	0.1
$Gly^- + H^+ \rightleftharpoons GlyH$	9.57	0.1
$Gly^- + 2H^+ \rightleftharpoons GlyH_2^+$	11.9	0.1

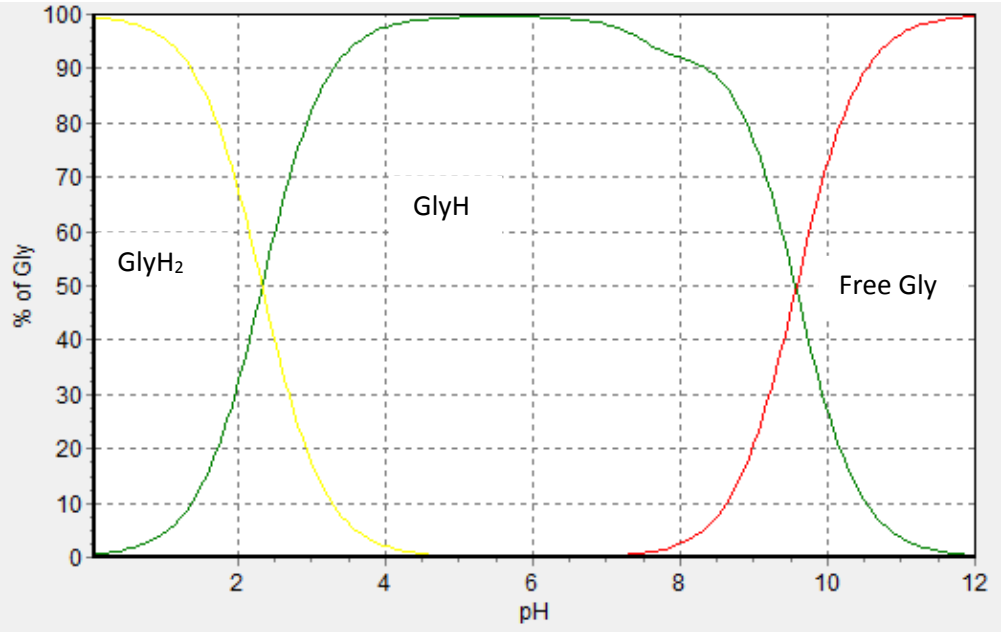


Figure A1.5: Species distribution diagram for the 0.1 M glycine in HNO_3. The species distribution diagram was plotted using the protonation constants im Table A1.3 at 25°C and the indicated ionic strengths.

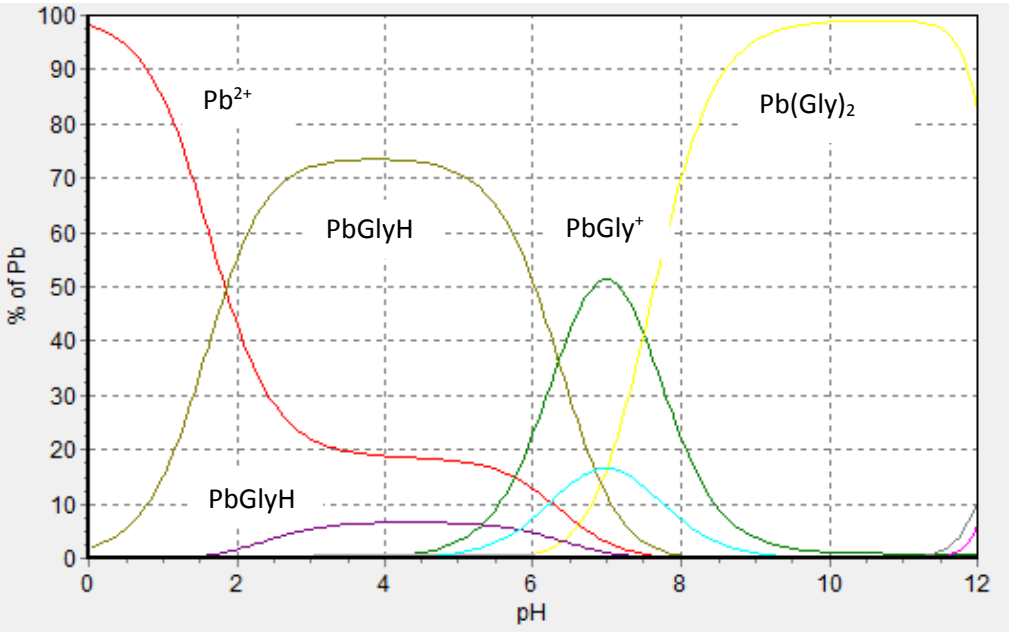


Figure A1.6: Species distribution diagram for 10^{-5} M Pb^{2+} and 0.12 M glycine in HNO_3 plotted using the formation constants in Table A1.3 at 25°C and the indicated ionic strength.

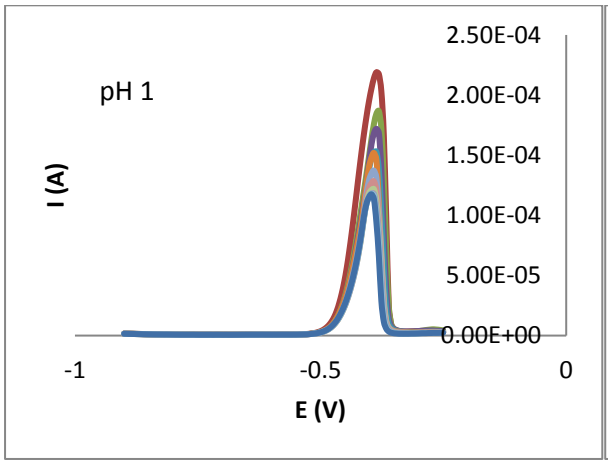
References

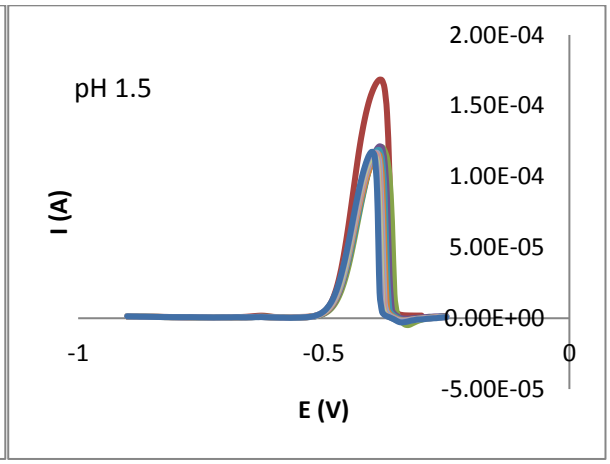
1) Petit, L. D., Powell, K. J. Sol-Eq, version 2.2; Academic Software, IUPAC, (2002).

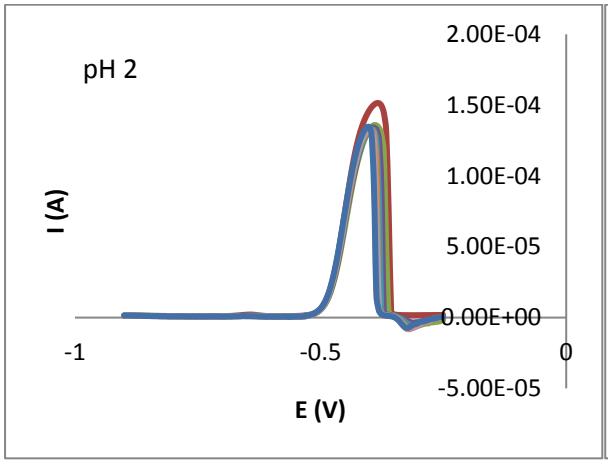
2) Martell, A.E., Smith, R.M.; Motekaitis,R.J. *NIST Standard Refernce Database*; version 8, (2004).

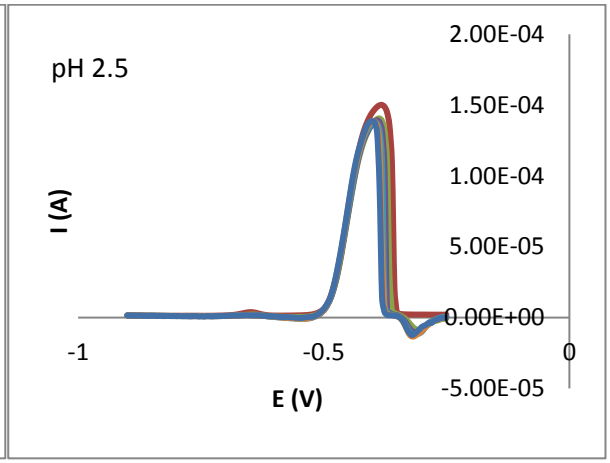
3) Shock, E. L. and Koretsky, M. K. *Geochimica. Cosmochim. Acta* **57,** 4899-4922 (1993).

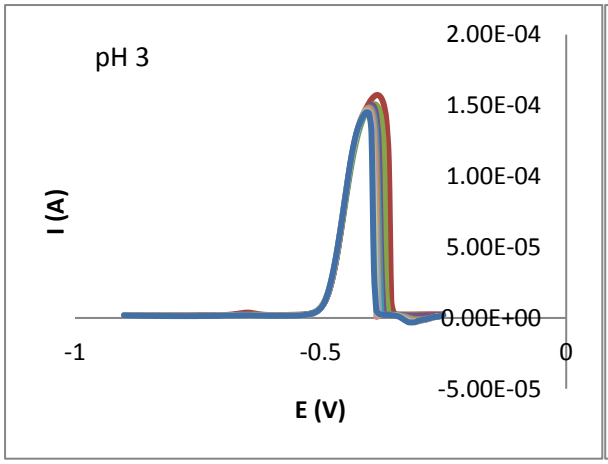
Appendix 2-Voltammograms

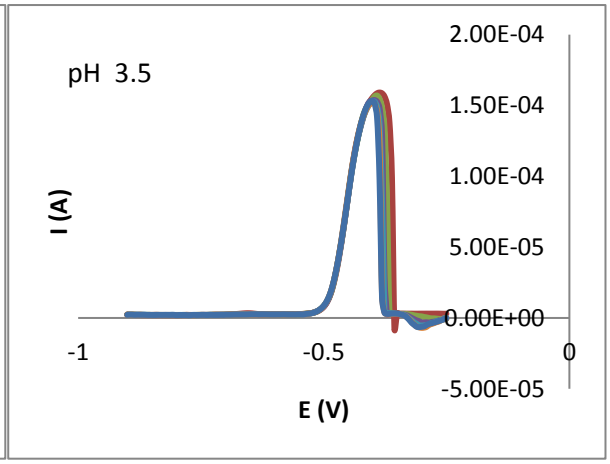












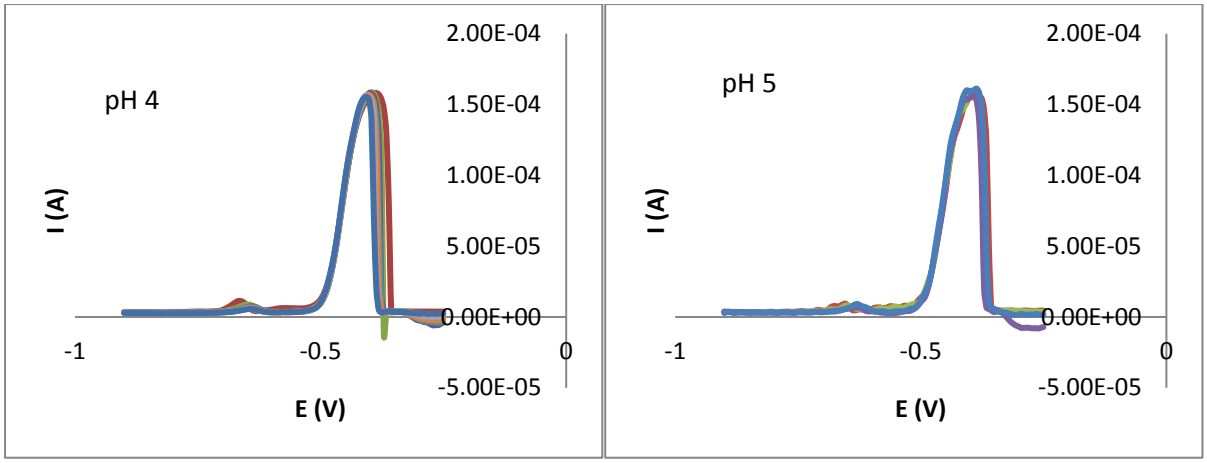


Figure A2.1: Voltammograms for the Pb^{2+} measured consecutively at 1×10^{-4} M and 1×10^{-3} M Hg^{2+} at different pH (E_{dep} and t_{dep} at -900 mV and 300 s). The same colour coding was used in all graphs and at pH 1 it can clearly be seen how the peak current decreases as consecutive measurements were made.

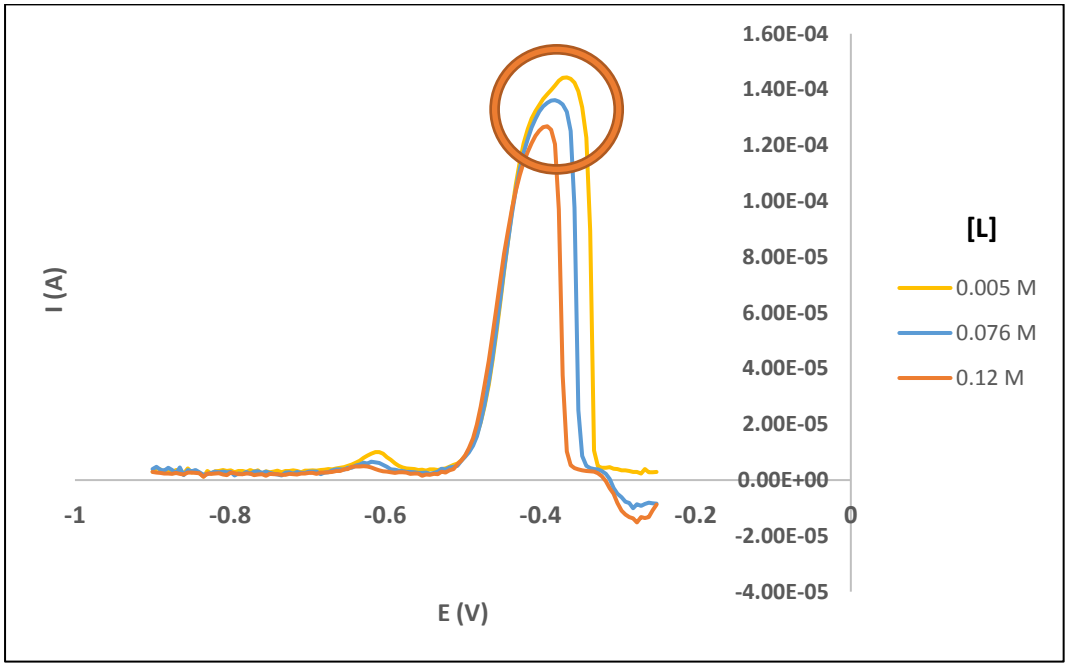


Figure A2.2: Selected Voltammograms from the Pb-Gly titration showing the almost split peaks.

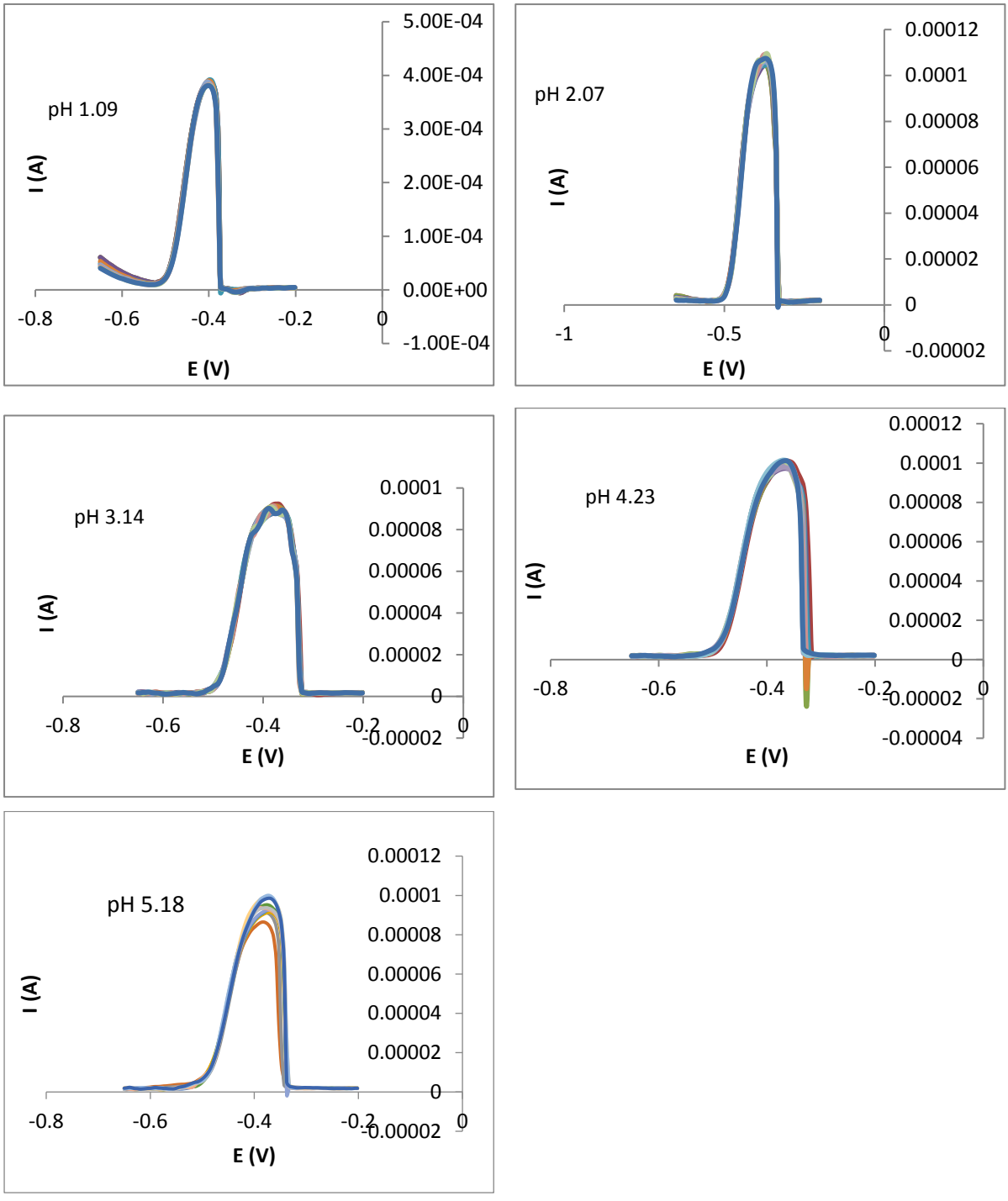


Figure A2.3: Voltammograms measured consecutively for 10^{-4} M Pb^{2+} (E_{dep} and t_{dep} at -650 mV and 120 s, respectively) at different pHs. Peak splitting can be seen in some voltammograms.